Cell

Global identification of SWI/SNF targets reveals compensation by EP400

Graphical abstract

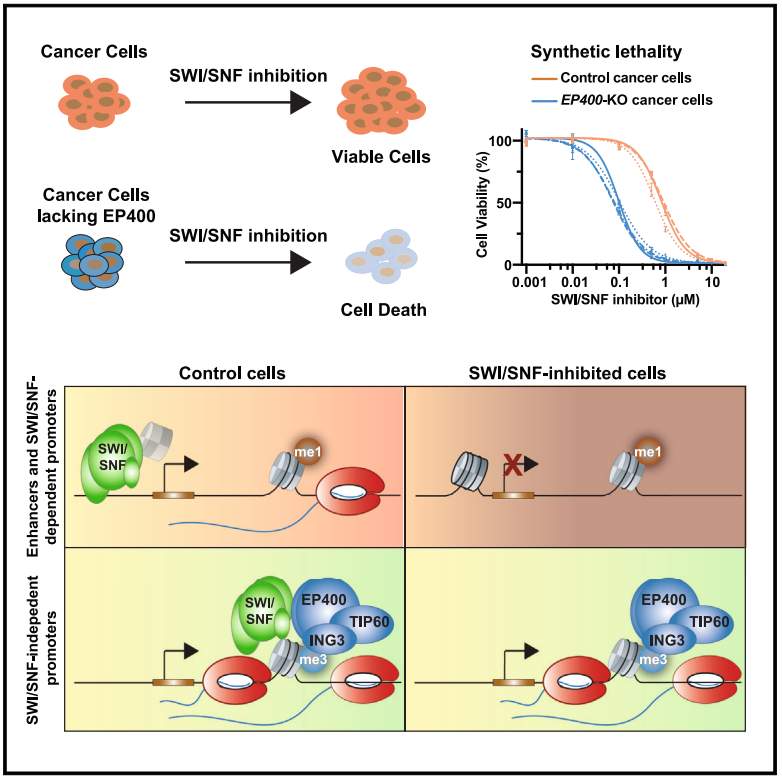

Highlights

- Genes repressed by long-term SWI/SNF loss do not accurately reflect direct targets
- Compensatory remodeler EP400/TIP60 allows many promoters to recover accessibility
- EP400 loss is synthetically lethal with perturbation of SWI/SNF
- SWI/SNF dependence in cancer cells can be predicted from the promoter chromatin state

Authors

Benjamin J.E. Martin, Eileen F. Ablondi, Christine Goglia, Claudia A. Mimoso, Piero R. Espinel-Cabrera, Karen Adelman

Correspondence

karen_adelman@hms.harvard.edu

In brief

Subunits of SWI/SNF chromatin remodeling complexes are often mutated in disease, but it has been difficult to predict gene sensitivity to SWI/SNF loss or inhibition. Time-resolved assays, however, reveal an initial global loss of chromatin accessibility and a mechanism of recovery at promoters following a regulatory logic dictated by the targeting of a compensatory remodeler, EP400.

Martin et al., 2023, Cell *186*, 5290–5307
November 22, 2023
https://doi.org/10.1016/j.cell.2023.10.006

CellPress

CellPress

Cell

Article

Global identification of SWI/SNF targets reveals compensation by EP400

Benjamin J.E. Martin,[1,2,4] Eileen F. Ablondi,[1,4] Christine Goglia,[1] Claudia A. Mimoso,[1] Piero R. Espinel-Cabrera,[1] and Karen Adelman[1,2,3,5,*]

[1]Department of Biological Chemistry and Molecular Pharmacology, Blavatnik Institute, Harvard Medical School, Boston, MA 02115, USA
[2]Ludwig Center at Harvard, Boston, MA 02115, USA
[3]Broad Institute of MIT and Harvard, Cambridge, MA 02142, USA
[4]These authors contributed equally
[5]Lead contact
*Correspondence: karen_adelman@hms.harvard.edu
https://doi.org/10.1016/j.cell.2023.10.006

SUMMARY

Mammalian SWI/SNF chromatin remodeling complexes move and evict nucleosomes at gene promoters and enhancers to modulate DNA access. Although SWI/SNF subunits are commonly mutated in disease, therapeutic options are limited by our inability to predict SWI/SNF gene targets and conflicting studies on functional significance. Here, we leverage a fast-acting inhibitor of SWI/SNF remodeling to elucidate direct targets and effects of SWI/SNF. Blocking SWI/SNF activity causes a rapid and global loss of chromatin accessibility and transcription. Whereas repression persists at most enhancers, we uncover a compensatory role for the EP400/TIP60 remodeler, which reestablishes accessibility at most promoters during prolonged loss of SWI/SNF. Indeed, we observe synthetic lethality between EP400 and SWI/SNF in cancer cell lines and human cancer patient data. Our data define a set of molecular genomic features that accurately predict gene sensitivity to SWI/SNF inhibition in diverse cancer cell lines, thereby improving the therapeutic potential of SWI/SNF inhibitors.

INTRODUCTION

Gene activation requires that transcription factors (TFs) and the transcription machinery can access DNA at gene promoters and at *cis*-regulatory enhancers.[1,2] DNA accessibility is generated by chromatin remodelers, such as the mammalian SWI/SNF complexes, which use energy from ATP to slide nucleosomes or evict them from DNA. These actions create nucleosome-depleted regions (NDRs) at promoters and enhancers that facilitate TF binding and transcription initiation.[3,4] Further, SWI/SNF has been implicated in rendering chromatin more dynamic to help RNA polymerase II (RNAPII) overcome nucleosome barriers within gene bodies.[5] Accordingly, chromatin remodeling by SWI/SNF is critical to the establishment of appropriate gene expression patterns.[6–8]

Emphasizing the crucial role of SWI/SNF, the complex is mutated in >20% of cancers, with SWI/SNF subunits frequently found to contain driver mutations.[9,10] However, a comprehensive understanding of the targets and cellular consequences of SWI/SNF activity has remained elusive, as RNAi-mediated depletion, genomic knockout (KO), and mutational studies have reported varied, often conflicting, conclusions about the function of chromatin remodeling by SWI/SNF.[11–13] Specifically, current models for SWI/SNF function range from inhibition of enhancer transcription,[11,14] to repression of certain gene sets,[3,15,16] to activation of specific enhancers.[7,17,18] These discrepancies likely result from the extended time required to sufficiently deplete SWI/SNF proteins with these strategies, such that the direct effects of SWI/SNF loss are obscured by indirect effects and compensatory mechanisms.

For these reasons, the development of fast-acting and specific inhibitors and degraders of the paralogous SWI/SNF ATPase subunits BRG1 and BRM represent valuable tools toward elucidating the direct role of SWI/SNF-mediated nucleosome remodeling.[19] Indeed, treatment of mouse and human cells with fast-acting BRG1/BRM inhibitors BRM011 and BRM014 markedly reduced chromatin accessibility at many regulatory loci within minutes, indicating that the maintenance of open chromatin at these sites is dependent upon continuous catalytic activity of SWI/SNF.[20,21] These results are consistent with previous work in *S. cerevisiae* demonstrating that constant chromatin remodeling is required to maintain appropriate genomic accessibility patterns.[22–24] Importantly, the effects observed upon treatment of cells with BRM014 were highly similar to those obtained when BRG1 was subjected to targeted protein degradation, validating inhibitor specificity.[20,25] Further, the development of SWI/SNF mutants with resistance to inhibitor compounds selectively identified mutated residues

located within the catalytic active site of the BRM/BRG1 ATPases.[26]

Surprisingly, despite broad reduction in enhancer accessibility and TF occupancy observed when BRG1/BRM were inhibited or degraded, this resulted in limited and highly selective effects on gene expression.[20,21,25] These findings raised critical questions about the functional relevance of SWI/SNF-mediated remodeling at regulatory elements.

One possibility suggested by the recent data is that alternate mechanisms exist to allow most genes to maintain expression in the absence of BRG1/BRM activity. To address this possibility and to identify potential compensatory chromatin remodelers, we probed the direct impact of SWI/SNF inhibition on enhancer and gene activity using time-resolved assays of chromatin accessibility and active transcription in mouse embryonic stem cells (mESCs). We find that SWI/SNF is globally and continuously required for chromatin accessibility and transcription initiation at both enhancers and promoters. However, whereas enhancers are persistently repressed during SWI/SNF inhibition, many promoters recover accessibility and transcription activity. Promoters that fail to recover are characterized by low expression, weak chromatin accessibility, and an enrichment of histone H3K4 monomethylation (H3K4me1). Importantly, these features defined in mESCs can predict gene sensitivity to SWI/SNF perturbation in diverse cancer cell lines. Our work thus establishes a prognostic framework for identifying genes that will be sensitive to SWI/SNF loss or inhibition in disease contexts. Further, we demonstrate that the compensation for loss of SWI/SNF activity is mediated by the EP400/TIP60 coactivator complex, which interacts with and is recruited by trimethylation of H3K4 (H3K4me3). Accordingly, EP400 gains increased importance in cells wherein SWI/SNF is perturbed, and EP400 loss greatly sensitizes cells to loss of SWI/SNF activity.

RESULTS

SWI/SNF inhibition causes widespread reduction in enhancer activity

To characterize changes in chromatin accessibility upon SWI/SNF inhibition in mESCs, we systematically identified active promoters and enhancers genome-wide (Figure 1A). Assay for transposase-accessible chromatin with high-throughput sequencing (ATAC-seq) data from untreated mESCs was used to define a set of peaks corresponding to regions of accessible chromatin (N = 83,201). We then used precision run-on sequencing (PRO-seq), which captures nascent RNA associated with engaged RNAPII,[27] to define sites of active transcription. Approximately 20% of ATAC-seq peaks were located within 1.5 kb of an active annotated transcription start site (TSS), with a median distance of 112 bp between these peak centers and the nearest active TSS (Figure S1A; see STAR Methods). These peaks were therefore designated as "promoter peaks" and, to facilitate subsequent analysis, were centered on the active TSS (N = 13,536; Figure S1B). Because synthesis of enhancer RNA (eRNA) is a sensitive hallmark of active enhancers,[28–30] promoter-distal ATAC-seq peaks with associated PRO-seq signal[31] were classified as putative enhancers (N = 32,149). Consistent with this designation, transcribed ATAC-seq peaks were enriched for acetylated histone H3K27 compared with non-transcribed peaks (Figure S1C) and showed the enrichment of H3K4me1 that is considered a hallmark of enhancers (Figure S1D). Chromatin immunoprecipitation sequencing (ChIP-seq) for BRG1, the SWI/SNF ATPase subunit expressed in mESCs,[32] demonstrated BRG1 occupancy at both promoters and enhancers (Figure 1A), consistent with a broad role for SWI/SNF in chromatin remodeling.[2,33]

We then treated mESCs with BRM014 (at 1 μM) or DMSO for 2 h and performed ATAC-seq, with *Drosophila* spike-in controls to allow for accurate quantification. These data demonstrated that inhibition of SWI/SNF activity broadly reduces chromatin accessibility at enhancers (Figure 1B, >98% of enhancers affected). This result is consistent with prior work in mESCs, which found strongly reduced accessibility and occupancy of TFs at regulatory loci following SWI/SNF loss[8,20,21] and clarifies that this loss of accessibility occurs at nearly all enhancer loci. Supporting that these rapid consequences of SWI/SNF inhibition represent direct effects, the enhancers most strongly affected by SWI/SNF inhibition are those most highly bound by the complex (Figure 1B, BRG1 ChIP-seq). Investigation of BRG1 binding to chromatin using quantitative ChIP-seq after 2 h BRM014 treatment demonstrated an increase in BRG1 occupancy within the enhancer peak, centered over the NDR (Figure 1C). This augmented BRG1 occupancy is consistent with biochemical experiments, indicating that blocking ATP hydrolysis slows SWI/SNF release from chromatin.[36] Short-term inhibition of BRG1, thus, does not displace SWI/SNF from enhancers, as would protein depletion or degradation. Consequently, this system provides mechanistic insights into the role of the BRG1 ATPase under conditions wherein the SWI/SNF complex remains properly localized. Western blotting confirmed that treatment with BRM014 for up to 24 h had no detectable effect on levels of SWI/SNF subunits (Figure S1E).

We next determined chromatin accessibility following extended inhibition of SWI/SNF activity, focusing on BRM014 treatment for 4 and 8 h, time points at which we observed no defects in cell proliferation or morphology (Figures S1F and S1G). Indicative of a continued dependence of enhancers on SWI/SNF for maintenance of open chromatin, accessibility was reduced at 77% of enhancers throughout an 8 h treatment with BRM014 (Figure 1D). Given this striking loss of accessibility during prolonged inhibition of SWI/SNF, and recent reports that BRM014 markedly reduces the occupancy of key TFs at enhancers, one might predict that eRNA synthesis would also be repressed by BRM014. Accordingly, analysis of nascent RNA synthesis at enhancers using PRO-seq demonstrates a broad reduction in eRNA transcription across the BRM014 treatment time course (Figure 1E). These results contrast with earlier suggestions that SWI/SNF suppresses enhancer transcription based on long-term depletion approaches[11] but are consistent with recent work using acute SWI/SNF perturbation.[20,21,25] We conclude that chromatin remodeling by SWI/SNF is necessary for the sustained activity of most enhancers.

Notably, enhancers that were sensitive to loss of SWI/SNF activity across the 8 h time course (Figure 1D) were enriched in binding of the pluripotency-associated TFs OCT4, SOX2, and NANOG (OSN) compared with enhancers that recovered

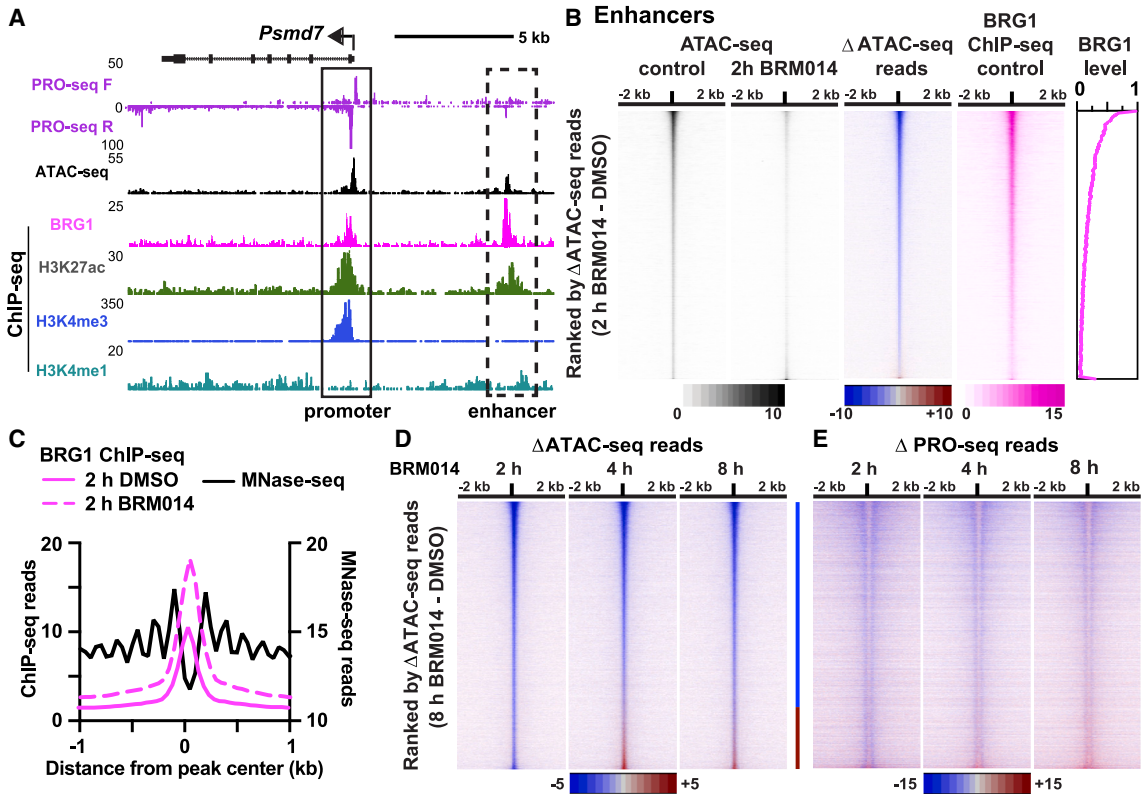

Figure 1. Enhancer accessibility and activity require SWI/SNF activity

(A) Genome browser view of the *Psmd7* promoter (solid box) and associated enhancer (dashed box) with PRO-seq, ATAC-seq, BRG1 ChIP-seq, H3K27ac ChIP-seq,[34] H3K4me3 ChIP-seq,[34] and H3K4me1 ChIP-seq data.[35]

(B) Heatmap representation of the effects of 2 h BRM014 treatment on ATAC-seq signal at enhancers (n = 32,149). Normalized data from combined replicates (n = 3 per condition) were aligned to the enhancer peak center. Sites are ranked by difference in ATAC-seq reads (enhancer center ± 300 bp) between 2 h BRM014 and 2 h DMSO control. BRG1 ChIP-seq signal is shown in the same rank order, as is relative BRG1 signal (summed ± 500 bp from peak centers).

(C) Aggregate plot of quantitative BRG1 ChIP-seq signal (n = 2 per condition) at enhancers from 2 h DMSO- and BRM014-treated cells. Average MNase-seq[28] profiles are shown to indicate the position of the NDR. Data are graphed in 50 bp bins.

(D and E) Difference in ATAC-seq signal (D) and PRO-seq signal (E) after BRM014 treatment (n ≥ 2 per condition) for all enhancers. Data were aligned to the enhancer center and rank ordered by the difference in enhancer ATAC-seq reads after 8 h treatment. Blue line between heatmaps indicates the 77% of enhancers that fail to recover accessibility, whereas red line indicates enhancers that regain accessibility.

See also Figures S1 and S2.

accessibility (Figures S2A–S2C). This finding emphasizes that the presence of TFs considered to be pioneer factors does not render an enhancer less dependent on chromatin remodelers.[8,21] By contrast, CTCF occupancy was enriched at the subset of enhancers that recovered accessibility following SWI/SNF inhibition (Figures S2A, S2D, and S2E).[4,21] This observation suggests that the CTCF-associated chromatin remodeler SNF2H (SMARCA5)[37,38] might serve to maintain open chromatin at these sites during SWI/SNF inhibition. Consistent with this idea, we found SNF2H enrichment at enhancers that retained accessibility following BRM014 treatment (Figure S2E). Moreover, accessibility at this subset of enhancers was sensitive to KO of SNF2H (Figure S2F), confirming a role for remodeling by SNF2H at these loci. Together, these data indicate that most enhancers in mESCs, including those bound by pioneer factors, require continuous SWI/SNF activity to maintain accessibility and activity. However, a subset of enhancers occupied by CTCF can employ the alternate chromatin remodeler SNF2H to sustain accessibility, even during prolonged absence of SWI/SNF activity.

A majority of gene promoters recover from loss of SWI/SNF activity

We then turned our attention to promoters, which have often been considered insensitive to SWI/SNF activity or even to be repressed by SWI/SNF-mediated remodeling.[3,12,20] Strikingly, analysis of promoter accessibility after 2 h of BRM014 treatment revealed a global reduction in chromatin accessibility, similar to that observed at enhancers (Figure 2A, 97% of promoters affected). As at enhancers, the promoters most affected by BRM014 inhibition are those with the highest levels of BRG1 ChIP-seq signal in control mESCs (Figure 2A), consistent with reduced accessibility reflecting a direct effect. Inhibitor treatment causes a marked increase in BRG1 binding at promoters, with the peak of BRG1 occupancy coinciding with the first (+1) well-positioned nucleosome (Figures 2A and 2B). We conclude

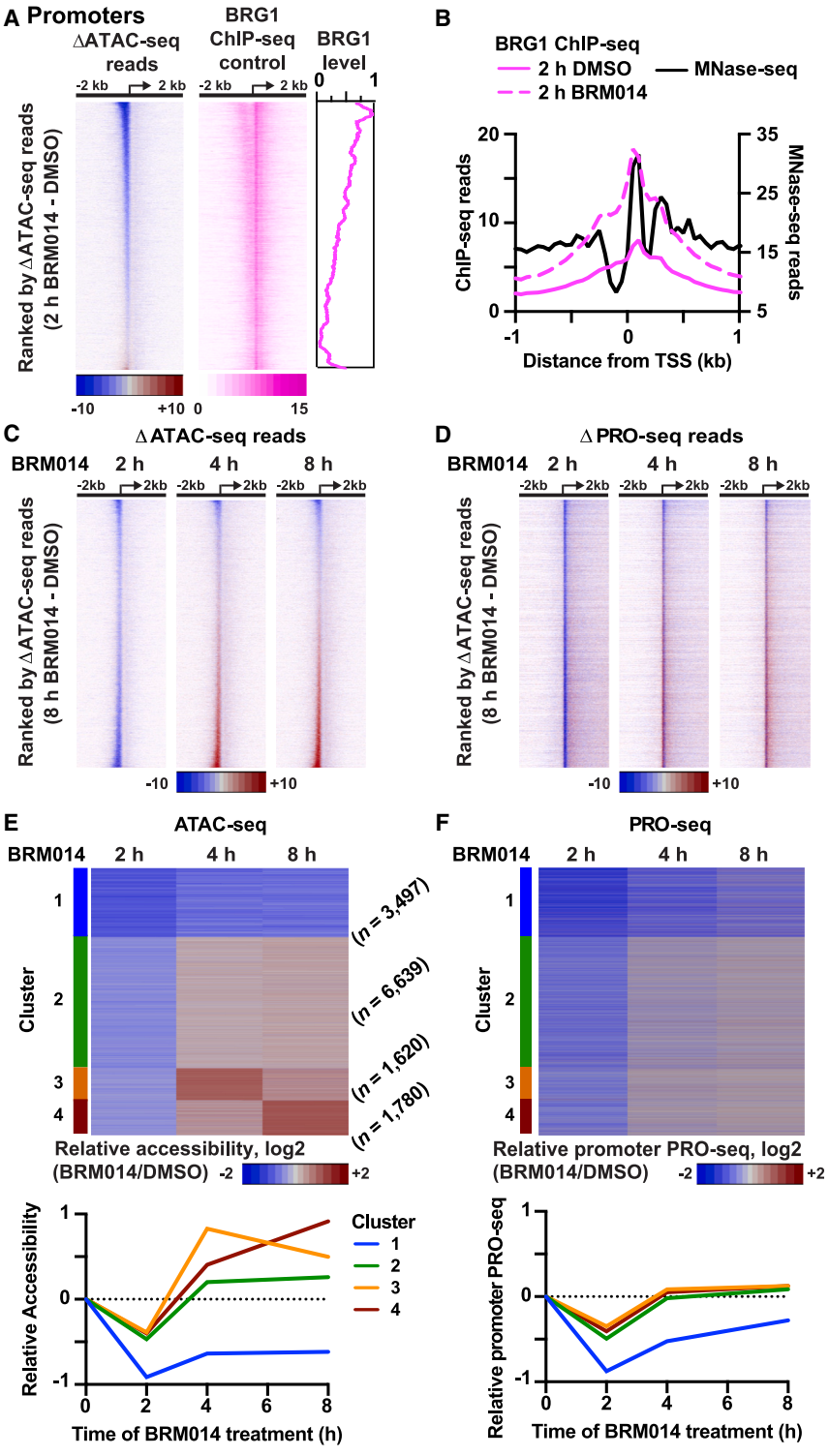

Figure 2. Promoters recover from SWI/SNF inhibition with variable kinetics

(A) Heatmaps showing the effects of 2 h BRM014 treatment on ATAC-seq signal at promoters (n = 13,536). Data are aligned to TSS. Sites are ranked by difference in ATAC-seq reads after 2 h BRM014 treatment (−450 to +149 bp from the TSS). BRG1 ChIP-seq signal is shown in the same rank order, as is relative BRG1 signal (summed from −750 to +249 bp relative to TSS).

(B) Aggregate plot of quantitative BRG1 ChIP-seq signal around promoters in DMSO- and BRM014-treated cells. Average MNase-seq[28] profile is shown to define the position of the NDR. Data are graphed in 50 bp bins.

(C and D) Difference in ATAC-seq (C) and PRO-seq (D) signal after BRM014 treatment (compared with time-matched DMSO controls, as in (A) for all promoters. Data were aligned to TSS and genes rank ordered by the difference in promoter ATAC-seq reads after 8 h treatment.

(E and F) Clustering based on relative differences in ATAC-seq reads (as in C) defines four classes of responses to extended BRM014 treatment. The average value in each cluster for the relative ATAC-seq (−450 to +149 bp from the TSS) and PRO-seq (TSS to +150 nt) signals across the time course are shown at bottom.

See also Figure S3.

that SWI/SNF broadly opens chromatin at promoters and that the immediate effects of inhibiting BRG1 are very similar at promoter and enhancer loci.

Extended BRM014 treatment, however, exhibited markedly different effects at promoters versus enhancers. In contrast to the persistent repression of accessibility observed at most enhancers, a majority of promoters effectively recover accessibility after 4 h of BRM014 treatment (Figure 2C). In fact, many promoters display even greater accessibility upon 4 h of SWI/SNF inhibition. These prominent accessibility changes were confirmed by ATAC-qPCR at selected loci (Figure S3A). The restoration of ATAC-seq signal at gene promoters following prolonged BRM014 treatment suggests that the loss of SWI/SNF activity can be functionally compensated at many promoters and even over-compensated at some loci.

To determine how the observed changes in promoter chromatin accessibility impact gene transcription, we evaluated PRO-seq signals over the BRM014 treatment time course. After 2 h of BRM014 treatment, the widespread reduction of promoter accessibility was accompanied by a strong repression of transcription activity (Figure 2D), with a loss of promoter-proximal RNAPII. These results are consistent with a requirement for accessible promoter chromatin to allow for transcription initiation. Upon longer SWI/SNF inhibition, as chromatin accessibility was restored at many gene promoters, transcription initiation, and gene activity recovered concomitantly.

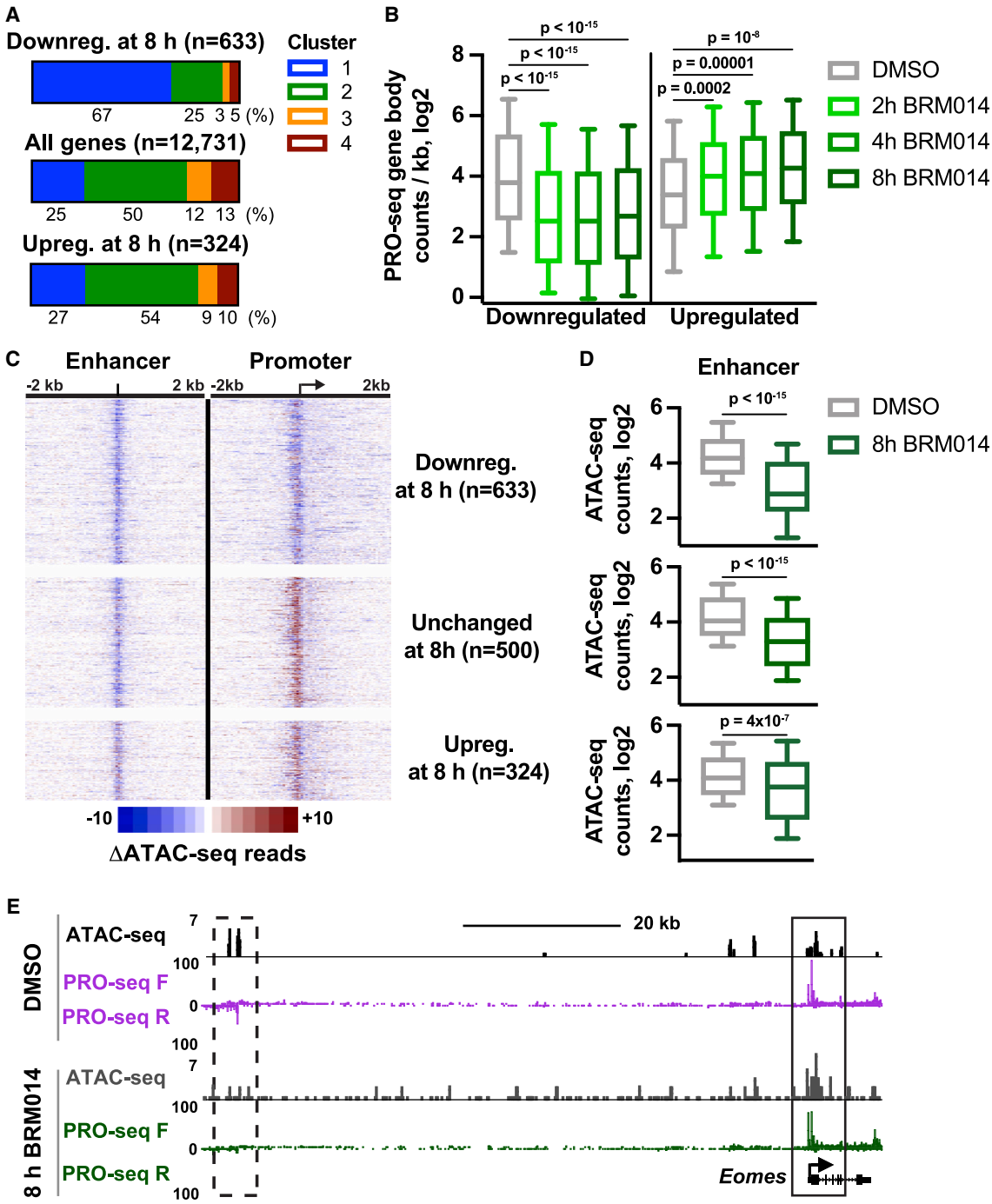

Figure 3. Recovery of gene expression during BRM014 treatment is not dependent on the activity of nearby enhancers

(A) Representation of promoter clusters among genes downregulated or upregulated after 8 h BRM014 treatment, compared with all active genes longer than 1 kb. Percentages of genes in each cluster are indicated. Differentially expressed genes were those with a fold-change > 1.5 and p adj < 0.001, based on PRO-seq read density in gene bodies (TSS + 250 to transcription end site [TES]).

(B) Gene body PRO-seq read density is shown at downregulated and upregulated genes. p values are from Mann-Whitney test.

(C) Heatmaps show the effects of 8 h BRM014 treatment on ATAC-seq signal at promoters (right) and their closest enhancers (left) for genes downregulated, unchanged (subsampled, n = 500), and upregulated upon BRM014 treatment. Data are aligned to the enhancer center or gene TSS.

(legend continued on next page)

To investigate the variable promoter recovery during BRM014 treatment, promoters were clustered based on their chromatin accessibility changes over the BRM014 time course (Figure 2E). Although most gene promoters (clusters 2–4) were able to readily reinstate chromatin accessibility following the loss of SWI/SNF activity, about one-quarter of promoters (cluster 1) remained repressed. Importantly, the inability of cluster 1 genes to reinstate accessibility in the absence of BRG1 activity is reproducible and persistent because these genes show substantially higher nucleosome occupancy in mESCs subjected to 24 h BRM014 treatment or following 72 h BRG1 KO (Figures S3B and S3C). Furthermore, degron-mediated depletion of the core SWI/SNF subunit ARID1A in mESCs[39] also caused a persistent reduction in accessibility of both cluster 1 genes and enhancers, whereas genes in clusters 2–4 recovered accessibility (Figure S3D). Our findings are thus not specific to the SWI/SNF ATPases but reflect a general consequence of SWI/SNF loss.

Graphing promoter-proximal PRO-seq signal across the four clusters (Figure 2F) confirmed that changes in accessibility are generally mirrored by transcriptional changes. However, although promoters in clusters 3 and 4 show evidence of elevated ATAC-seq signal at the 4 or 8 h time point compared with DMSO controls, we find no evidence that transcription is broadly increased above control levels under these conditions (Figure 2F and below). Overall, these findings indicate that accessible promoter chromatin is necessary, but not sufficient, for gene transcription. Further, they support a model wherein the direct, immediate consequence of SWI/SNF inhibition is reduced accessibility and transcription at both promoters and enhancers. Whereas most promoters can compensate for loss of SWI/SNF activity to reestablish accessible chromatin and gene expression, a subset of promoters and most enhancers are dependent upon SWI/SNF-mediated remodeling for appropriate accessibility and activity.

To test whether the accumulation of inactive BRG1 on chromatin observed after 2 h BRM014 treatment (Figures 1C and 2B) might persist at enhancers and cluster 1 promoters, preventing the recovery of accessibility, we performed BRG1 ChIP-seq after 4 h of SWI/SNF inhibition (Figures S3E–S3H). However, in contrast to this model, we found that release of inactive BRG1 occurs most efficiently at enhancers, which largely fail to recover accessibility. Thus, the retention of inactive SWI/SNF complexes does not underlie the failure to reinstate accessibility in BRM014-treated cells.

Recovery from SWI/SNF inhibition is largely promoter autonomous

We hypothesized that the variable ability of gene promoters to reinstate expression during prolonged BRM014 treatment might be connected to the activity of nearby enhancers. To test this model, we stringently defined differentially expressed genes in 8 h BRM014-treated cells vs. DMSO controls, using the PRO-seq signal within gene bodies. This analysis revealed 633 downregulated genes and 324 upregulated genes (Figure 3A). As anticipated, cluster 1 promoters were markedly enriched among genes with sustained downregulation of transcription compared with all genes (Figure 3A). To confirm these gene sets, we assessed gene-body PRO-seq density over the BRM014 treatment time course (Figure 3B). For the downregulated genes, repression was notable at the earliest time point, suggesting that these genes are rapidly and persistently repressed by BRM014. In contrast, the upregulated genes showed gradually increased PRO-seq signal to a maximum at 8 h, suggesting that upregulation occurs more slowly following BRM014 treatment. For comparison, we defined a set of unchanged genes (fold-change < 1.1 and p adj > 0.5) that showed no appreciable differences in PRO-seq signal in BRM014-treated cells (Figure S3I).

We then assessed chromatin accessibility at the nearest enhancer of the downregulated, unchanged, and upregulated genes using heatmaps of ATAC-seq signal and boxplot analyses of read counts (Figures 3C and 3D). At the downregulated genes (Figures 3C and 3D, top), consistent with their enrichment for cluster 1 genes, promoter chromatin accessibility remained reduced after 8 h BRM014 treatment. Enhancers associated with downregulated genes also remained significantly repressed. For unchanged genes, where promoter chromatin accessibility was restored or even increased by 8 h BRM014, we observed persistent repression of the nearest enhancers (Figures 3C and 3D, middle). This result suggests that recovery of chromatin accessibility and gene activity at promoters can occur independently of enhancer inputs. Indeed, investigation of individual loci with well-defined enhancers that are essential for maintaining expression in mESCs, such as the *Eomes* gene[40] (Figure 3E, validated enhancer shown in dashed box), demonstrates that gene activity is fully restored after 8 h of BRM014 treatment, despite continued reduction of both accessibility and eRNA synthesis at the cognate enhancer. Even at upregulated genes, which showed continually increasing activity during BRM014 treatment (Figure 3B), we find only partial recovery at nearby enhancers, with 38% of the associated enhancers recovering to starting accessibility levels (Figures 3C and 3D, bottom). Thus, even genes that have increased expression following BRM014 treatment are generally near enhancers with reduced accessibility and activity.

To address the relationship between enhancer and nearby promoter recovery in a different way, we divided enhancers into quartiles based on the level of accessibility after 8 h of BRM014 treatment and assessed ATAC-seq signal at the promoters nearest these enhancers. This analysis provided no evidence that enhancer recovery affects the reinstatement of accessibility at nearby promoters (Figure S3J), with promoters near the most persistently repressed enhancers just as capable of restoring accessibility during extended BRM014 treatment as were promoters associated with enhancers that recovered

(D) ATAC-seq counts (±300 bp relative to the enhancer center) at the closest enhancers for the genes downregulated (top), unchanged (middle), or upregulated (bottom) after 8 h BRM014 treatment. p values are from Mann-Whitney test.

(E) Genome browser image of ATAC-seq and PRO-seq data at the *Eomes* promoter (solid box) and associated enhancer (dashed box) in cells treated with BRM014 or DMSO for 8 h.

See also Figure S3.

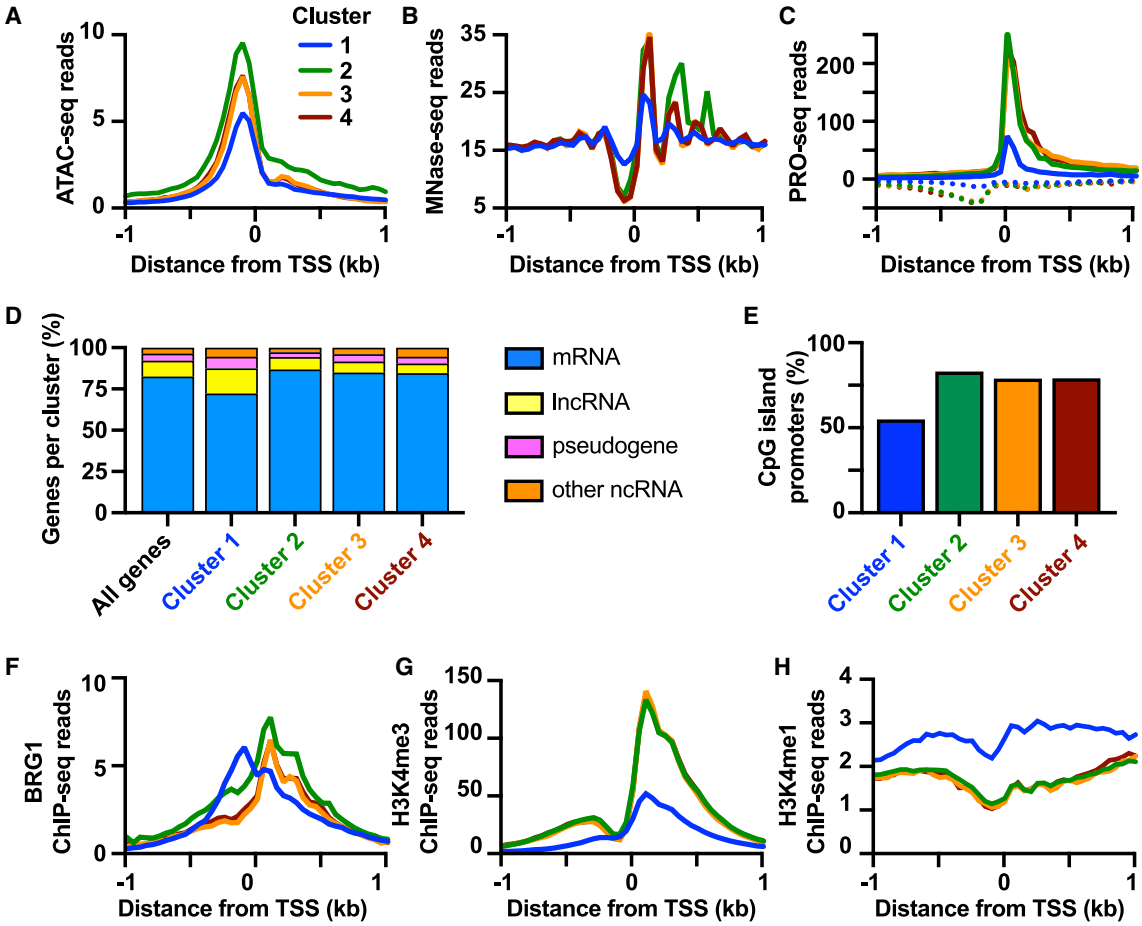

Figure 4. Promoters that are sensitive to SWI/SNF inhibition have distinct epigenetic characteristics

(A–C) Aggregate plots of average reads at promoters by cluster for ATAC-seq (A), MNase-seq[28] (B), and PRO-seq (C) signal. Data are graphed in 50 bp bins. Dotted lines in (C) represent antisense strand reads.

(D) Percentage of genes by transcript biotype for all annotated genes in each cluster.

(E) Bar graph showing percentage of promoters by cluster overlapping a CpG island.[44]

(F–H) Aggregate plots of average reads at promoters by cluster for BRG1 ChIP-seq (F), H3K4me3 ChIP-seq[34] (G), and H3K4me1 ChIP-seq[35] (H) signal. Data are graphed in 50 bp bins.

See also Figure S4.

entirely. We conclude that the restoration of accessibility and activity at gene promoters occurs autonomously of nearby enhancers. A similar, widespread disruption of enhancer-promoter communication following SWI/SNF perturbation was recently documented in prostate cancer cells.[25] Together, these findings imply that enhancer dysfunction is a general feature of prolonged SWI/SNF inhibition, which can occur in healthy, as well as diseased, cells.

SWI/SNF-dependent promoters have chromatin features that are characteristic of enhancers

We then sought to define the features that discriminate SWI/SNF-dependent, cluster 1 promoters from those that can compensate for loss of SWI/SNF activity. Investigation of chromatin architecture in untreated mESCs revealed that cluster 1 promoters are characterized by lower average accessibility and exhibit particularly small and weak NDRs compared with cluster 2–4 promoters (Figures 4A and 4B). Analysis of PRO-seq data showed that cluster 1 genes displayed lower occupancy by engaged RNAPII in both sense and antisense directions (Figure 4C), as well as lower levels of RNA expression (Figure S4A). Cluster 1 genes are enriched for Gene Ontology (GO) terms associated with cell signaling, development, and specific cell types or developmental lineages (Figure S4B). Notably, cluster 1 is enriched for genes involved in neuron development and the cardiovascular system, lineages known to require BRG1,[41–43] suggesting that BRG1 helps to poise these genes in mESCs for activation during development. Consistent with their enrichment in developmental genes, 25% of cluster 1 genes were considered bivalent,[33] compared with 13% of all expressed genes (Figure S4C). However, 75% of cluster 1 genes were not bivalent, indicating that bivalency and SWI/SNF dependence are distinct.

Cluster 1 is enriched for non-coding RNA species, including lncRNAs, pseudogenes, and pre-miRNAs (Figure 4D). Analysis

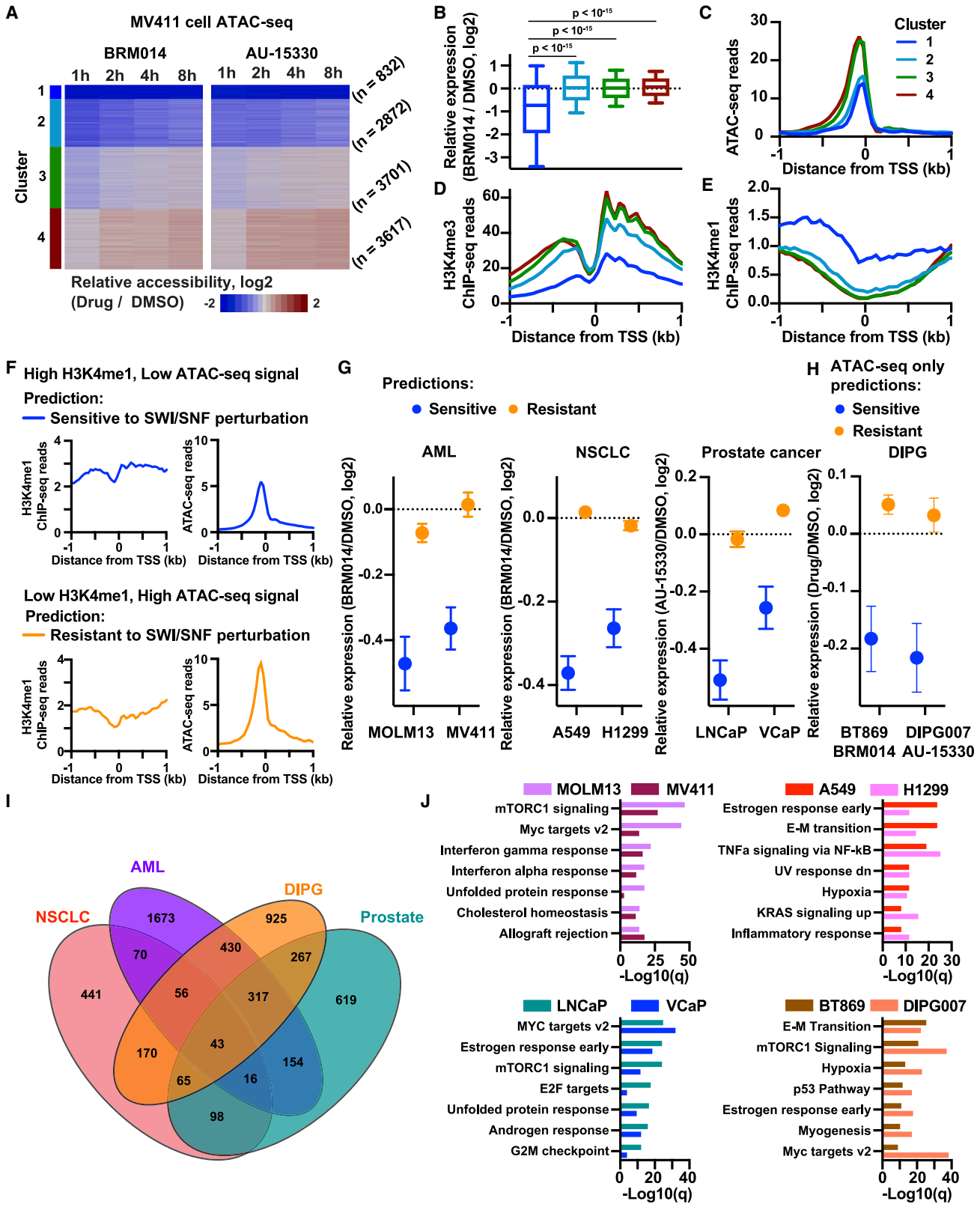

(legend on next page)

of evolutionary conservation revealed that cluster 1 promoters are less conserved on average than other promoters (Figure S4D). Cluster 1 promoters are less likely to overlap a CpG island than other clusters; however, more than 54% of cluster 1 promoters are embedded in CpG islands (Figure 4E), and the profile of GC enrichment across cluster 1 promoters is similar to that of clusters 2–4 promoters (Figure S4E).

Thus, SWI/SNF inhibition can repress CpG-island promoters as well as those with lower GC content, demonstrating that SWI/SNF dependence is not dictated by GC content, as has been previously suggested.[45,46]

Although BRG1 occupancy over most gene promoters is focused over the +1 nucleosome, cluster 1 promoters are instead bound by BRG1 over the NDR (Figure 4F). This pattern is reminiscent of BRG1 localization at enhancers (Figure 1C), suggesting that BRG1 may be executing an essential, nucleosome eviction activity at cluster 1 promoters and enhancers. Characterization of histone modifications revealed that, in comparison with other genes, cluster 1 promoters feature lower levels of H3K4me3 and significantly higher levels of H3K4me1 (Figures 4G and 4H). This finding is consistent with our determination that cluster 1 genes tend to be lowly expressed because levels of histone H3K4 methylation are known to reflect levels of transcriptional activity.[28,47] Moreover, this finding emphasizes the similarities between non-recovering promoters and distal enhancers, which often exhibit enrichment of H3K4me1. Overall, our data highlight the importance of SWI/SNF activity at genes with low expression, weak nucleosome depletion, and enhancer-like chromatin features.

SWI/SNF perturbation results in acute loss and variable recovery of chromatin accessibility at promoters in cancer cells

To determine if the effects of SWI/SNF perturbation observed in mESCs were generalizable, we investigated chromatin accessibility in MV411 acute myeloid leukemia (AML) cells. SWI/SNF inhibitors are in clinical trial for the treatment of patients with advanced hematologic malignancies (ClinicalTrials.gov identifier NCT04891757), and AML cells are exquisitely sensitive to these compounds.[48,49] We thus treated MV411 cells with BRM014 and a recently characterized proteolysis targeting chimera (PROTAC) degrader of BRG1/BRM (AU-15330),[25] allowing us to compare the effects of catalytic inhibition with those of degrading SWI/SNF ATPase subunits. AU-15330 treatment resulted in rapid depletion of BRG1, with protein levels undetectable following 1 h treatment (Figure S5A).

We performed ATAC-seq on MV411 cells treated with BRM014 or AU-15330 for 1, 2, 4, and 8 h, time points at which we observed no defects in cell growth or viability (Figure S5B). *Drosophila* spike-in controls were included to enable accurate quantification of ATAC-seq signal. Enhancers in MV411 cells showed rapid and persistent loss of accessibility following treatment with BRM014 or AU-15330, with 95% of enhancers exhibiting reduced accessibility across 8 h of treatment (Figures S5C and S5D). By contrast, reduced accessibility at many promoters was rapidly followed by recovery and/or overcompensation (Figure S5E), as seen in mESCs.

Clustering of promoters based on accessibility following BRM014 treatment yielded four clusters with different recovery kinetics (Figures 5A, left and S5H). As in mESCs, this analysis identified a cluster of genes (cluster 1) that were persistently repressed through the duration of treatment, and clusters that recovered (cluster 3) or overcompensated (cluster 4) when SWI/SNF activity was lost. Notably, cluster 2 exhibited an intermediate phenotype, with promoters only partially restoring accessibility by 8 h of treatment. Similar dynamics were observed for all clusters following treatment of MV411 cells with AU-15330 (Figures 5A, right and S5E–S5I), indicating that the effects of BRG1/BRM ATPase inhibition closely resemble BRG1/BRM protein degradation. Analysis of gene expression following prolonged treatment with BRM014[48] demonstrated that genes in cluster 1 were persistently repressed, confirming the sensitivity of these genes to SWI/SNF inhibition, whereas expression of genes in other clusters was resistant to perturbation by BRM014 (Figure 5B).

Similar to that in mESCs, the BRM014-sensitive cluster 1 promoters identified in MV411 cells are characterized by low average accessibility (Figure 5C) and weak RNA expression (Figure S5J). Moreover, cluster 1 promoters exhibit lower levels of H3K4me3 and higher levels of H3K4me1 compared with genes in clusters 2–4 (Figures 5D and 5E). Thus, in agreement with our analysis of mESCs, SWI/SNF activity in MV411 cells is critically important at genes with weak nucleosome depletion, low expression, and enhancer-like chromatin features.

Figure 5. Epigenetic features of promoters can predict sensitivity to SWI/SNF inhibition or degradation

(A) Clustering based on relative differences in MV411 ATAC-seq reads defines four classes of responses to extended BRM014 treatment.

(B) Average relative RNA-seq[48] expression following 24 h BRM014 treatment, by promoter cluster. p values are from Mann-Whitney test.

(C–E) Aggregate plots of average reads at promoters by cluster for ATAC-seq (C), H3K4me3[50] (D), and H3K4me1[51] (E) signal. Data are graphed in 50 bp bins.

(F) Strategy to predict gene response to prolonged SWI/SNF disruption, using H3K4me1 ChIP-seq and ATAC-seq data.

(G) Mean expression changes at genes predicted to be sensitive (blue) or resistant (orange) to SWI/SNF perturbation. The average $\log_2$ fold-change in RNA-seq following SWI/SNF inhibition by 24 h BRM014 treatment in AML cell lines (left),[48] 12 h BRM014 treatment in NSCLC lines (middle), or 12 h degradation by AU-15330 in prostate cancer lines (right)[25] is shown. Error bars represent SEM. See STAR Methods for data sources and number of genes in each group.

(H) Mean expression changes at genes predicted to be sensitive to SWI/SNF perturbation in DIPG cell lines using ATAC-seq data. Shown are the average $\log_2$ fold-changes in RNA-seq following 24 h treatment with BRM014 (BT869)[52] or AU-15330 (DIPG007).[53] Error bars represent SEM. See STAR Methods for data sources and number of genes in each group.

(I) Venn diagram showing the overlap between genes downregulated following SWI/SNF inhibition or degradation as described for (G) and (H). Downregulated genes had a fold-change > 1.5 and p adj < 0.001 in RNA-seq.

(J) Top enriched Hallmark gene sets in genes downregulated by SWI/SNF inhibition or degradation in each cell line.

See also Figure S5.

Promoter characteristics can predict gene expression changes following SWI/SNF perturbation in cancer cells

We next asked whether features distinguishing SWI/SNF-dependent promoters in mESCs and MV411 cells, specifically elevated H3K4me1 ChIP-seq and low ATAC-seq signals, could be used to predict gene responses to SWI/SNF inhibition in other systems (Figure 5F). We first evaluated this in three types of cancer for which SWI/SNF is being pursued as a therapeutic target: AML, non-small cell lung cancer (NSCLC), and prostate cancer.[25,26,48,49,54,55] Using existing H3K4me1 ChIP-seq and ATAC-seq datasets from MOLM13 and MV411 AML cells, A549 and H1299 NSCLC cells, and LNCaP and VCaP prostate cancer cells (see STAR Methods), we identified promoters within both the top 15% of H3K4me1 signal and bottom 15% of ATAC-seq signal. These promoters were predicted to be sensitive to SWI/SNF inhibition and thus repressed by loss of SWI/SNF activity. Conversely, genes within the bottom 15% of H3K4me1 signal and top 15% of ATAC-seq signal were predicted to recover activity during SWI/SNF perturbation and thus to be resistant to long-term changes in gene expression.

Analysis of published RNA sequencing (RNA-seq) data from AML cells treated with BRM014 for 24 h[48] showed that the genes predicted as SWI/SNF sensitive were indeed downregulated following SWI/SNF inhibition, whereas genes predicted as resistant to SWI/SNF were relatively unchanged (Figure 5G, left). We next performed RNA-seq on NSCLC cells (A549 and H1299) treated with BRM014 for 12 h at 5 μM, a concentration at which cell growth was not affected (Figure S5K). In the NSCLC lines, genes predicted to be SWI/SNF sensitive were downregulated following SWI/SNF inhibition, whereas genes predicted to be resistant to BRM014 were unaffected (Figure 5G, middle). We then analyzed published RNA-seq data from prostate cancer cells (LNCaP and VCaP) treated for 12 h with the BRG1/BRM PROTAC degrader AU-15330.[25] Again, genes predicted to be sensitive to SWI/SNF activity based on their chromatin signatures showed significant downregulation upon loss of the SWI/SNF ATPases, whereas genes predicted to recover activity displayed unchanged activity (Figure 5G, right). Importantly, these data demonstrate that features associated with SWI/SNF dependence in mESCs can accurately predict gene responses to SWI/SNF inhibition or degradation in markedly different cellular contexts.

To extend these findings, we wondered if a single, readily available dataset such as ATAC-seq could be used to predict downregulated genes following SWI/SNF perturbation. Indeed, we found that ATAC-seq data alone could identify SWI/SNF-dependent genes in AML, NSCLC, and prostate cancer cells, albeit with somewhat reduced accuracy compared with using multiple datasets (Figure S5L). We leveraged published ATAC-seq data to predict gene responses to SWI/SNF perturbation in two additional cell lines from diffuse intrinsic pontine glioma (DIPG) samples (Figure 5H). Genes predicted to be sensitive to SWI/SNF perturbation again showed reduced expression levels following drug treatment, demonstrating that commonly available ATAC-seq datasets can be implemented to predict which genes will be most sensitive to SWI/SNF inhibition. This is a powerful possibility given the high-level interest in suppressing SWI/SNF activity in cancer. Notably, the 8 cell lines investigated here contain a diverse array of background mutations, including lines with wild-type SWI/SNF activity as well as those with SWI/SNF mutations.

That ATAC-seq signals, which vary across cell types, can predict gene sensitivity to SWI/SNF perturbation suggests that SWI/SNF dependence is determined by the chromatin state at gene promoters, rather than being hard-wired by DNA sequence. Indeed, genes downregulated following SWI/SNF perturbation differ substantially across cell lines (Figures 5I, S5M, and S5N), and gene ontology analysis revealed largely different pathways repressed upon long-term SWI/SNF perturbation (Figure 5J). Thus, in agreement with the variability in gene targets affected by SWI/SNF disruption in disease states, we find that genes repressed by sustained perturbation of SWI/SNF exhibit cell-type specificity. Consequently, SWI/SNF dependence of gene expression cannot be predicted by sequence content. Our work reveals, however, that SWI/SNF dependence can be inferred from the chromatin state at promoters.

EP400/TIP60 drives recovery of gene activity at most promoters

The above data suggest that cluster 1 promoters lack a compensatory remodeler that enables recovery of chromatin accessibility following inhibition of SWI/SNF. To probe this possibility, we investigated ChIP-seq localization for several chromatin remodelers in mESCs. We found many remodelers to be present at similar levels across promoter clusters regardless of recovery capacity (Figure 6A), including SNF2H, which was implicated in the recovery of accessibility at CTCF-bound enhancers (Figure S2). However, cluster 1 genes were strongly depleted of both EP400 and TIP60, key subunits of the EP400/TIP60 complex (Figures 6A, S6A, and S6B).[56] The EP400/TIP60 complex both deposits and acetylates histone H2A.Z (H2A.Zac), such that H2A.Zac is a specific marker of complex activity in mammalian cells.[57] Accordingly, we found that H2A.Zac was significantly depleted from cluster 1 promoters (Figures 6A, S6A, and S6B) compared with promoters in clusters 2–4. The finding that EP400/TIP60 is preferentially localized to promoters that recover from SWI/SNF inhibition was intriguing in light of previous reports that EP400/TIP60 binds H3K4me3 through its ING3 subunit.[58–60] Selective recruitment of EP400/TIP60 to promoters enriched in H3K4me3 would thus provide a mechanistic explanation for the localization of this complex at cluster 2–4 promoters. Indeed, heatmaps of active promoters rank ordered by increasing H3K4me3 levels show a clear relationship between the H3K4me3 modification and levels of EP400, TIP60, and H2A.Zac (Figure 6B).

Based on our evaluation of individual genes (Figure 6C), as well as earlier reports that BRG1 and EP400 may work together to regulate chromatin accessibility,[3] we tested whether EP400 enables efficient recovery of accessibility at cluster 2–4 genes following BRM014 treatment. We performed small interfering RNA (siRNA) knockdown of EP400 for 72 h, which substantially reduced both EP400 mRNA and protein levels (Figures S6C and S6D) without altering cell viability (Figures S6E and S6F) in comparison with a non-targeting control siRNA (siNT). ATAC-seq was then performed on siNT and siEP400-treated cells,

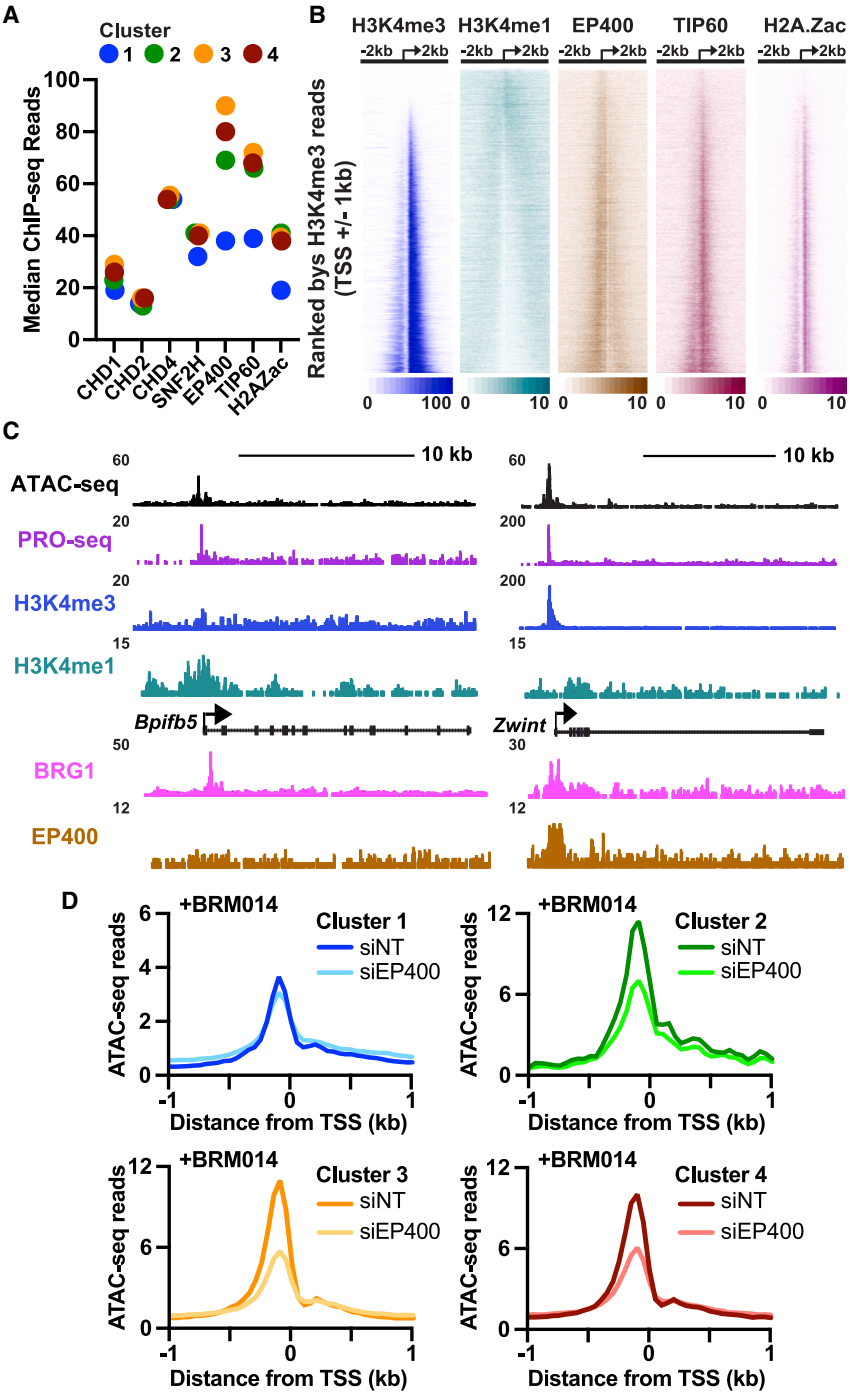

Figure 6. Recovery of accessibility at promoters following SWI/SNF inhibition is dependent on EP400/TIP60

(A) Median ChIP-seq signal (±500 bp relative to TSS) for CHD1,[3] CHD2,[3] CHD4,[3] SNF2H,[61] EP400,[3] TIP60,[62] and H2A.Zac[63] across each promoter cluster.

(B) Heatmaps of H3K4me3,[34] H3K4me1,[35] EP400,[3] TIP60,[62] and H2A.Zac.[63] Data are aligned to TSS and genes rank ordered by promoter H3K4me3 signal (±1 kb around TSS).

(C) Genome browser images of representative SWI/SNF sensitive gene *Bpifb5* (left) and resistant gene *Zwint* (right).

(D) Aggregate plots of ATAC-seq signal at promoters in each cluster, following 4 h BRM014 treatment under siNT conditions ($n \geq 2$ per condition), graphed in 50 bp bins.

See also Figure S6.

with and without BRM014 treatment, using spike-in for accurate quantitation. In the absence of SWI/SNF inhibitors, knockdown of EP400 was not associated with appreciable changes to promoter chromatin accessibility at genes in any cluster (Figure S6G). EP400 was previously suggested to selectively regulate bivalent genes in mESCS.[3] However, analysis of EP400 ChIP-seq revealed that EP400 binding is at background levels at bivalent genes (Figure S6H). Further, EP400 knockdown had minimal effects on chromatin accessibility at bivalent genes (Figure S6I). We conclude that other remodelers dominate the profile of chromatin accessibility during normal mESC growth, including at bivalent loci.

Supporting an increased role for EP400 following loss of SWI/SNF activity, ATAC-seq data from cells depleted of EP400 and treated with BRM014 for 4 h showed clear effects of EP400 siRNA (Figure 6D). EP400 depletion strongly reduced chromatin accessibility at cluster 2–4 promoters (Figures 6D, S6J, and S6K), whereas cluster 1 promoters showed only a subtle response to EP400 depletion. These findings were confirmed by ATAC-qPCR analysis at selected genes (Figure S6L). To determine if compensation for SWI/SNF loss involved altered recruitment of EP400, we performed ChIP-seq for EP400 following 2 and 4 h treatment with BRM014 (or DMSO). We found that EP400 binding increased at cluster 2–4 promoters within 2 h of BRM014 treatment and remained elevated at 4 h of treatment (Figures S6M and S6N). This result suggests that acute inhibition of SWI/SNF causes cells to rapidly mobilize alternative remodelers, such as EP400, to help reestablish chromatin accessibility. These analyses further suggest that EP400-mediated recovery takes time, with a delay observed between maximal EP400 promoter occupancy and the reestablishment of fully open promoter chromatin. Together, our data provide strong evidence that the activity of EP400/TIP60 enables the recovery of accessibility at cluster 2–4 promoters in the absence of SWI/SNF activity. Mechanistically, this model implies that the role played by SWI/SNF at many promoters can be functionally compensated by EP400/TIP60.

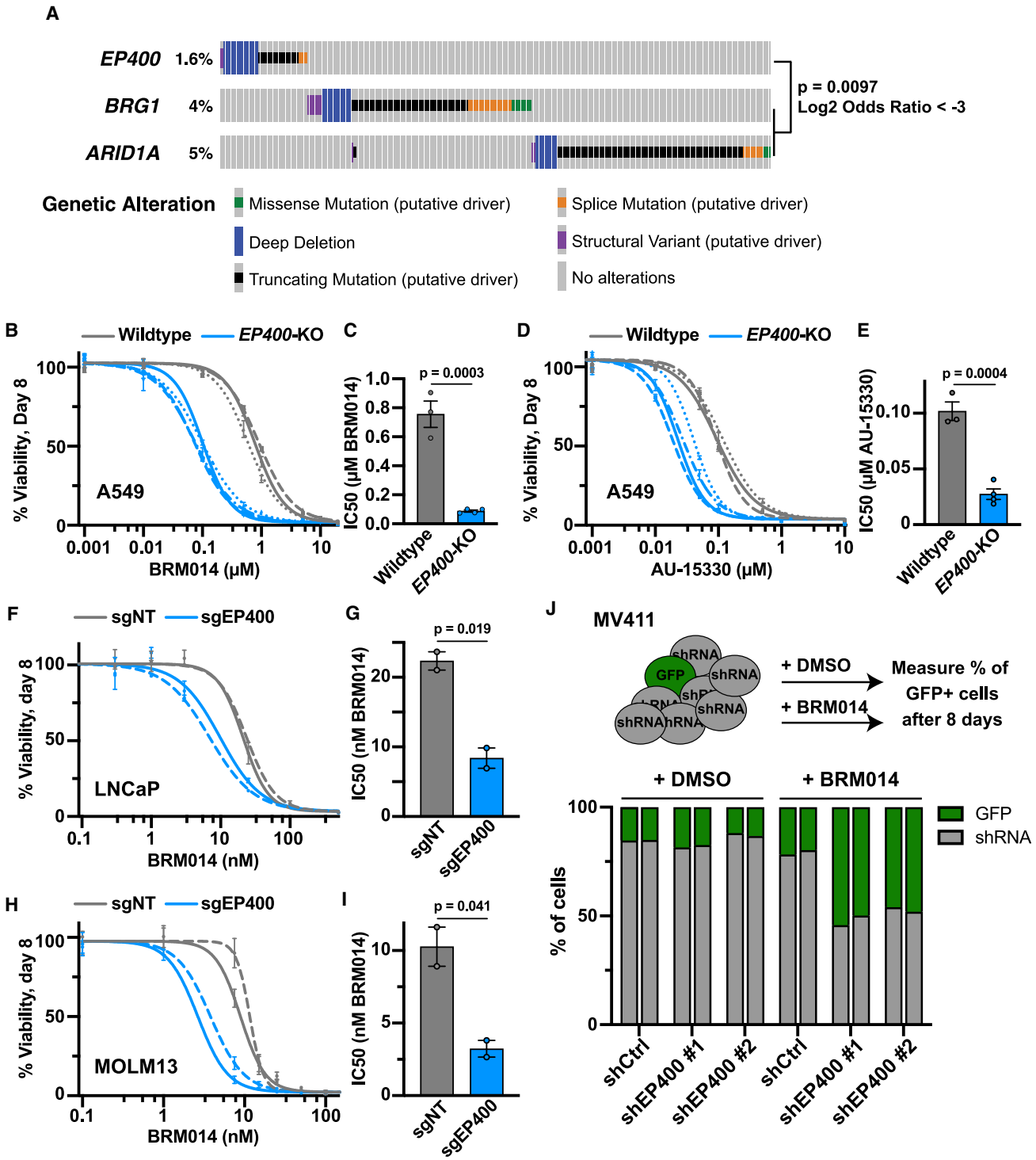

Figure 7. SWI/SNF activity is essential in non-small cell lung cancer cells lacking EP400

(A) NSCLC mutation data accessed through the cBio Portal (n = 3,311). Mutations of unknown significance were removed, and only samples profiling all 3 genes were analyzed. Fisher's exact test performed for mutually exclusive relationship between *EP400* and *BRG1/ARID1A* mutations. The percentage of samples with the indicated mutations are indicated.

(B) Drug dose response curves of wild-type and *EP400*-KO NSCLC (A549) cells following 8 days of treatment with BRM014. Each curve represents an independent experiment of the indicated cell line (n = 3 for wild type and n = 4 for *EP400*-KO). Error bars represent the SEM of three technical replicates.

(legend continued on next page)

EP400 loss creates a dependency on SWI/SNF

Our findings suggest that EP400/TIP60 may be critical for the establishment of appropriate chromatin architecture in cells lacking functional SWI/SNF. In support of this idea, synthetic lethality between subunits of the EP400/TIP60 and SWI/SNF complexes was previously reported in a genetic screen.[64] Further, analysis of all cell lines represented in DepMap[65–68] with damaging mutations in genes encoding SWI/SNF subunits BRG1, BRM, or ARID1A demonstrated that these lines were more sensitive to CRIPSR-mediated knockdown of EP400 than lines lacking such mutations (Figure S7A). To probe synthetic lethality in patient samples, we accessed The Cancer Genome Atlas (TCGA) data from NSCLC, for which mutations in SWI/SNF subunits *BRG1* and *ARID1A* are common. Indeed, mutations in *EP400* are mutually exclusive with mutations in *BRG1* and *ARID1A* (Figure 7A).

To directly test whether loss of *EP400* is synthetically lethal with disruption of SWI/SNF in isogenic cell lines, we used CRISPR-Cas9 editing to introduce homozygous loss-of-function mutations into *EP400* in A549 NSCLC cells (Figures S7B and S7C). The *EP400*-KO line recapitulated a previously described increase in expression of epithelial-mesenchymal transition markers (Figure S7D), consistent with the enrichment of *EP400* mutations in metastatic tumors.[69] We then tested whether EP400 loss affects cell growth in the presence of BRM014 (Figures 7B and 7C). We found that *EP400*-KO A549 cells displayed dramatically increased sensitivity to inhibition of SWI/SNF, with IC50 values dropping from 756 to 87 nM. To perturb SWI/SNF function using an orthogonal approach, we tested whether the *EP400*-KO cells displayed increased sensitivity to BRG1/BRM degradation by AU-15330. Loss of EP400 sensitized cells to treatment with AU-15330, with IC50 values decreasing from 102 to 27 nM (Figures 7D and 7E). Similar results were obtained with another NSCLC line, H1299 (Figures S7E–S7I).

To determine if the genetic interaction between EP400 and SWI/SNF perturbation is generalizable to other cancer contexts, we used lentiviruses to target EP400 by CRISPR-Cas9 in prostate cancer and AML cell lines. KO of EP400 consistently increased sensitivity to SWI/SNF inhibition (Figures 7F–7I and S7I). As an orthogonal approach, we used short hairpin RNA (shRNA) to knock down EP400 in MV411 AML cells. Under competitive growth conditions, we observed a strong drop-out of EP400-depleted cells following BRM014 treatment (Figures 7J and S7J), confirming the interaction between EP400 and SWI/SNF perturbation. Importantly, this panel of cell lines encompasses a wide range of cancer lineages and background mutations (Figure S7K). We conclude that EP400 loss broadly sensitizes cells to perturbation of SWI/SNF activity, supporting a model wherein EP400/TIP60 becomes essential for recovery of chromatin architecture when SWI/SNF function is perturbed.

DISCUSSION

We find that compensation by EP400/TIP60 masks a global role for SWI/SNF in promoting chromatin accessibility. We propose a model wherein SWI/SNF functions ubiquitously and continuously at nearly all promoters and enhancers to enable binding of TFs and the general transcription machinery. In mESCs, which lack mutations in SWI/SNF or other remodelers, this activity of SWI/SNF is sufficient to independently maintain open chromatin. Therefore, loss of EP400/TIP60 elicits little change in accessibility or gene activity under these conditions (Figure S6G[3,70,71]). However, perturbation of SWI/SNF unveils a role for EP400/TIP60 in reestablishing accessibility at most promoters. This model provides a mechanistic explanation for the minor effects on gene activity often observed upon disruption of SWI/SNF or EP400/TIP60 alone (Figure 3A[3,20,21,25]) and highlights the power of fast-acting inhibitors in assigning direct functions and untangling compensatory mechanisms. Critically, our work demonstrates that promoters and enhancers that are persistently repressed following perturbation of SWI/SNF do not represent the only direct targets of this remodeler; instead, they represent the subset of sites at which compensation for SWI/SNF loss does not occur.

We find that the recovery of promoter accessibility and gene activity following SWI/SNF inhibition occurs largely independently of nearby enhancer activity, consistent with recent work in prostate cancer cells, demonstrating that SWI/SNF degradation uncouples enhancer-promoter communication.[25] Collectively, these results suggest that a common consequence of prolonged SWI/SNF perturbation would be promoter-autonomous gene activity.

(C) Quantification of IC50 values from the dose response curves plotted in (B). Error bars represent SEM. Individual values plotted as circles. p values calculated by t test.
(D) Drug dose response curves of wild-type and *EP400*-KO A549 cells following 8 days of treatment with AU-15330. Each curve represents an independent experiment of the indicated cell line (n = 3 for wild type and n = 4 for *EP400*-KO). Error bars represent the SEM of three technical replicates.
(E) Quantification of IC50 values from the dose response curves plotted in (D). Error bars represent SEM. Individual values plotted as circles. p values calculated by t test.
(F) Drug dose response curves of non-targeting guide (sgNT) and sg*EP400* expressing prostate cancer (LNCaP) cells following 8 days of treatment with BRM014. Each curve represents an independent experiment of the indicated cell line (n = 2). Error bars represent the SEM of three technical replicates.
(G) Quantification of IC50 values from the dose response curves plotted in (F). Error bars represent SEM. Individual values plotted as circles. p values calculated by t test.
(H) Drug dose response curves of sgNT and sg*EP400* expressing AML (MOLM13) cells following 8 days of treatment with BRM014. Each curve represents an independent experiment of the indicated cell line (n = 2). Error bars represent the SEM of three technical replicates.
(I) Quantification of IC50 values from the dose response curves plotted in (H). Error bars represent SEM. Individual values plotted as circles. p values calculated by t test.
(J) Competitive growth of GFP or shRNA expressing AML (MV411) cells. GFP cells were initially mixed at 15% of the population. Following 8 days of treatment with BRM014 or DMSO the % of GFP cells was measured by flow cytometry. Each bar represents independently grown replicates (n = 2).
See also Figure S7.

Despite the ability of both SWI/SNF and EP400/TIP60 to increase promoter chromatin accessibility, these complexes possess distinct biochemical activities. SWI/SNF generates DNA accessibility through nucleosome sliding or eviction, whereas EP400/TIP60 exchanges H2A for H2A.Z and acetylates histone tails. H2A.Z-containing nucleosomes were reported to be hyper-labile,[72,73] reducing the nucleosomal barrier to transcription by RNAPII, and acetylation of H2A.Z is tightly linked to transcription activation.[74–77] Understanding how the disparate activities of SWI/SNF and EP400/TIP60 converge to enable promoter opening and transcription activation merits future investigation.

The ability for cells to compensate for SWI/SNF loss is relevant in disease, where SWI/SNF is frequently mutated and is being explored as a therapeutic target. Our work reveals that the promoters most sensitive to loss of SWI/SNF have distinct features. Intriguingly, the promoters that fail to recover activity (cluster 1) are those with weak accessibility and an enrichment of H3K4me1, features shared by enhancers. The prognostic value of these features is demonstrated by our ability to predict whether a gene will be sensitive to SWI/SNF perturbation in diverse cancer cell lines, using ATAC-seq and H3K4me1 ChIP-seq data at promoters (Figures 5F–5H and S5L).

The synthetic lethality observed between EP400 and SWI/SNF uncovers a dependency that could be targeted in cancer therapies because the redundancy between SWI/SNF and EP400/TIP60 buffers the transcriptional response against loss of either remodeler. Accordingly, our experiments demonstrate that EP400 depletion in cancer cells create a specific dependency on SWI/SNF, which may widen the therapeutic window for SWI/SNF-targeting compounds. In pan-cancer analysis, EP400 mutations are enriched in metastatic tumors[69]; thus, EP400 mutations may represent attractive indicators for targeting SWI/SNF more generally. Further, considering the prevalence of SWI/SNF mutations, we propose that inhibitors of the EP400/TIP60 complex present an attractive and unexplored therapeutic approach.

Limitations of the study

First, we used BRM014 to target SWI/SNF, which might have off-target effects. To mitigate this concern, we confirmed key results with the BRG1/BRM degrader compound AU-15330, which acts through a disparate mechanism to perturb SWI/SNF function. Second, the depletion of EP400 was carried out using slow-acting strategies (siRNA, shRNA, or CRISPR-Cas9), which may have occluded the acute effects of EP400 loss. Future work will use fast-acting methods to rapidly deplete EP400 for mechanistic examination. Third, cancer cell lines contain an array of background mutations, limiting the generalities of findings from a single cell line. To alleviate this issue, we performed experiments in multiple cancer cell lines and mouse ESCs.

STAR★METHODS

Detailed methods are provided in the online version of this paper and include the following:

- KEY RESOURCES TABLE
- RESOURCE AVAILABILITY
  - Lead contact
  - Materials availability
  - Data and code availability
- EXPERIMENTAL MODEL AND STUDY PARTICIPANT DETAILS
  - Cell Culture and Inhibitor Treatments
- METHOD DETAILS
  - Western Blots
  - mESC ATAC-seq Library Preparation
  - ChIP-seq Library Preparation
  - PRO-seq Library Preparation
  - siRNA Transfection
  - MV411 ATAC-seq Library Preparation
  - RNA-seq Library Preparation
  - Generation of *EP400*-KO A549 cells
  - Generation of EP400 shRNA and Cas9 guide pools
  - Cell Proliferation Assays
- QUANTIFICATION AND STATISTICAL ANALYSIS
  - mESC ATAC-seq data processing and mapping
  - PRO-seq data processing and mapping
  - Genome annotation
  - Peak calling and filtering
  - BRG1 ChIP-seq data processing and mapping
  - EP400 ChIP-seq data processing and mapping
  - Genome browser images
  - Metagenes and heatmaps
  - Clustering
  - Relative Accessibility Analysis
  - Relative PRO-seq Analysis
  - Differential Gene Expression Analysis
  - Gene Ontology Analysis
  - Analysis of Publicly Available mESC Data
  - Cancer Cell Line RNA-seq and ATAC-seq Analysis
  - DepMap analysis of SWI/SNF subunit mutations
  - Box plots and statistical analysis

SUPPLEMENTAL INFORMATION

Supplemental information can be found online at https://doi.org/10.1016/j.cell.2023.10.006.

ACKNOWLEDGMENTS

We thank Fred Winston, Bob Kingston, Konrad Hochedlinger, Marie Bao, Jacques Côté, and Blaine Bartholomew for helpful discussions. We also thank Julia Rogers for providing spike-in S2 cells for the MV411 ATAC-seq experiments, Zainab Jagani and the Novartis Institute for Biomedical Research for providing BRM014 under MTA, and the Harvard Medical School Biopolymers Facility, Bauer Core Facility at Harvard University and Apoorva Baluapuri for sequencing. This work was supported by the Van Maanen Fellowship from Harvard Medical School and a National Science Foundation Graduate Research Fellowship under grant no. DGE1745303 to E.F.A., a CIHR Banting Postdoctoral Fellowship to B.J.E.M. and the Ludwig Center at Harvard (to K.A. and B.J.E.M.).

AUTHOR CONTRIBUTIONS

Conceptualization, K.A., E.F.A., and B.J.E.M.; methodology, K.A., E.F.A., B.J.E.M., C.G., C.A.M., and P.R.E.-C.; investigation, E.F.A., B.J.E.M., C.G., C.A.M., and P.R.E.-C.; data analysis, E.F.A., B.J.E.M., C.A.M., and K.A.;

visualization: E.F.A., K.A., B.J.E.M., and C.A.M.; project administration, K.A.; funding acquisition, K.A.; supervision, K.A.; writing, E.F.A., B.J.E.M., and K.A.

DECLARATION OF INTERESTS

K.A. is a consultant to Syros Pharmaceuticals and Odyssey Therapeutics, is on the SAB of CAMP4 Therapeutics, and received research funding from Novartis not related to this work.

INCLUSION AND DIVERSITY

We support inclusive, diverse, and equitable conduct of research.

Received: February 12, 2023
Revised: August 11, 2023
Accepted: October 3, 2023
Published: November 2, 2023

REFERENCES

1. Clapier, C.R., Iwasa, J., Cairns, B.R., and Peterson, C.L. (2017). Mechanisms of action and regulation of ATP-dependent chromatin-remodelling complexes. Nat. Rev. Mol. Cell Biol. *18*, 407–422. https://doi.org/10.1038/nrm.2017.26.
2. Narlikar, G.J., Sundaramoorthy, R., and Owen-Hughes, T. (2013). Mechanisms and functions of ATP-dependent chromatin-remodeling enzymes. Cell *154*, 490–503. https://doi.org/10.1016/j.cell.2013.07.011.
3. de Dieuleveult, M., Yen, K., Hmitou, I., Depaux, A., Boussouar, F., Bou Dargham, D.B., Jounier, S., Humbertclaude, H., Ribierre, F., Baulard, C., et al. (2016). Genome-wide nucleosome specificity and function of chromatin remodellers in ES cells. Nature *530*, 113–116. https://doi.org/10.1038/nature16505.
4. Barisic, D., Stadler, M.B., Iurlaro, M., and Schübeler, D. (2019). Mammalian ISWI and SWI/SNF selectively mediate binding of distinct transcription factors. Nature *569*, 136–140. https://doi.org/10.1038/s41586-019-1115-5.
5. Brown, S.A., Imbalzano, A.N., and Kingston, R.E. (1996). Activator-dependent regulation of transcriptional pausing on nucleosomal templates. Genes Dev. *10*, 1479–1490. https://doi.org/10.1101/gad.10.12.1479.
6. Nakayama, R.T., Pulice, J.L., Valencia, A.M., McBride, M.J., McKenzie, Z.M., Gillespie, M.A., Ku, W.L., Teng, M., Cui, K., Williams, R.T., et al. (2017). SMARCB1 is required for widespread BAF complex–mediated activation of enhancers and bivalent promoters. Nat. Genet. *49*, 1613–1623. https://doi.org/10.1038/ng.3958.
7. Alver, B.H., Kim, K.H., Lu, P., Wang, X., Manchester, H.E., Wang, W., Haswell, J.R., Park, P.J., and Roberts, C.W.M. (2017). The SWI/SNF chromatin remodelling complex is required for maintenance of lineage specific enhancers. Nat. Commun. *8*, 14648. https://doi.org/10.1038/ncomms14648.
8. King, H.W., and Klose, R.J. (2017). The pioneer factor OCT4 requires the chromatin remodeller BRG1 to support gene regulatory element function in mouse embryonic stem cells. eLife *6*, e22631. https://doi.org/10.7554/eLife.22631.
9. Kadoch, C., Hargreaves, D.C., Hodges, C., Elias, L., Ho, L., Ranish, J., and Crabtree, G.R. (2013). Proteomic and bioinformatic analysis of mammalian SWI/SNF complexes identifies extensive roles in human malignancy. Nat. Genet. *45*, 592–601. https://doi.org/10.1038/ng.2628.
10. Centore, R.C., Sandoval, G.J., Soares, L.M.M., Kadoch, C., and Chan, H.M. (2020). Mammalian SWI/SNF chromatin remodeling complexes: emerging mechanisms and therapeutic strategies. Trends Genet. *36*, 936–950. https://doi.org/10.1016/j.tig.2020.07.011.
11. Hainer, S.J., Gu, W., Carone, B.R., Landry, B.D., Rando, O.J., Mello, C.C., and Fazzio, T.G. (2015). Suppression of pervasive noncoding transcription in embryonic stem cells by esBAF. Genes Dev. *29*, 362–378. https://doi.org/10.1101/gad.253534.114.
12. Tolstorukov, M.Y., Sansam, C.G., Lu, P., Koellhoffer, E.C., Helming, K.C., Alver, B.H., Tillman, E.J., Evans, J.A., Wilson, B.G., Park, P.J., et al. (2013). Swi/Snf chromatin remodeling/tumor suppressor complex establishes nucleosome occupancy at target promoters. Proc. Natl. Acad. Sci. USA *110*, 10165–10170. https://doi.org/10.1073/pnas.1302209110.
13. Hodges, H.C., Stanton, B.Z., Cermakova, K., Chang, C.Y., Miller, E.L., Kirkland, J.G., Ku, W.L., Veverka, V., Zhao, K., and Crabtree, G.R. (2018). Dominant-negative SMARCA4 mutants alter the accessibility landscape of tissue-unrestricted enhancers. Nat. Struct. Mol. Biol. *25*, 61–72. https://doi.org/10.1038/s41594-017-0007-3.
14. Flynn, R.A., Do, B.T., Rubin, A.J., Calo, E., Lee, B., Kuchelmeister, H., Rale, M., Chu, C., Kool, E.T., Wysocka, J., et al. (2016). 7SK-BAF axis controls pervasive transcription at enhancers. Nat. Struct. Mol. Biol. *23*, 231–238. https://doi.org/10.1038/nsmb.3176.
15. Weber, C.M., Hafner, A., Kirkland, J.G., Braun, S.M.G., Stanton, B.Z., Boettiger, A.N., and Crabtree, G.R. (2021). mSWI/SNF promotes Polycomb repression both directly and through genome-wide redistribution. Nat. Struct. Mol. Biol. *28*, 501–511. https://doi.org/10.1038/s41594-021-00604-7.
16. Zhang, X., Li, B., Li, W., Ma, L., Zheng, D., Li, L., Yang, W., Chu, M., Chen, W., Mailman, R.B., et al. (2014). Transcriptional repression by the BRG1-SWI/SNF complex affects the pluripotency of human embryonic stem cells. Stem Cell Rep. *3*, 460–474. https://doi.org/10.1016/j.stemcr.2014.07.004.
17. Bossen, C., Murre, C.S., Chang, A.N., Mansson, R., Rodewald, H.R., and Murre, C. (2015). The chromatin remodeler Brg1 activates enhancer repertoires to establish B cell identity and modulate cell growth. Nat. Immunol. *16*, 775–784. https://doi.org/10.1038/ni.3170.
18. Park, Y.K., Lee, J.E., Yan, Z., McKernan, K., O'Haren, T., Wang, W., Peng, W., and Ge, K. (2021). Interplay of BAF and MLL4 promotes cell type-specific enhancer activation. Nat. Commun. *12*, 1630. https://doi.org/10.1038/s41467-021-21893-y.
19. Papillon, J.P.N., Nakajima, K., Adair, C.D., Hempel, J., Jouk, A.O., Karki, R.G., Mathieu, S., Möbitz, H., Ntaganda, R., Smith, T., et al. (2018). Discovery of orally active inhibitors of Brahma Homolog (BRM)/SMARCA2 ATPase activity for the treatment of Brahma Related Gene 1 (BRG1)/SMARCA4-mutant cancers. J. Med. Chem. *61*, 10155–10172. https://doi.org/10.1021/acs.jmedchem.8b01318.
20. Schick, S., Grosche, S., Kohl, K.E., Drpic, D., Jaeger, M.G., Marella, N.C., Imrichova, H., Lin, J.-M.G., Hofstätter, G., Schuster, M., et al. (2021). Acute BAF perturbation causes immediate changes in chromatin accessibility. Nat. Genet. *53*, 269–278. https://doi.org/10.1038/s41588-021-00777-3.
21. Iurlaro, M., Stadler, M.B., Masoni, F., Jagani, Z., Galli, G.G., and Schübeler, D. (2021). Mammalian SWI/SNF continuously restores local accessibility to chromatin. Nat. Genet. *53*, 279–287. https://doi.org/10.1038/s41588-020-00768-w.
22. Biggar, S.R., and Crabtree, G.R. (1999). Continuous and widespread roles for the Swi–Snf complex in transcription. EMBO J. *18*, 2254–2264. https://doi.org/10.1093/emboj/18.8.2254.
23. Schwabish, M.A., and Struhl, K. (2007). The Swi/Snf complex is important for histone eviction during transcriptional activation and RNA polymerase II elongation in vivo. Mol. Cell. Biol. *27*, 6987–6995. https://doi.org/10.1128/MCB.00717-07.
24. Sudarsanam, P., Cao, Y., Wu, L., Laurent, B.C., and Winston, F. (1999). The nucleosome remodeling complex, Snf/Swi, is required for the maintenance of transcription in vivo and is partially redundant with the histone acetyltransferase, Gcn5. EMBO J. *18*, 3101–3106. https://doi.org/10.1093/emboj/18.11.3101.
25. Xiao, L., Parolia, A., Qiao, Y., Bawa, P., Eyunni, S., Mannan, R., Carson, S.E., Chang, Y., Wang, X., Zhang, Y., et al. (2022). Targeting SWI/SNF

ATPases in enhancer-addicted prostate cancer. Nature *601*, 434–439. https://doi.org/10.1038/s41586-021-04246-z.

26. Jagani, Z., Chenail, G., Xiang, K., Bushold, G., Bhang, H.-E.C., Li, A., Elliott, G., Zhu, J., Vattay, A., Gilbert, T., et al. (2019). In-depth characterization and validation in BRG1-mutant lung cancers define novel catalytic inhibitors of SWI/SNF chromatin remodeling. Preprint at bioRxiv. https://doi.org/10.1101/812628.
27. Mahat, D.B., Kwak, H., Booth, G.T., Jonkers, I.H., Danko, C.G., Patel, R.K., Waters, C.T., Munson, K., Core, L.J., and Lis, J.T. (2016). Base-pair-resolution genome-wide mapping of active RNA polymerases using precision nuclear run-on (PRO-seq). Nat. Protoc. *11*, 1455–1476. https://doi.org/10.1038/nprot.2016.086.
28. Henriques, T., Scruggs, B.S., Inouye, M.O., Muse, G.W., Williams, L.H., Burkholder, A.B., Lavender, C.A., Fargo, D.C., and Adelman, K. (2018). Widespread transcriptional pausing and elongation control at enhancers. Genes Dev. *32*, 26–41. https://doi.org/10.1101/gad.309351.117.
29. Tippens, N.D., Liang, J., Leung, A.K., Wierbowski, S.D., Ozer, A., Booth, J.G., Lis, J.T., and Yu, H. (2020). Transcription imparts architecture, function and logic to enhancer units. Nat. Genet. *52*, 1067–1075. https://doi.org/10.1038/s41588-020-0686-2.
30. Wang, Z., Chivu, A.G., Choate, L.A., Rice, E.J., Miller, D.C., Chu, T., Chou, S.P., Kingsley, N.B., Petersen, J.L., Finno, C.J., et al. (2022). Prediction of histone post-translational modification patterns based on nascent transcription data. Nat. Genet. *54*, 295–305. https://doi.org/10.1038/s41588-022-01026-x.
31. Danko, C.G., Hyland, S.L., Core, L.J., Martins, A.L., Waters, C.T., Lee, H.W., Cheung, V.G., Lis Kraus, W.L., J.T., and Siepel, A. (2015). Identification of active transcriptional regulatory elements with GRO-seq. Nat. Methods *12*, 433–438. https://doi.org/10.1038/nmeth.3329.
32. Ho, L., Ronan, J.L., Wu, J., Staahl, B.T., Chen, L., Kuo, A., Lessard, J., Nesvizhskii, A.I., Ranish, J., and Crabtree, G.R. (2009). An embryonic stem cell chromatin remodeling complex, esBAF, is essential for embryonic stem cell self-renewal and pluripotency. Proc. Natl. Acad. Sci. USA *106*, 5181–5186. https://doi.org/10.1073/pnas.0812889106.
33. Bartholomew, B. (2014). Regulating the chromatin landscape: structural and mechanistic perspectives. Annu. Rev. Biochem. *83*, 671–696. https://doi.org/10.1146/annurev-biochem-051810-093157.
34. Vlaming, H., Mimoso, C.A., Field, A.R., Martin, B.J.E., and Adelman, K. (2022). Screening thousands of transcribed coding and non-coding regions reveals sequence determinants of RNA polymerase II elongation potential. Nat. Struct. Mol. Biol. *29*, 613–620. https://doi.org/10.1038/s41594-022-00785-9.
35. Buecker, C., Srinivasan, R., Wu, Z., Calo, E., Acampora, D., Faial, T., Simeone, A., Tan, M., Swigut, T., and Wysocka, J. (2014). Reorganization of enhancer patterns in transition from naive to primed pluripotency. Cell Stem Cell *14*, 838–853. https://doi.org/10.1016/j.stem.2014.04.003.
36. Tilly, B.C., Chalkley, G.E., van der Knaap, J.A., Moshkin, Y.M., Kan, T.W., Dekkers, D.H., Demmers, J.A., and Verrijzer, C.P. (2021). In vivo analysis reveals that ATP-hydrolysis couples remodeling to SWI/SNF release from chromatin. eLife *10*, e69424. https://doi.org/10.7554/eLife.69424.
37. Wiechens, N., Singh, V., Gkikopoulos, T., Schofield, P., Rocha, S., and Owen-Hughes, T. (2016). The chromatin remodelling enzymes SNF2H and SNF2L position nucleosomes adjacent to CTCF and other transcription factors. PLoS Genet. *12*, e1005940. https://doi.org/10.1371/journal.pgen.1005940.
38. Bomber, M.L., Wang, J., Liu, Q., Barnett, K.R., Layden, H.M., Hodges, E., Stengel, K.R., and Hiebert, S.W. (2023). Human SMARCA5 is continuously required to maintain nucleosome spacing. Mol. Cell *83*, 507–522.e6. https://doi.org/10.1016/j.molcel.2022.12.018.
39. Blümli, S., Wiechens, N., Wu, M.Y., Singh, V., Gierlinski, M., Schweikert, G., Gilbert, N., Naughton, C., Sundaramoorthy, R., Varghese, J., et al. (2021). Acute depletion of the ARID1A subunit of SWI/SNF complexes reveals distinct pathways for activation and repression of transcription. Cell Rep. *37*, 109943. https://doi.org/10.1016/j.celrep.2021.109943.
40. Engreitz, J.M., Haines, J.E., Perez, E.M., Munson, G., Chen, J., Kane, M., McDonel, P.E., Guttman, M., and Lander, E.S. (2016). Local regulation of gene expression by lncRNA promoters, transcription and splicing. Nature *539*, 452–455. https://doi.org/10.1038/nature20149.
41. Hota, S.K., Johnson, J.R., Verschueren, E., Thomas, R., Blotnick, A.M., Zhu, Y., Sun, X., Pennacchio, L.A., Krogan, N.J., and Bruneau, B.G. (2019). Dynamic BAF chromatin remodeling complex subunit inclusion promotes temporally distinct gene expression programs in cardiogenesis. Development *146*, dev174086. https://doi.org/10.1242/dev.174086.
42. Matsumoto, S., Banine, F., Struve, J., Xing, R., Adams, C., Liu, Y., Metzger, D., Chambon, P., Rao, M.S., and Sherman, L.S. (2006). Brg1 is required for murine neural stem cell maintenance and gliogenesis. Dev. Biol. *289*, 372–383. https://doi.org/10.1016/j.ydbio.2005.10.044.
43. Lessard, J., Wu, J.I., Ranish, J.A., Wan, M., Winslow, M.M., Staahl, B.T., Wu, H., Aebersold, R., Graef, I.A., and Crabtree, G.R. (2007). An essential switch in subunit composition of a chromatin remodeling complex during neural development. Neuron *55*, 201–215. https://doi.org/10.1016/j.neuron.2007.06.019.
44. Karolchik, D., Hinrichs, A.S., Furey, T.S., Roskin, K.M., Sugnet, C.W., Haussler, D., and Kent, W.J. (2004). The UCSC Table Browser data retrieval tool. Nucleic Acids Res. *32*, D493–D496. https://doi.org/10.1093/nar/gkh103.
45. Ramirez-Carrozzi, V.R., Braas, D., Bhatt, D.M., Cheng, C.S., Hong, C., Doty, K.R., Black, J.C., Hoffmann, A., Carey, M., and Smale, S.T. (2009). A unifying model for the selective regulation of inducible transcription by CpG islands and nucleosome remodeling. Cell *138*, 114–128. https://doi.org/10.1016/j.cell.2009.04.020.
46. Fenouil, R., Cauchy, P., Koch, F., Descostes, N., Cabeza, J.Z., Innocenti, C., Ferrier, P., Spicuglia, S., Gut, M., Gut, I., et al. (2012). CpG islands and GC content dictate nucleosome depletion in a transcription-independent manner at mammalian promoters. Genome Res. *22*, 2399–2408. https://doi.org/10.1101/gr.138776.112.
47. Core, L.J., Martins, A.L., Danko, C.G., Waters, C.T., Siepel, A., and Lis, J.T. (2014). Analysis of nascent RNA identifies a unified architecture of initiation regions at mammalian promoters and enhancers. Nat. Genet. *46*, 1311–1320. https://doi.org/10.1038/ng.3142.
48. Chambers, C., Cermakova, K., Chan, Y.S., Kurtz, K., Wohlan, K., Lewis, A.H., Wang, C., Pham, A., Dejmek, M., Sala, M., et al. (2023). SWI/SNF blockade disrupts PU.1-directed enhancer programs in normal hematopoietic cells and acute myeloid leukemia. Cancer Res. *83*, 983–996. https://doi.org/10.1158/0008-5472.can-22-2129.
49. Rago, F., Rodrigues, L.U., Bonney, M., Sprouffske, K., Kurth, E., Elliott, G., Ambrose, J., Aspesi, P., Oborski, J., Chen, J.T., et al. (2022). Exquisite sensitivity to dual BRG1/BRM ATPase inhibitors reveals broad SWI/SNF dependencies in acute myeloid leukemia. Mol. Cancer Res. *20*, 361–372. https://doi.org/10.1158/1541-7786.MCR-21-0390.
50. Erb, M.A., Scott, T.G., Li, B.E., Xie, H., Paulk, J., Seo, H.S., Souza, A., Roberts, J.M., Dastjerdi, S., Buckley, D.L., et al. (2017). Transcription control by the ENL YEATS domain in acute leukaemia. Nature *543*, 270–274. https://doi.org/10.1038/nature21688.
51. Ellegast, J.M., Alexe, G., Hamze, A., Lin, S., Uckelmann, H.J., Rauch, P.J., Pimkin, M., Ross, L.S., Dharia, N.V., Robichaud, A.L., et al. (2022). Unleashing cell-intrinsic inflammation as a strategy to kill AML blasts. Cancer Discov. *12*, 1760–1781. https://doi.org/10.1158/2159-8290.CD-21-0956.
52. Panditharatna, E., Marques, J.G., Wang, T., Trissal, M.C., Liu, I., Jiang, L., Beck, A., Groves, A., Dharia, N.V., Li, D., et al. (2022). BAF complex maintains glioma stem cells in pediatric H3K27M glioma. Cancer Discov. *12*, 2880–2905. https://doi.org/10.1158/2159-8290.CD-21-1491.
53. Mota, M., Sweha, S.R., Pun, M., Natarajan, S.K., Ding, Y., Chung, C., Hawes, D., Yang, F., Judkins, A.R., Samajdar, S., et al. (2023). Targeting SWI/SNF ATPases in H3.3K27M diffuse intrinsic pontine gliomas. Proc. Natl. Acad. Sci. USA *120*, e2221175120. https://doi.org/10.1073/pnas.2221175120.

54. Oike, T., Ogiwara, H., Tominaga, Y., Ito, K., Ando, O., Tsuta, K., Mizukami, T., Shimada, Y., Isomura, H., Komachi, M., et al. (2013). A synthetic lethality–based strategy to treat cancers harboring a genetic deficiency in the chromatin remodeling factor BRG1. Cancer Res. *73*, 5508–5518. https://doi.org/10.1158/0008-5472.CAN-12-4593.

55. Vangamudi, B., Paul, T.A., Shah, P.K., Kost-Alimova, M., Nottebaum, L., Shi, X., Zhan, Y., Leo, E., Mahadeshwar, H.S., Protopopov, A., et al. (2015). The SMARCA2/4 ATPase domain surpasses the bromodomain as a drug target in SWI/SNF-mutant cancers: insights from cDNA rescue and PFI-3 inhibitor studies. Cancer Res. *75*, 3865–3878. https://doi.org/10.1158/0008-5472.CAN-14-3798.

56. Doyon, Y., Selleck, W., Lane, W.S., Tan, S., and Côté, J. (2004). Structural and functional conservation of the NuA4 histone acetyltransferase complex from yeast to humans. Mol. Cell. Biol. *24*, 1884–1896. https://doi.org/10.1128/MCB.24.5.1884-1896.2004.

57. Wichmann, J., Pitt, C., Eccles, S., Garnham, A.L., Li-Wai-Suen, C.S.N., May, R., Allan, E., Wilcox, S., Herold, M.J., Smyth, G.K., et al. (2022). Loss of TIP60 (KAT5) abolishes H2AZ lysine 7 acetylation and causes p53, INK4A, and ARF-independent cell cycle arrest. Cell Death Dis. *13*, 627. https://doi.org/10.1038/s41419-022-05055-6.

58. Kim, S., Natesan, S., Cornilescu, G., Carlson, S., Tonelli, M., McClurg, U.L., Binda, O., Robson, C.N., Markley, J.L., Balaz, S., et al. (2016). Mechanism of histone H3K4me3 recognition by the plant homeodomain of inhibitor of growth 3. J. Biol. Chem. *291*, 18326–18341. https://doi.org/10.1074/jbc.M115.690651.

59. Shi, X., Hong, T., Walter, K.L., Ewalt, M., Michishita, E., Hung, T., Carney, D., Peña, P., Lan, F., Kaadige, M.R., et al. (2006). ING2 PHD domain links histone H3 lysine 4 methylation to active gene repression. Nature *442*, 96–99. https://doi.org/10.1038/nature04835.

60. Peña, P.V., Davrazou, F., Shi, X., Walter, K.L., Verkhusha, V.V., Gozani, O., Zhao, R., and Kutateladze, T.G. (2006). Molecular mechanism of histone H3K4me3 recognition by plant homeodomain of ING2. Nature *442*, 100–103. https://doi.org/10.1038/nature04814.

61. Song, Y., Liang, Z., Zhang, J., Hu, G., Wang, J., Li, Y., Guo, R., Dong, X., Babarinde, I.A., Ping, W., et al. (2022). CTCF functions as an insulator for somatic genes and a chromatin remodeler for pluripotency genes during reprogramming. Cell Rep. *39*, 110626. https://doi.org/10.1016/j.celrep.2022.110626.

62. Ravens, S., Yu, C., Ye, T., Stierle, M., and Tora, L. (2015). Tip60 complex binds to active Pol II promoters and a subset of enhancers and co-regulates the c-Myc network in mouse embryonic stem cells. Epigenetics Chromatin *8*, 45. https://doi.org/10.1186/s13072-015-0039-z.

63. Hu, G., Cui, K., Northrup, D., Liu, C., Wang, C., Tang, Q., Ge, K., Levens, D., Crane-Robinson, C., and Zhao, K. (2013). H2A.Z facilitates access of active and repressive complexes to chromatin in embryonic stem cell self-renewal and differentiation. Cell Stem Cell *12*, 180–192. https://doi.org/10.1016/j.stem.2012.11.003.

64. Hopkins, S.R., McGregor, G.A., Murray, J.M., Downs, J.A., and Savic, V. (2016). Novel synthetic lethality screening method identifies TIP60-dependent radiation sensitivity in the absence of BAF180. DNA Repair *46*, 47–54. https://doi.org/10.1016/j.dnarep.2016.05.030.

65. Dempster, J.M., Rossen, J., Kazachkova, M., Pan, J., Kugener, G., Root, D.E., and Tsherniak, A. (2019). Extracting biological insights from the Project Achilles genome-scale CRISPR screens in cancer cell lines. Preprint at bioRxiv. https://doi.org/10.1101/720243.

66. Dempster, J.M., Boyle, I., Vazquez, F., Root, D., Boehm, J.S., Hahn, W.C., Tsherniak, A., and McFarland, J.M. (2021). Chronos: a CRISPR cell population dynamics model. Genome Biol. *22*, 343. https://doi.org/10.1186/s13059-021-02540-7.

67. Meyers, R.M., Bryan, J.G., McFarland, J.M., Weir, B.A., Sizemore, A.E., Xu, H., Dharia, N.V., Montgomery, P.G., Cowley, G.S., Pantel, S., et al. (2017). Computational correction of copy number effect improves specificity of CRISPR–Cas9 essentiality screens in cancer cells. Nat. Genet. *49*, 1779–1784. https://doi.org/10.1038/ng.3984.

68. Pacini, C., Dempster, J.M., Boyle, I., Gonçalves, E., Najgebauer, H., Karakoc, E., van der Meer, D., Barthorpe, A., Lightfoot, H., Jaaks, P., et al. (2021). Integrated cross-study datasets of genetic dependencies in cancer. Nat. Commun. *12*, 1661. https://doi.org/10.1038/s41467-021-21898-7.

69. Halaburkova, A., Cahais, V., Novoloaca, A., Araujo, M.G.D.S., Khoueiry, R., Ghantous, A., and Herceg, Z. (2020). Pan-cancer multi-omics analysis and orthogonal experimental assessment of epigenetic driver genes. Genome Res. *30*, 1517–1532. https://doi.org/10.1101/gr.268292.120.

70. Fazzio, T.G., Huff, J.T., and Panning, B. (2008). An RNAi screen of chromatin proteins identifies Tip60-p400 as a regulator of embryonic stem cell identity. Cell *134*, 162–174. https://doi.org/10.1016/j.cell.2008.05.031.

71. Fazzio, T.G., Huff, J.T., and Panning, B. (2008). Chromatin regulation Tip(60)s the balance in embryonic stem cell self-renewal. Cell Cycle *7*, 3302–3306. https://doi.org/10.4161/cc.7.21.6928.

72. Jin, C., Zang, C., Wei, G., Cui, K., Peng, W., Zhao, K., and Felsenfeld, G. (2009). H3.3/H2A.Z double variant-containing nucleosomes mark 'nucleosome-free regions' of active promoters and other regulatory regions. Nat. Genet. *41*, 941–945. https://doi.org/10.1038/ng.409.

73. Jin, C., and Felsenfeld, G. (2007). Nucleosome stability mediated by histone variants H3.3 and H2A.Z. Genes Dev. *21*, 1519–1529. https://doi.org/10.1101/gad.1547707.

74. Colino-Sanguino, Y., Clark, S.J., and Valdes-Mora, F. (2016). H2A.Z acetylation and transcription: ready, steady, go!. Epigenomics *8*, 583–586. https://doi.org/10.2217/epi-2016-0016.

75. Halley, J.E., Kaplan, T., Wang, A.Y., Kobor, M.S., and Rine, J. (2010). Roles for H2A.Z and its acetylation in GAL1 transcription and gene induction, but not GAL1-transcriptional memory. PLoS Biol. *8*, e1000401. https://doi.org/10.1371/journal.pbio.1000401.

76. Law, C., and Cheung, P. (2015). Expression of non-acetylatable H2A.Z in myoblast cells blocks myoblast differentiation through disruption of MyoD expression. J. Biol. Chem. *290*, 13234–13249. https://doi.org/10.1074/jbc.M114.595462.

77. Janas, J.A., Zhang, L., Luu, J.H., Demeter, J., Meng, L., Marro, S.G., Mall, M., Mooney, N.A., Schaukowitch, K., Ng, Y.H., et al. (2022). Tip60-mediated H2A.Z acetylation promotes neuronal fate specification and bivalent gene activation. Mol. Cell *82*, 4627–4646.e14. https://doi.org/10.1016/j.molcel.2022.11.002.

78. Justice, M., Carico, Z.M., Stefan, H.C., and Dowen, J.M. (2020). A WIZ/Cohesin/CTCF complex anchors DNA loops to define gene expression and cell identity. Cell Rep. *31*, 107503. https://doi.org/10.1016/j.celrep.2020.03.067.

79. Baumgart, S.J., Nevedomskaya, E., Lesche, R., Newman, R., Mumberg, D., and Haendler, B. (2020). Darolutamide antagonizes androgen signaling by blocking enhancer and super-enhancer activation. Mol. Oncol. *14*, 2022–2039. https://doi.org/10.1002/1878-0261.12693.

80. Sugiura, M., Sato, H., Okabe, A., Fukuyo, M., Mano, Y., Shinohara, K.I., Rahmutulla, B., Higuchi, K., Maimaiti, M., Kanesaka, M., et al. (2021). Identification of AR-V7 downstream genes commonly targeted by AR/AR-V7 and specifically targeted by AR-V7 in castration resistant prostate cancer. Transl. Oncol. *14*, 100915. https://doi.org/10.1016/j.tranon.2020.100915.

81. The ENCODE Project Consortium (2012). An integrated encyclopedia of DNA elements in the human genome. Nature *489*, 57–74. https://doi.org/10.1038/nature11247.

82. Suzuki, A., Makinoshima, H., Wakaguri, H., Esumi, H., Sugano, S., Kohno, T., Tsuchihara, K., and Suzuki, Y. (2014). Aberrant transcriptional regulations in cancers: genome, transcriptome and epigenome analysis of lung adenocarcinoma cell lines. Nucleic Acids Res. *42*, 13557–13572. https://doi.org/10.1093/nar/gku885.

83. Kim, D., Kim, Y., Lee, B.B., Cho, E.Y., Han, J., Shim, Y.M., and Kim, D.H. (2021). Metformin reduces histone H3K4me3 at the promoter regions of

positive cell cycle regulatory genes in lung cancer cells. Cancers *13*, 739. https://doi.org/10.3390/cancers13040739.

84. Riedel, S.S., Lu, C., Xie, H.M., Nestler, K., Vermunt, M.W., Lenard, A., Bennett, L., Speck, N.A., Hanamura, I., Lessard, J.A., et al. (2021). Intrinsically disordered Meningioma-1 stabilizes the BAF complex to cause AML. Mol. Cell *81*, 2332–2348.e9. https://doi.org/10.1016/j.molcel.2021.04.014.
85. Langmead, B., Trapnell, C., Pop, M., and Salzberg, S.L. (2009). Ultrafast and memory-efficient alignment of short DNA sequences to the human genome. Genome Biol. *10*, R25. https://doi.org/10.1186/gb-2009-10-3-r25.
86. Dobin, A., Davis, C.A., Schlesinger, F., Drenkow, J., Zaleski, C., Jha, S., Batut, P., Chaisson, M., and Gingeras, T.R. (2013). STAR: ultrafast universal RNA-seq aligner. Bioinformatics *29*, 15–21. https://doi.org/10.1093/bioinformatics/bts635.
87. Liao, Y., Smyth, G.K., and Shi, W. (2019). The R package Rsubread is easier, faster, cheaper and better for alignment and quantification of RNA sequencing reads. Nucleic Acids Res. *47*, e47. https://doi.org/10.1093/nar/gkz114.
88. Love, M.I., Huber, W., and Anders, S. (2014). Moderated estimation of fold change and dispersion for RNA-seq data with DESeq2. Genome Biol. *15*, 550. https://doi.org/10.1186/s13059-014-0550-8.
89. Martin, M. (2011). Cutadapt removes adapter sequences from high-throughput sequencing reads. EMBnet.journal *17*, 10–12. https://doi.org/10.14806/ej.17.1.200.
90. Wang, Z., Chu, T., Choate, L.A., and Danko, C.G. (2019). Identification of regulatory elements from nascent transcription using dREG. Genome Res. *29*, 293–303. https://doi.org/10.1101/gr.238279.118.
91. Li, H., Handsaker, B., Wysoker, A., Fennell, T., Ruan, J., Homer, N., Marth, G., Abecasis, G., and Durbin, R.; 1000 Genome Project Data Processing Subgroup (2009). The Sequence Alignment/Map format and SAMtools. Bioinformatics *25*, 2078–2079. https://doi.org/10.1093/bioinformatics/btp352.
92. Bray, N.L., Pimentel, H., Melsted, P., and Pachter, L. (2016). Near-optimal probabilistic RNA-seq quantification. Nat. Biotechnol. *34*, 525–527. https://doi.org/10.1038/nbt.3519.
93. Heinz, S., Benner, C., Spann, N., Bertolino, E., Lin, Y.C., Laslo, P., Cheng, J.X., Murre, C., Singh, H., and Glass, C.K. (2010). Simple combinations of lineage-determining transcription factors prime cis-regulatory elements required for macrophage and B cell identities. Mol. Cell *38*, 576–589. https://doi.org/10.1016/j.molcel.2010.05.004.
94. Huang, D.W., Sherman, B.T., and Lempicki, R.A. (2009). Systematic and integrative analysis of large gene lists using DAVID bioinformatics resources. Nat. Protoc. *4*, 44–57. https://doi.org/10.1038/nprot.2008.211.
95. Huang, D.W., Sherman, B.T., and Lempicki, R.A. (2009). Bioinformatics enrichment tools: paths toward the comprehensive functional analysis of large gene lists. Nucleic Acids Res. *37*, 1–13. https://doi.org/10.1093/nar/gkn923.
96. Buenrostro, J.D., Giresi, P.G., Zaba, L.C., Chang, H.Y., and Greenleaf, W.J. (2013). Transposition of native chromatin for fast and sensitive epigenomic profiling of open chromatin, DNA-binding proteins and nucleosome position. Nat. Methods *10*, 1213–1218. https://doi.org/10.1038/nmeth.2688.
97. Tian, B., Yang, J., and Brasier, A.R. (2012). Two-step cross-linking for analysis of protein-chromatin interactions. Methods Mol. Biol. *809*, 105–120. https://doi.org/10.1007/978-1-61779-376-9_7.
98. Grandi, F.C., Modi, H., Kampman, L., and Corces, M.R. (2022). Chromatin accessibility profiling by ATAC-seq. Nat. Protoc. *17*, 1518–1552. https://doi.org/10.1038/s41596-022-00692-9.
99. Conant, D., Hsiau, T., Rossi, N., Oki, J., Maures, T., Waite, K., Yang, J., Joshi, S., Kelso, R., Holden, K., et al. (2022). Inference of CRISPR edits from Sanger Trace Data. CRISPR J. *5*, 123–130. https://doi.org/10.1089/crispr.2021.0113.
100. Yates, A.D., Achuthan, P., Akanni, W., Allen, J., Allen, J., Alvarez-Jarreta, J., Amode, M.R., Armean, I.M., Azov, A.G., Bennett, R., et al. (2020). Ensembl 2020. Nucleic Acids Res. *48*, D682–D688. https://doi.org/10.1093/nar/gkz966.
101. Martin, B.J., Adelman, K., and Nelson, G. (2021). AdelmanLab/NIH_scripts: AdelmanLab/NIH_scripts/v1Zenodo. https://doi.org/10.5281/zenodo.5519915.
102. Kent, W.J., Sugnet, C.W., Furey, T.S., Roskin, K.M., Pringle, T.H., Zahler, A.M., and Haussler, D. (2002). The human genome browser at UCSC. Genome Res. *12*, 996–1006. https://doi.org/10.1101/gr.229102.
103. Stein, C.B., Field, A.R., Mimoso, C.A., Zhao, C., Huang, K.L., Wagner, E.J., and Adelman, K. (2022). Integrator endonuclease drives promoter-proximal termination at all RNA polymerase II-transcribed loci. Mol. Cell *82*, 4232–4245.e11. https://doi.org/10.1016/j.molcel.2022.10.004.
104. Mimoso, C.A., and Adelman, K. (2023). U1 snRNP increases RNA Pol II elongation rate to enable synthesis of long genes. Mol. Cell *83*, 1264–1279.e10. https://doi.org/10.1016/j.molcel.2023.03.002.
105. Ku, M., Koche, R.P., Rheinbay, E., Mendenhall, E.M., Endoh, M., Mikkelsen, T.S., Presser, A., Nusbaum, C., Xie, X., Chi, A.S., et al. (2008). Genomewide analysis of PRC1 and PRC2 occupancy identifies two classes of bivalent domains. PLoS Genet. *4*, e1000242. https://doi.org/10.1371/journal.pgen.1000242.
106. Martin, B.J., Mimoso, C.A., and Adelman, K. (2021). AdelmanLab/GetGeneAnnotation_GGA: AdelmanLab/GetGeneAnnotation_GGA/v1Zenodo. https://doi.org/10.5281/zenodo.5519928.
107. Martin, B.J.E., Brind'Amour, J., Kuzmin, A., Jensen, K.N., Liu, Z.C., Lorincz, M., and Howe, L.J. (2021). Transcription shapes genome-wide histone acetylation patterns. Nat. Commun. *12*, 210. https://doi.org/10.1038/s41467-020-20543-z.
108. Ghandi, M., Huang, F.W., Jané-Valbuena, J., Kryukov, G.V., Lo, C.C., McDonald, E.R., Barretina, J., Gelfand, E.T., Bielski, C.M., Li, H., et al. (2019). Next-generation characterization of the Cancer Cell Line Encyclopedia. Nature *569*, 503–508. https://doi.org/10.1038/s41586-019-1186-3.
109. Wong, A.K., Shanahan, F., Chen, Y., Lian, L., Ha, P., Hendricks, K., Ghaffari, S., Iliev, D., Penn, B., Woodland, A.M., et al. (2000). BRG1, a component of the SWI-SNF complex, is mutated in multiple human tumor cell lines. Cancer Res. *60*, 6171–6177.
110. Filbin, M.G., Tirosh, I., Hovestadt, V., Shaw, M.L., Escalante, L.E., Mathewson, N.D., Neftel, C., Frank, N., Pelton, K., Hebert, C.M., et al. (2018). Developmental and oncogenic programs in H3K27M gliomas dissected by single-cell RNA-seq. Science *360*, 331–335. https://doi.org/10.1126/science.aao4750.

STAR★METHODS

KEY RESOURCES TABLE

REAGENT or RESOURCE	SOURCE	IDENTIFIER
Antibodies		
Rabbit monoclonal, BRG1	Cell Signaling Technology	Cat # 49360, RRID:AB_2728743
Rabbit monoclonal, BAF155	Cell Signaling Technology	Cat # 11956, RRID:AB_2797776
Rabbit monoclonal, ARID1A	Cell Signaling Technology	Cat # 12354, RRID:AB_2637010
Rabbit polyclonal, EP400	Abcam	Cat # ab70301, RRID:AB_1269644
Rabbit polyclonal, H3	Abcam	Cat # ab1791, RRID:AB_302613
Rabbit monoclonal, BRG1	Abcam	Cat # ab110641, RRID: AB_10861578
Rabbit polyclonal, EP400	Bethyl Antibodies	Cat # A300-541A, RRID:AB_2098208
Rabbit polyclonal, MYC	Santa Cruz Biotechnology	Cat # sc-764, RRID: AB_631276
Rabbit polyclonal, VINCULIN	Abcam	Cat # AB129002, RRID:AB_11144129
Bacterial and virus strains		
pXPR101 (Cas9 expression lentivirus)	Broad Institute Genetic Perturbation Platform	pXPR101
Chemicals, peptides, and recombinant proteins		
BRM014	Novartis Institutes for BioMedical Research	N/A
LIF	Cell Guidance Systems	Cat # GFM200
PD0325901	Reprocell	Cat # 04-0006
CHIR99021	Reprocell	Cat # 04-0004
Puromycin	Invivogen	Cat # ant-pr-1
Blasticidin	Invivogen	Cat # ant-bl-05
Polybrene	Sigma-Aldrich	Cat # TR-1003-G
TransIT-LT1 transfection reagent	VWR	Cat # 10767-116
Digitonin	Promega	Cat # G9441
Biotin-11-NTPs	Perkin Elmer	Cat # NEL54(2/3/4/5)001
AU-15330	MedChem Express	Cat # HY-145388
Protease Inhibitor Cocktail	Roche	Cat # 11836170001
Lipofectamine RNAiMAX	Thermo Fisher	Cat # 13778075
TRIzol reagent	Invitrogen	Cat # 15596018
Trypan Blue	VWR	Cat # AAA18600-14
DSG crosslinker	Cova Chem	Cat # 13301-5x100
Formaldehyde	Sigma-Aldrich	Cat # F8775
Protein A agarose beads	Millipore	Cat # 16-125
Proteinase K	NEB	Cat # P8107
Phenol:chloroform:isoamyl alcohol	Sigma-Aldrich	Cat # P3803
IGEPAL CA-630	Sigma-Aldrich	Cat # I8896
SUPERase-In	Thermo Fisher	Cat # AM26976
Dynabeads MyOne Streptavidin C1	Thermo Fisher	Cat # 65001
T4 RNA Ligase I	NEB	Cat # M0437
RNA 5' Pyrophosphohydrolase	NEB	Cat # M0356
T4 PNK Reaction Buffer	NEB	Cat # B0201
T4 PNK	NEB	Cat # M0201
SuperScript IV Reverse Transcriptase	Thermo Fisher	Cat # 18090010
ProNex Size-Selective Purification System	Promega	Cat # NG2001

(*Continued on next page*)

Continued

REAGENT or RESOURCE	SOURCE	IDENTIFIER
DNase I, amplification grade	Invitrogen	Cat # 18068015
Critical commercial assays		
NEBNext Ultra II DNA Library Prep Kit for Illumina	NEB	Cat # E7103S
Illumina TruSeq Stranded Total RNA Library Prep Gold	Illumina	Cat # 20020598
Illumina Tagment DNA Enzyme and Buffer Small Kit	Illumina	Cat # 20034197
MinElute PCR Purification Kit	Qiagen	Cat # 28004
DNA Clean and Concentrator-5 Kit	Zymo Research	Cat # D4014
NEBNext High-Fidelity 2X PCR Master Mix	NEB	Cat # M01541
Total RNA Purification Kit	Norgen Biotek	Cat # 17250
RNeasy Mini Kit	Qiagen	Cat # 74104
Direct-zol RNA miniprep kit	VWR	Cat # 76211-340
CellTiter-Glo 2.0 Assay	Promega	Cat # G9242
Deposited data		
Raw and analyzed data	This paper	GEO: GSE198517
Original western blot images	This paper	https://doi.org/10.17632/z3f6pm86w3.1
mESC MNase-seq	Henriques et al.[28]	GEO: GSE85191
mESC TT-seq	Vlaming et al.[34]	GEO: GSE178230
MNase-seq from control and BRM014 treated mESCs	Iurlaro et al.[21]	GEO: GSE158345
ATAC-seq from control and *BRG1*-KO mESCs	King and Klose[8]	GEO: GSE87822
ATAC-seq from control and *SNF2H*-KO mESCs	Barisic et al.[4]	GEO: GSE112130
mESC H3K27ac ChIP-seq	Vlaming et al.[34]	4DN: 4DNESQ33L4G7
mESC H3K4me3 ChIP-seq	Vlaming et al.[34]	GEO: GSE178230
mECS H3K4me1 ChIP-seq	Buecker et al.[35]	GEO: GSE56098
mESC H2A.Z and H2A.Zac ChIP-seq	Hu et al.[63]	GEO: GSE34483
mESC CHD1, CHD2, CHD4, and EP400 ChIP-seq	Dieuleveult et al.[3]	GEO: GSE64825
mESC TIP60 ChIP-seq	Ravens et al.[62]	GEO: GSE69671
mESC CTCF ChIP-seq	Justice et al.[78]	GEO: GSE137272
mESC SNF2H ChIP-seq	Song et al.[61]	GEO: GSE123670
mESC OCT4, SOX2, and NANOG ChIP-seq	King and Klose[8]	GEO: GSE87822
LNCaP and VCaP RNA-seq and ATAC-seq	Xiao et al.[25]	GEO: GSE171523
VCaP H3K4me1 ChIP-seq	Baumgart et al.[79]	GEO: GSE148400
LNCaP H3K4me1 ChIP-seq	Sugiura et al.[80]	GEO: GSE122922
A549 H3K4me1 ChIP-seq	The ENCODE Project Consortium[81]	GEO: GSE29611
A549 ATAC-seq	The ENCODE Project Consortium[81]	GEO: GSE169955
H1299 H3K4me1 ChIP-seq	Suzuki et al.[82]	SRA: DRR016953
H1299 ATAC-seq	Kim et al.[83]	GEO: GSE141060
MV411 and MOLM13 RNA-seq and ATAC-seq	Chambers et al.[48]	GEO: GSE190721
MV411 H3K4me1 ChIP-seq	Ellegast et al.[51]	GEO: GSE168647
MV411 H3K27ac ChIP-seq	Erb et al.[50]	GEO: GSE82116
MOLM13 H3K4me1 ChIP-seq	Riedel et al.[84]	GEO: GSE154985
BT869 RNA-seq and ATAC-seq	Panditharatna et al.[52]	GEO: GSE212718
DIPG007 RNA-seq and ATAC-seq	Mota et al.[53]	GEO: GSE229452
Experimental models: Cell lines		
F121-9	Jaenisch/Gribnau labs	4DNSRMG5APUM
A549 cell line	ATCC	CCL-185
H1299 cell line	ATCC	CRL-5803

(*Continued on next page*)

Continued		
REAGENT or RESOURCE	SOURCE	IDENTIFIER
A549 *EP400*-KO	This paper	N/A
MV411 cell line	ATCC	CRL9591
MOLM13 cell line	DSMZ	ACC 554
LNCaP cell line	ATCC	CRL-1740
Recombinant DNA		
Packaging plasmid (psPAX2)	psPAX2 was a gift from Didier Trono	Addgene Plasmid #12260, RRID:Addgene_12260
Envelope plasmid (pMD2.G)	psPAX2 was a gift from Didier Trono	Addgene Plasmid #12259; RRID:Addgene_12259
Non-targeting guide lentiviral plasmid	Broad Institute Genetic Perturbation Platform	BRDN0002985967
EP400-targeting guide lentiviral plasmid	Broad Institute Genetic Perturbation Platform	BRDN0003790195
EP400-targeting guide lentiviral plasmid	Broad Institute Genetic Perturbation Platform	BRDN0003483852
Ctrl shRNA lentiviral plasmid	Broad Institute Genetic Perturbation Platform	TRCN0000072181
GFP expressing lentiviral plasmid	Broad Institute Genetic Perturbation Platform	TRCN0000231782
EP400 shRNA lentiviral plasmid #1	Broad Institute Genetic Perturbation Platform	TRCN0000312676
EP400 shRNA lentiviral plasmid #2	Broad Institute Genetic Perturbation Platform	TRCN0000312686
Oligonucleotides		
Table S1	This paper	N/A
siEP400, Dharmacon J-058750-12	Dharmacon	J-058750-12
Non-Targeting siRNA	Dharmacon	D-001210-02-05
ERCC RNA Spike-In Mix	Thermo Fisher	Cat # 4456740
Software and algorithms		
trim_and_filter_PE.pl	This paper	https://doi.org/10.5281/zenodo.5519915
extract_fragments.pl	This paper	https://doi.org/10.5281/zenodo.5519915
normalize_bedGraph.pl	This paper	https://doi.org/10.5281/zenodo.5519915
bedgraphs2stdBedGraph.pl	This paper	https://doi.org/10.5281/zenodo.5519915
make_heatmap	This paper	https://doi.org/10.5281/zenodo.5519915
get_gene_annotations.sh	This paper	https://doi.org/10.5281/zenodo.5519928
bowtie 1.2.2	Langmead et al.[85]	https://bowtie-bio.sourceforge.net/index.shtml
STAR 2.7.3a	Dobin et al.[86]	https://github.com/alexdobin/STAR
R 3.6.1	www.r-project.org	https://www.r-project.org/
Rsubread 2.0.1	Liao et al.[87]	https://bioconductor.org/packages/release/bioc/html/Rsubread.html
DESeq2 1.26.0	Love et al.[88]	https://bioconductor.org/packages/release/bioc/html/DESeq2.html
Prism	GraphPad	https://www.graphpad.com/
Partek Genomics Suite 6.16.0812	www.partek.com	https://www.partek.com/partek-genomics-suite/
cutadapt	Martin[89]	https://cutadapt.readthedocs.io/en/stable/
dREG	Wang et al.[90]	https://github.com/Danko-Lab/dREG
Samtools 1.9	Li et al.[91]	http://www.htslib.org/
Kallisto 0.45.1	Bray et al.[92]	https://pachterlab.github.io/kallisto/
HOMER 4.10.3	Heinz et al.[93]	http://homer.ucsd.edu/homer/
The Database for Annotation, Visualization and Integrated Discovery (DAVID) v6.8	Huang et al.[94,95]	https://david.ncifcrf.gov/

RESOURCE AVAILABILITY

Lead contact

Further information and requests for resources and reagents should be directed to and will be fulfilled by the lead contact, Karen Adelman (karen_adelman@hms.harvard.edu).

Materials availability

Unique and stable reagents generated in this study are available upon request.

Data and code availability

- All PRO-seq, ChIP-seq, ATAC-seq, and RNA-seq data have been deposited at GEO and are publicly available as of the date of publication. Accession numbers are listed in the key resources table (GEO: GSE198517). Original western blot images have been deposited at Mendeley and are publicly available as of the date of publication. The DOI is listed in the key resources table. This paper also analyzes existing, publicly available data. These accession numbers for these datasets are listed in the key resources table.
- All custom scripts have been deposited at Zenodo and are publicly available as of the date of publication. DOIs are listed in the key resources table.
- Any additional information required to reanalyze the data reported in this paper is available from the lead contact upon request.

EXPERIMENTAL MODEL AND STUDY PARTICIPANT DETAILS

Cell Culture and Inhibitor Treatments

Cell Culture

F121-9-CASTx129 female mouse hybrid embryonic stem cells (mESCs) were obtained from David Gilbert (Florida State University) and cultured at 37°C in 5% CO_2. Cells were maintained in serum-free ES medium (SFES) composed of 50% Neurobasal Media (Gibco 21103-049), 50% DMEM/F12 (Gibco 11320-033), 0.5X N2 Supplement (Gibco 17502-048), 0.5X B27(+RA) (Gibco 17504-044) and 0.05% BSA (Gibco 15260-037) and supplemented with 2 mM glutamine (Gibco 25030-081), $1.5x10^{-4}$ M monothioglycerol (Sigma M6145), 1 μM MEK inhibitor (PD03259010; Reprocell 04-0006-02), 3 μM GSK3 inhibitor (CHIR99021;Reprocell 04-0004-02), and 1,000 U/mL leukemia inhibiting factor (LIF; Cell Guidance Systems GFM200). *Drosophila* S2 cells were grown at 27°C in Shields and Sang M3 Insect Medium (Sigma S3652) supplemented with bactopeptone (Difco 2116), yeast extract (Sigma Y-1000), and 10% FBS (Invitrogen 16000044). A549 cells were obtained from the ATCC and cultured at 37°C in 5% CO_2. Cells were maintained in F12-K medium composed of F12-K +L-glutamine (Gibco 21127-022), 10% fetal bovine serum (Fisher Scientific 16-000-044) and Penicillin-Streptomycin (Thermo Fisher 15140163). Male H1299 (ATCC), LNCaP (ATCC), MV411 (ATCC), and MOLM13 (DSMZ) cells were cultured at 37°C in 5% CO_2. Cells were maintained in RPMI medium consisting of RPMI 1640 with L-glutamine (Corning MT 10-040-CV), 10% fetal bovine serum (Fisher Scientific 16-000-044) and Penicillin-Streptomycin (Thermo Fisher 15140163). All cells were tested routinely for mycoplasma contamination.

BRM014 Treatment

SWI/SNF inhibitor BRM014[19] was provided by Novartis Institutes for BioMedical Research (Cambridge, MA) and was resuspended in dimethyl sulfoxide (DMSO) for a 10 mM stock. mESCs were treated at a final concentration of 1 μM. For viability experiments, a TC20 Automated Cell Counter (Bio-Rad) was used to collect cell counts in duplicate for both unstained cells and cells stained with Trypan Blue (VWR AAA18600-14). Average cell counts for each condition were used to generate cell growth and viability curves.

METHOD DETAILS

Western Blots

mESC whole cell extracts were resolved using a Novex™ WedgeWell™ 6% Tris-Glycine Mini Protein Gel (Thermo Fisher XP00065BOX). Samples were transferred to a polyvinylidene difluoride (PVDF) membrane (Bio-Rad 1620177). After blocking in 5% BSA, membranes were incubated overnight with primary antibodies: BRG1 (Cell Signaling Technology #49360), BAF155 (Cell Signaling Technology #11956), ARID1A (Cell Signaling Technology #12354), EP400 (Abcam #ab70301), or H3 (Abcam #ab1791). Membranes were incubated with horseradish-peroxidase-conjugated secondary antibodies (Jackson ImmunoResearch 111-035-144) before being visualized using SuperSignal™ West Pico PLUS Chemiluminescent Substrate (Thermo Fisher 34579) and the ChemiDoc Imaging System (Bio-Rad). For MV411 samples, whole cell extracts were resolved using a Biorad 4-20% Mini-PROTEAN® TGX™ Precast Protein Gel (Bio-Rad 456-1096). Samples were transferred to a nitrocellulose membrane (VWR 10120-004). After blocking with 5% milk, membranes were incubated overnight with primary antibodies: BRG1 (Cell Signaling Technology #49360), MYC (SCBT #SC764), or H3 (Abcam #ab1791), or VINCULIN (Abcam #ab129002). Membranes were incubated with horseradish-peroxidase-conjugated secondary antibodies (Jackson ImmunoResearch 111-035-144) before being visualized using SuperSignal™ West Pico PLUS Chemiluminescent Substrate (Thermo Fisher 34579) and the ChemiDoc Imaging System (Bio-Rad).

mESC ATAC-seq Library Preparation

Cell Preparation and Transposition

ATAC-seq was performed as described in Buenrostro et al.,[96] with some modifications. In brief, 1 x 10^5 cells per sample were washed with ice-cold 1X PBS and centrifuged at 500 × *g* for 5 min at 4°C. Cells were then resuspended in 50 μL CSK Lysis Buffer (10 mM PIPES, pH 6.8, 100 mM NaCl, 300 mM sucrose, 3 mM $MgCl_2$, 0.1% Triton-X-100), incubated on ice for 5 min, and centrifuged for 5 min at 500 × *g* and 4°C. To allow for downstream spike normalization, *Drosophila* S2 cells were harvested in parallel and processed as described above, with spin speeds increased to 1000 x *g*. For each reaction, 1 x 10^5 mESCs and 5 x 10^4 S2 cells were resuspended in Tagment DNA Buffer and treated with 3 μL TDE1 Tagment DNA Enzyme (Illumina 20034197). After thorough mixing, samples were incubated at 37°C for 30 minutes. Tagmented DNA was subsequently purified using a MinElute PCR Purification Kit (Qiagen 28004).

Library Preparation

Purified samples were combined with NEBNext High-Fidelity 2X PCR Master Mix (New England Biolabs M01541) for amplification. As described in Buenrostro et al.,[96] custom primers were used to incorporate Illumina adaptors and index sequences into sample fragments. Libraries were sequenced at The Bauer Core Facility at Harvard University on an Illumina NovaSeq using an S1 flow cell and a paired-end 100-bp cycle run.

ATAC-qPCR

To validate ATAC-seq results, qPCR was performed using experimental primers (Table S1) targeting a panel of candidate genes and enhancer regions, as well as a set of three 'background' primer pairs targeting nongenic regions of closed chromatin. For each sample, Cq values of experimental primers were normalized to the average Cq value across all background primers for that same sample, allowing differences in accessibility between conditions to be expressed in terms of "normalized accessibility."

ChIP-seq Library Preparation

Chromatin Isolation and Sonication

After the indicated treatment interval, cells were fixed for 1 h in 2 mM DSG with the addition of 1% formaldehyde for the final 12.5 min, as described in Tian et al.[97] Crosslinking was quenched by the addition of glycine to a final concentration of 0.125 M. Cells were collected and washed with ice-cold 1X PBS before being resuspended in Sonication Buffer (20 mM Tris, pH 8.0, 2 mM EDTA, 0.5 mM EGTA, 1X Complete Mini EDTA-free Protease Inhibitor Cocktail [Roche 11836170001], 0.5% SDS, and 0.5 mM PMSF) at a concentration of 1 x 10^8 cells per mL. Chromatin was sheared to an average fragment size of ~200 bp using a QSonica sonicator, flash-frozen in liquid nitrogen, and stored at -80°C until use.

Immunoprecipitation

ChIP material was diluted into IP buffer (20 mM Tris pH 8.0, 2 mM EDTA, 0.5% Triton X-100, 150 mM NaCl, 10% Glycerol, 5% BSA) and pre-cleared with 30 μL of Protein A agarose beads (Millipore Cat No. 16-125) for 1 h at 4°C. Cleared samples were collected and combined with primary antibody before overnight incubation at 4°C with rotation. For 2 h BRM014 treated samples, 30 μL BRG1 antibody (Abcam ab110641 - EPNCIR111A) was used. For 4 h BRM014 treated samples, the antibody amount was reduced to 10 μL, based on antibody titrations. All EP400 immunoprecipitations were all performed with 30 μL of antibody (Bethyl A300-541A). Subsequently, 200 μL Protein A beads were added to each IP reaction, and samples were rotated for 2 h at 4°C. Samples were washed once with Low-Salt Buffer (20 mM Tris pH 8.0, 2 mM EDTA, 1% Triton X-100, 150 mM NaCl, 0.1% SDS), three times with High-Salt Buffer (20 mM Tris pH 8.0, 2 mM EDTA, 1% Triton X-100, 500 mM NaCl, 0.1% SDS), once with Lithium Chloride Buffer (20 mM Tris pH 8.0, 2 mM EDTA, 250 mM LiCl, 1% IGEPAL CA-630, 1% sodium deoxycholate), and twice with TE Buffer (10 mM Tris-HCl, 1mM EDTA). Each wash was performed by rotating samples for 3 minutes with 1 mL volume of ice-cold wash solution. Two elutions were performed by resuspending beads in Elution Buffer (100 mM $NaHCO_3$, 1% SDS) and rotating for 15 min at room temperature (22°C). The combined eluate was supplemented with 200 mM NaCl and incubated overnight in a 65°C water bath. Samples were treated with Proteinase K (New England Biolabs P8107), extracted with phenol:chloroform:isoamyl alcohol (25:24:1, Sigma P3803), and resuspended in 65 μl H_2O. To enable accurate sample normalization, an equal amount of fragmented *D. melanogaster* DNA was added to the eluate of each sample.

Library Preparation

Libraries were prepared using the NEBNext Ultra II DNA Library Prep Kit for Illumina (New England Biolabs) according to the manufacturer's instructions. Libraries were sequenced on an Illumina NovaSeq using an S1 flow cell and a paired-end 100-bp cycle run, with sequencing performed by The Bauer Core Facility at Harvard University.

PRO-seq Library Preparation

Cell Permeabilization

Precision run-on sequencing (PRO-seq) was performed based on the protocol described in Mahat et al.,[27] with some modifications. All steps of PRO-seq sample preparation were performed on ice, and all buffers were thoroughly chilled on ice before being added to the reaction. Cells were released using Accutase, collected with ice-cold media, washed with PBS, and resuspended in 0.25 mL Buffer W (10 mM Tris-HCL pH 8.0, 10 mM KCl, 250 mM sucrose, 5 mM $MgCl_2$, 1 mM EGTA, 0.5 mM DTT, 10% glycerol). Then 10 mL Buffer P (Buffer W + 0.1% IGEPAL CA-630 (Sigma I8896) was carefully added to each sample. Samples were incubated on ice for 5 min, then centrifuged at 4°C and 400 x *g* for 4 min. Permeabilized cells were resuspended in 10 mL of Buffer W and centrifuged at 4°C and 400 x *g* for 4 min, before being resuspended in Buffer F (50 mM Tris-CL pH 8.0, 5 mM $MgCl_2$, 1.1 mM EDTA, 0.5 mM

DTT, 40% glycerol, 1 μL/mL SUPERase-In (Thermo Fisher AM26976) at a final volume of 1 x 10^6 permeabilized cells per 50 μL. Immediately after processing, samples were flash-frozen using liquid nitrogen and stored at -80°C.

Biotin Run-On and RNA Purification

For each sample, 1 x 10^6 permeabilized mES cells were spiked with previously prepared permeabilized *Drosophila* S2 cells at a proportion of 5% to enable downstream data normalization. Permeabilized cells were then combined with 2X Run-On Master Mix (10 mM Tris-Cl pH 8.0, 300 mM KCl, 1% Sarkosyl, 5 mM $MgCl_2$, 1 mM DTT, 200 μM biotin-11-A/C/G/UTP (Perkin-Elmer NEL544001EA / NEL542001EA / NEL541001EA / NEL543001EA), 0.8 U/μL SUPERase-In (Thermo Fisher AM26976) and incubated at 30°C for 5 min to allow the biotin-NTP run-on reaction to proceed. Following run-on, RNA was isolated using the Total RNA Purification Kit (Norgen Biotek 17250) according to the manufacturer's instructions.

Library Preparation

Purified RNA was subject to chemical fragmentation with 2X RNA Fragmentation Buffer (150 mM Tris-Cl pH 8.3, 225 mM KCl, 9 mM $MgCl_2$) for 5 min at 94°C. Chilled fragmented RNA was combined with 48 μL Dynabeads MyOne Streptavidin C1 (Thermo Fisher 65001) in Binding Buffer (300 mM NaCl, 10 mM Tris-HCl pH 7.4, 0.1% Triton-X-100) and rotated for 20 min at room-temperature. RNA-bound beads were washed two times each with High-Salt Buffer (2 M NaCl, 50 mM Tris-HCl pH 7.4, 0.5% Triton-X-100), Binding Buffer (described above), and Low-Salt Buffer (5 mM Tris-HCl pH 7.4, 0.1% Triton-X-100), then resuspended in TRIzol Reagent (Invitrogen 15596026). RNA was eluted from the beads via two sequential rounds of incubation, each for 5 min at 65°C. Chloroform extraction was used to purify isolated RNA. Purified RNA was resuspended in 10 μM VRA3 adaptor (/5Phos/rGrArUrCrGrUrCrGrGrArCrUrGrUrArGrArArCrUrCrUrGrArArC/3InvdT/) and treated with T4 RNA Ligase I (New England Biolabs M0437) for 2 h at room temperature (22°C) to enable 3' adaptor ligation. Desired RNA species were captured with Dynabeads MyOne Streptavidin C1 in the presence of a blocking oligo (TCCGACGATCCCACGTTCCCGTGG/3InvdT), after which the beads were sequentially washed with High-Salt, Binding, Low-Salt, and 1X Thermo Pol (New England Biolabs B9004) Buffers. Beads were next resuspended in 1X Thermo Pol Buffer and treated with 2 μL RNA 5' Pyrophosphohydrolase (New England Biolabs M0356) at 37°C for 1 h to promote decapping of 5' RNA ends. Beads were washed in High-Salt Buffer and Low-Salt Buffer, then resuspended in 1X T4 PNK Reaction Buffer (New England Biolabs B0201). Samples were incubated at 37°C for 1 h after the addition of T4 PNK (New England Biolabs M0201) to allow 5'-hydroxyl repair. A second ligation step was performed as described above to ligate the VRA5 5' RNA adaptor (rCrCrUrUrGrGrCrArCrCrCrGrArGrArArUrUrCrCrA). Beads were washed twice each with High-Salt, Binding, and Low-Salt Buffers, then washed once in 0.25X FS Buffer (12.5 mM Tris-HCl pH 8.3, 18.75 mM KCl, 0.75 mM $MgCl_2$). Twenty-five pmol of RP1 primer (AATGATACGGCGACCACCGAGATCTACACGTTCAGAGTTCTACAGTCCGA) was added to samples, after which reverse transcription was performed using SuperScript IV Reverse Transcriptase (Thermo Fisher 18090010). Final library products were eluted by heating samples twice to 95°C for 30 sec each, then amplified by 12 cycles of PCR with primer RP1, Illumina TruSeq PCR primer RPI-X, and Phusion Polymerase (New England Biolabs M0530). The ProNex Size-Selective Purification System (Promega NG2001) was used at a 2.8X ratio to purify amplified libraries. Libraries were sequenced at The Bauer Core Facility at Harvard University on an Illumina NovaSeq using an S4 flow cell and a paired-end 100-bp cycle run.

siRNA Transfection

Cell Culture

For EP400 knockdown experiments, mESCs were transfected with either a non-targeting control siRNA (siNT) or a commercially available on-target siRNA against mouse *Ep400* (Dharmacon J-058750-12) (siEP400) using Lipofectamine RNAiMAX Transfection Reagent (Thermo Fisher 13778075). Cells were maintained for 72 h before harvest.

Knockdown Validation

To ensure that effective knockdown of *Ep400* was achieved under the conditions described above, cells transfected with either non-targeting (siNT) or on-target (siEP400) siRNA were harvested after 72 h for analysis of mRNA and protein levels. To analyze mRNA expression, RNA was extracted using the RNeasy Mini Kit (Qiagen 74104). cDNA synthesis was performed using hexamer primers and SuperScript IV Reverse Transcriptase (Thermo Fisher 18090010). Processed samples were then subjected to RT-qPCR analysis using primer pairs targeting *Ep400* (Table S1). To analyze protein expression, cells were harvested and subjected to western blot according to the conditions described above. To enable estimation of residual EP400 protein levels, a serial dilution of control (siNT-treated) sample was run alongside experimental samples.

BRM014 Treatment and ATAC Library Preparation

Fresh media containing 1 μM BRM014 was provided 72 h after the initial transfection, and cells were harvested after an additional 4 h of inhibitor treatment (for a total time 76 h between transfection and harvest). Cells were observed regularly to ensure that no large-scale defects in growth or viability occurred under these treatment conditions. After harvest, ATAC libraries were prepared according to the protocol detailed above. Libraries were sequenced at The Bauer Core Facility at Harvard University on an Illumina NovaSeq using an S4 flow cell and a paired-end 100-bp cycle run

MV411 ATAC-seq Library Preparation

Cell Preparation and Transposition

ATAC-seq was performed as described in Grandi et al.,[98] with some modifications. Briefly 100,000 cells were mixed with 10,000 S2 *Drosophila* cells and pelleted at 500g for 5 minutes at 4°C. Cells were washed with 100 μL ice-cold DPBS (Corning 21-031-CV), and

pelleted at 500 x g for 5 minutes at 4°C. The cell pellet was resuspended in 50 μL of ATAC-seq Lysis Buffer (0.1% NP40, 0.1% Tween-20, 0.01% digitonin, 10 mM Tris–HCl pH 7.5, 10 mM NaCl and 3 mM MgCl2) and incubated on ice for 3 minutes. Then 1 mL of ATAC-seq Wash Buffer (0.1% Tween-20, 10 mM Tris–HCl pH 7.5, 10 mM NaCl and 3 mM MgCl2) was added to dilute the lysis reagents, and nuclei were pelleted by spinning at 500 x g for 10 minutes at 4°C. Nuclei were then resuspended in 50 μL Transposition Mix (1X Tagment DNA Buffer, 0.33X DPBS, 0.01% digitonin, 0.1% Tween-20) treated with 3 μL TDE1 Tagment DNA Enzyme (Illumina 20034197). The reaction was incubated at 37°C for 30 minutes with shaking at 1,000 rpm. Tagmented DNA was subsequently purified using the DNA Clean and Concentrator-5 Kit (Zymo Research, cat. no. D4014).

Purified samples were combined with NEBNext High-Fidelity 2X PCR Master Mix (New England Biolabs M01541) for amplification. As described,[98] custom primers were used to incorporate Illumina adaptors and index sequences into sample fragments. Libraries were sequenced by Apoorva Baluapuri on an Illumina NextSeq 550 using paired-end 36 bp reads.

RNA-seq Library Preparation

H1299 and A549 cells were treated in triplicate with 5 μM BRM014 for 12 hours. Cells were harvested and resuspended in 500 μL TRIzol. To each sample an equal amount of the ERCC spike-in was added per cell to allow absolute quantification. RNA was extracted by chloroform precipitation and DNase (Invitrogen DNase I 18068015) treated. 500 ng of total RNA was used to make libraries with the TruSeq Stranded Total RNA Gold sequencing kit (Illumina 20020598). Two modifications to the manufacturer's protocol were made. First, Superscript III was used rather than SuperScript II for the reverse transcription. Second, the A549 and H1299 samples were subject to 9 and 8 cycles of PCR amplification, respectively. Libraries were sequenced at The Bauer Core Facility at Harvard University on an Illumina NovaSeq using an SP flow cell and a paired-end 100-bp cycle run.

Generation of *EP400*-KO A549 cells

Alt-R CRISPR-Cas9 crRNA targeting EP400 was ordered from IDT and annealed with ATTO550-labelled Alt-R tracrRNA (IDT 1072533), in an equimolar mixture at a final concentration of 100 μM. 1 μL of annealed RNAs was incubated with 1 μL of 10 mg/mL Cas9 protein (PNA Bio # CP01-200) at room temperature (22°C) for 25 minutes. The resultant riboprotein complex was introduced into cells by nucleofection (4D-Nucleofector X unit, Lonza bioscience), using the SF cell line kit and A549 cell program (CM 130). Two days after nucleofection, single cells positive for ATTO550 were isolated by fluorescence-activated cell sorting (FACS). After expanding single cell clones, homozygous disruption of *EP400* was confirmed by PCR of genomic DNA flanking the Cas9 cut site and Sanger sequencing. Sanger sequencing traces were compared using Inference of CRISPR Edits (ICE).[99] Wildtype and clonal cell lines were then interrogated for *EP400* expression. To analyze mRNA expression, RNA was extracted using the Direct-zol RNA miniprep kit (VWR 76211-340). cDNA synthesis was performed using hexamer primers and SuperScript IV Reverse Transcriptase (Thermo Fisher 18090010). Processed samples were then subjected to RT-qPCR analysis using primer pairs targeting *EP400* and *ACTB* for normalization.

Generation of EP400 shRNA and Cas9 guide pools

Virus production

HEK293T cells were used to package lentiviruses. HEK293Ts were co-transfected with 500 ng of packaging plasmid (psPAX2), 50 ng envelope plasmid (pMD2.G) and 500 ng of the desired lentivirus construct using the TransIT-LT1 transfection reagent. The following day, the media was exchanged for high-serum (30%) DMEM media. Virus was collected from the supernatant over the following 2 days, and the fractions were pooled. The collected virus suspension was spun at 1250 rpm for 5 minutes, and the supernatant was aliquoted and stored at -80°C until use.

shRNA lentivirus transduction

MV411 cells were transduced with lentivirus expressing GFP (TRCN0000231782, no shRNA), control shRNA (TRCN0000072181, target: ACAACAGCCACAACGTCTATA), shRNA EP400 #1 (TRCN0000312676, target: CAGCCGTACCACAGGTATAAA), and shRNA EP400 #2 (TRCN0000312686, target: AGCACTGGGAAAGATATAATT). For transductions, 1.5 million MV411 cells were spinfected with 300 μL lentivirus and 8 μg/mL polybrene, spinning at 900 x g for 2 hours. Virus-containing cells were selected for by 2 μg/mL puromycin.

Cas9 guide lentivirus transduction

H1299 cells were transduced with EP400-targeting guide virus BRDN0003483852 (guide: GTCATTGTCATAAAACACGA), while MOLM13 and LNCaP cells were transduced with EP400-taragеting guide virus BRDN0003790195 (guide: AGTGGTCATA AGGTTACACA). All cell lines were transduced with the non-targeting guide virus BRDN0002985967 (guide: TCTCGTAG CCTAATGCGCCA). For MOLM13 transductions, 1.5 million cells were spinfected with 300 μL lentivirus and 8 μg/mL polybrene, spinning at 900 x g for 2 hours. For LNCaP and H1299 cells, cells were plated with virus. For Cas9 guide experiments, cells were first transduced with the Cas9 expressing lentivirus (pXPR101) followed by treatment with 8 μg/mL blasticidin to select for Cas9-expressing cells. The Cas9-expressing pool of cells was then transduced with guide expressing lentivirus, followed by treatment with 2 μg/mL puromycin to select for cells expressing the guides.

Cell Proliferation Assays

For adherent cells (A549, H1299 and LNCaP), control and EP400-depleted cells were plated in 100 μL media in 96 well plates. The following day, cells were treated with BRM014 or AU-15330, then assayed after 8 days. For suspension cells (MOLM13), cells were diluted into 100 μL media in 96 well plates, treated the same day with BRM014, and assayed after 8 days. Cell growth was determined using Cell Titer-Glo 2.0 Cell Viability Assay (Promega G9242). IC50 values were calculated in Prism using a four-parameter non-linear fit inhibitor vs response model. For MV411 competition assays, shRNA expressing cells were mixed with 15% GFP-expressing control cells. These were plated in 24-well plates and treated with DMSO or 50 nM BRM014. After 8 days the percentage of GFP-expressing cells was measured by flow cytometry.

QUANTIFICATION AND STATISTICAL ANALYSIS

mESC ATAC-seq data processing and mapping

All custom scripts described here are accessible at Zenodo (DOIs listed in the key resources table). Cutadapt 1.14[89] was used to trim paired-end reads to 40 bp to remove adaptor sequences and low-quality reads. In order to identify spike-in reads, read pairs were next aligned to the *D. melanogaster* genome (dm6) using bowtie 1.2.2 (-k1 -v2 -X1000, —best -3 1 -p 5 —allow-contain —un).[85] All reads that failed to align to the spike genome were subsequently aligned to the *M. musculus* genome (mm10) using bowtie 1.2.2 (-k1 -v2 -X1000 —best -3 1 -p 5 -S —allow-contain). The markdup tool (samtools 1.9)[91] was used to flag duplicate reads, which were then discarded. Fragments were filtered to retain unique reads between 10 and 150 bp, representing regions of accessible chromatin, which were then converted to bedGraph format using the custom script extract_fragments.pl. As the replicate samples were highly correlated across ATAC-seq peaks and spike-in return rates were generally consistent across mESC samples, biological replicates were merged and depth-normalized using the custom scripts bedgraphs2stdBedGraph.pl and normalize_bedGraph.pl. Data was binned in 50 bp windows to generate bedGraph files for UCSC Genome Browser visualization and downstream analysis. Mapped reads and Spearman correlations between replicates are shown below:

Sample	Total reads	Number of mapped reads	Replicate Spearman correlations (reads summed +/- 300 bp from peak centers)
mESC WT ATAC-seq rep1	62697825	40927157	0.94-0.96
mESC WT ATAC-seq rep2	58980583	36080172	0.94-0.96
mESC WT ATAC-seq rep3	168574624	100198015	0.94-0.96
mESC WT ATAC-seq rep4	46502293	27779825	0.94-0.96
mESC DMSO 2h ATAC-seq rep1	130212716	64415064	0.92-0.93
mESC DMSO 2h ATAC-seq rep2	157163723	92364211	0.92-0.93
mESC DMSO 2h ATAC-seq rep3	101477699	48635293	0.92-0.93
mESC BRM014 2h ATAC-seq rep1	69377420	42103200	0.94-0.95
mESC BRM014 2h ATAC-seq rep2	56773634	29270581	0.94-0.95
mESC BRM014 2h ATAC-seq rep3	10070588	5522290	0.94-0.95
mESC DMSO 4h ATAC-seq rep1	31363319	17925819	0.94
mESC DMSO 4h ATAC-seq rep2	40843256	18687002	0.94
mESC BRM014 4h ATAC-seq rep1	16319382	8573425	0.94
mESC BRM014 4h ATAC-seq rep2	28491265	16413884	0.93
mESC DMSO 8h ATAC-seq rep1	19153700	9695625	0.92-0.94
mESC DMSO 8h ATAC-seq rep2	29033108	12731907	0.92-0.94
mESC DMSO 8h ATAC-seq rep3	30886422	13344105	0.92-0.94
mESC BRM014 8h ATAC-seq rep1	24320127	11377650	0.94-0.94
mESC BRM014 8h ATAC-seq rep2	34579052	17553798	0.94-0.94
mESC BRM014 8h ATAC-seq rep3	62829283	35207217	0.94-0.94
mESC siNT DMSO 4h ATAC-seq rep1	32310317	24645541	0.95
mESC siNT DMSO 4h ATAC-seq, rep2	29360108	22036024	0.95
mESC siNT BRM014 4h ATAC-seq rep1	29177680	13353373	0.94
mESC siNT BRM014 4h ATAC-seq rep2	43344493	32931732	0.94
mESC siEP400 DMSO 4h ATAC-seq rep1	31235724	22889689	0.93-0.95
mESC siEP400 DMSO 4h ATAC-seq rep2	27756232	20984256	0.93-0.95
mESC siEP400 DMSO 4h ATAC-seq rep3	27405134	20467472	0.93-0.95

(*Continued on next page*)

Continued

Sample	Total reads	Number of mapped reads	Replicate Spearman correlations (reads summed +/- 300 bp from peak centers)
mESC siEP400 BRM014 4h ATAC-seq rep1	25189856	18890986	0.92-0.95
mESC siEP400 BRM014 4h ATAC-seq rep2	36974588	27560990	0.92-0.95
mESC siEP400 BRM014 4h ATAC-seq rep3	26767737	18633718	0.92-0.95

PRO-seq data processing and mapping

All custom scripts described here are accessible at Zenodo (DOIs listed in the key resources table). The custom script trim_and_filter_PE.pl was used to trim FASTQ files to 41 bp and remove read pairs with minimum average base quality scores below 20. Subsequent removal of adaptor sequences and low-quality reads was performed using cutadapt 1.14, and any reads shorter than 20 nt were discarded. The 3'-most nucleotide was removed from each trimmed read, after which bowtie (1.2.2) was used to map reads to the *Drosophila* dm6 genome (-k1 -v2 -best -X100 –un) and determine spike return across samples. Unaligned reads were mapped to the mm10 reference genome using the same parameters. Uniquely aligned read pairs were separated, and the custom script bowtie2stdBedGraph.pl was used to generate single-nucleotide resolution bedGraph files based on 3' end mapping positions. Biological replicates were depth normalized using the custom script normalize_bedGraph.pl. As biological replicates were highly correlated (as indicated in the table below) replicates were merged using the custom script bedgraphs2stdbedGraph.pl, and data was binned in 50 bp windows.

Sample	Total reads	Number of mapped reads	Replicate Spearman correlations (reads summed from TSS to +150 nt)
mESC DMSO 4h PRO-seq rep1	82516247	56488766	0.97
mESC DMSO 4h PRO-seq rep2	92652645	59095009	0.97
mESC DMSO 8h PRO-seq rep1	96563644	70835757	0.97
mESC DMSO 8h PRO-seq rep2	101470974	75493782	0.97
mESC BRM014 2h PRO-seq rep1	94431263	40923008	0.94
mESC BRM014 2h PRO-seq rep2	94658080	45160907	0.94
mESC BRM014 4h PRO-seq rep1	101647384	75810022	0.97
mESC BRM014 4h PRO-seq rep2	132694572	98250874	0.97
mESC BRM014 8h PRO-seq rep1	97770657	73572986	0.96
mESC BRM014 8h PRO-seq rep2	108501424	82388844	0.96

Genome annotation

Transcription start sites

Genome-wide annotation of active transcripts and associated dominant transcription start site (TSS) and transcription end site (TES) locations was performed using the publicly available GetGeneAnnotations (GGA) pipeline (DOI listed in the key resources table). Briefly, GGA uses the 5' end of PRO-seq reads to call TSSs and assign the dominant TSS for each gene. RNA-seq transcript isoform expression, quantified by kallisto (version 0.45.1),[92] is then used to identify the most commonly used TES for each gene. GGA also enables comprehensive annotation of non-dominant TSSs and divergent obsTSSs (uaTSSs) associated with expressed genes. For this analysis, a total of 18,339 dominant and 1,671 non-dominant TSSs (and their associated TESs) were defined by GGA.

RNA Biotype Analysis

Biotypes were derived from Ensembl annotations for mouse assembly GRCm38,p6 (v102).[100] Promoters associated with biotypes in the "protein coding" category were designated as mRNA genes. Promoters associated with biotypes in the "long noncoding" and "short noncoding" categories were designated as ncRNA genes. Promoters associated with biotypes in the "pseudogene" category were designated as pseudogenes.

Candidate enhancer identification

To identify putative regulatory elements, peaks of bidirectional transcription were called from PRO-seq data using the dREG analysis tool[90] under default parameters, generating a list of significant peaks (FDR < 0.05) with associated dREG scores, p-values, and peak center coordinates. Gene-distal elements (greater than 1.5 kb from a gene TSS) were retained as putative enhancers for downstream analysis. Peaks were subsequently filtered by read count, with peaks required to contain a minimum of 30 PRO-seq reads, giving rise to a final list of 71,330 dREG-identified candidate enhancer peaks.

Peak calling and filtering

Final bed files from untreated mESC ATAC-seq libraries (N=4) were merged for peak-calling with HOMER (4.10.3) findPeaks using the "-style factor" argument.[93] An initial list of 141,175 peaks was generated by this analysis, which was then filtered by peak score > 4.5 to generate a final list of 83,201 peaks. The HOMER annotatePeaks.pl command was used to associate each peak with nearby TSSs, as defined above. Peaks that were located within 1.5 kb of a dominant TSS (n = 17,160) were classified as proximal and shifted to center the associated TSS before subsequent analysis. After removal of duplicate TSSs, a final list of 13,536 sites was produced. For clarity, peaks that were located within 1.5 kb of a non-dominant TSS (n = 768) were excluded from further analysis. Remaining peaks were classified as distal (n = 65,273). Peaks that were located within 500 bp of a dREG-identified candidate enhancer were classified as enhancers (n = 32,149) and retained for analysis. To facilitate analysis of promoter-enhancer coordination, the HOMER annotatePeaks.pl command was also used to associate each promoter with its nearest enhancer and vice versa.

BRG1 ChIP-seq data processing and mapping

All custom scripts described here are accessible at Zenodo (DOIs listed in the key resources table). Adapter sequences were trimmed using cutadapt 1.14. Reads were first aligned to the *Drosophila* dm6 genome using bowtie 1.2.2, after which unaligned reads were mapped to the mm10 reference genome using analogous parameters. The custom script extract_fragments.pl was used to generate a final bedGraph file for each sample using uniquely mapped reads between 50 and 500 bp. 2 h BRM014- and DMSO-treated BRG1 ChIP-seq samples differed significantly in terms of spike-in read return. Therefore, the custom script normalize_bedGraph.pl was used to normalize individual libraries. For 4 h BRM014- and DMSO-treated BRG1 ChIP-seq samples, no significant difference in spike-in read return was seen, and samples were depth-normalized using the custom script normalize_bedGraph.pl. As biological replicates were highly correlated (as indicated in the table below) replicates were merged using the custom script bedgraphs2stdbedGraph.pl, and data was binned in 50 bp windows.

Sample	Total reads	Number of mapped reads	Replicate Spearman correlations (reads summed +/- 500 bp from TSS)
mESC DMSO 2h ChIP-seq BRG1 rep1	64215668	50979397	0.92
mESC DMSO 2h ChIP-seq BRG1 rep2	64177288	50292050	0.92
mESC BRM014 2h ChIP-seq BRG1 rep1	64271407	51100557	0.95
mESC BRM014 2h ChIP-seq BRG1 rep2	74916410	59849481	0.95
mESC DMSO 4h ChIP-seq BRG1 rep1	38211742	29750352	0.8-0.86
mESC DMSO 4h ChIP-seq BRG1 rep2	37114825	29381300	0.8-0.86
mESC DMSO 4h ChIP-seq BRG1 rep3	28759029	23505743	0.8-0.86
mESC BRM014 4h ChIP-seq BRG1 rep1	46768229	36425379	0.8-0.91
mESC BRM014 4h ChIP-seq BRG1 rep2	39886870	31863514	0.8-0.91
mESC BRM014 4h ChIP-seq BRG1 rep3	32806163	26167224	0.8-0.91

EP400 ChIP-seq data processing and mapping

All custom scripts described here are accessible at Zenodo (DOIs listed in the key resources table)[101]. Adapter sequences were trimmed using cutadapt 1.14. Reads were first aligned to the *Drosophila* dm6 genome using bowtie 1.2.2, after which unaligned reads were mapped to the mm10 reference genome using analogous parameters. The custom script extract_fragments.pl was used to generate a final bedGraph file for each sample using uniquely mapped reads between 50 and 500 bp. As no significant difference in spike-in read return was seen, samples were depth normalized using the custom script normalize_bedGraph.pl. As biological replicates were positively correlated (as indicated in the table below) replicates were merged using the custom script bedgraphs2stdbedGraph.pl, and data was binned in 50 bp windows.

Sample	Total reads	Number of mapped reads	Replicate Spearman correlations (reads summed +/- 5000 bp from TSS)
mESC DMSO 2h ChIP-seq EP400 rep1	24719193	20173843	0.47
mESC DMSO 2h ChIP-seq EP400 rep2	25007427	20098880	0.47
mESC BRM014 2h ChIP-seq EP400 rep1	26191431	21314430	0.51
mESC BRM014 2h ChIP-seq EP400 rep2	22408586	17690065	0.51
mESC DMSO 4h ChIP-seq EP400 rep1	24383212	19737328	0.56-0.58
mESC DMSO 4h ChIP-seq EP400 rep2	24480704	19970222	0.56-0.58

(*Continued on next page*)

Continued

Sample	Total reads	Number of mapped reads	Replicate Spearman correlations (reads summed +/- 5000 bp from TSS)
mESC DMSO 4h ChIP-seq EP400 rep3	25860987	20841903	0.56-0.58
mESC BRM014 4h ChIP-seq EP400 rep1	27054324	19064718	0.52-0.54
mESC BRM014 4h ChIP-seq EP400 rep2	24801234	19872439	0.52-0.54
mESC BRM014 4h ChIP-seq EP400 rep3	25562190	20687107	0.52-0.54

Genome browser images

All genome browser images were generated from the UCSC Genome Browser (http://genome.ucsc.edu/)[102] using genome build GRCm38/mm10.

Metagenes and heatmaps

Composite metagene plots were generated by summing reads in 50 bp/nt bins at each indicated position relative to the TSS (promoters) or peak center (enhancers) using the custom script make_heatmap.pl (DOI listed in the key resources table),[101] then dividing by the total number of sites. For PRO-seq data, 17 rRNA loci with aberrantly high signal were removed before final composite metagene plots were generated. Heatmaps were generated using Partek Genomics Suite (version 6.16.0812) from matrices summing reads in 50 bp/nt bins +/- 2 kb relative to the TSS (promoters) or peak center (enhancers). ΔATAC-seq and ΔPRO-seq heatmaps were generated by subtracting DMSO matrix values from the matrix values of the associated BRM014-treated sample, such that negative values correspond to regions of reduced signal following BRM014 treatment, and positive values correspond to regions of increased signal following BRM014 treatment. To order heatmaps, ATAC-seq signal from BRM014- and DMSO-treated samples was summed over a 600 bp window (-450 to +149 bp relative to TSS for promoters, -300 to +299 bp relative to peak center for enhancers). The raw difference in signal (# reads BRM014 - # reads DMSO) was calculated for each site at each time point, and sites were ranked in ascending order such that sites with the largest losses of signal are oriented at the top of the heatmap, and sites with the largest gains of signal are oriented at the bottom of the heatmap. For plot of relative BRG1 signal at promoters, BRG1 ChIP-seq reads for each promoter were summed from -750 to +149 bp relative to the TSS. For plot of relative BRG1 signal at enhancers, BRG1 ChIP-seq reads for each enhancer were summed from +/- 500 bp relative to the peak center. With sites ranked by difference in ATAC-seq signal after 2 h BRM014, pruning was performed in Prism 8 (8.4.3) to report average values over 10 rows. Data was smoothed across adjacent bins, and minimum and maximum values were used to normalize values across a range of 0 to 1.

Clustering

Partek Genomics Suite (6.16.0812) was used to perform partitioning (k-means) clustering on all promoters (n = 13,536) based on relative ATAC-seq signal (normalized to DMSO control) across the BRM014 treatment time course (summed over a 600 bp window from -450 to +149 relative to the TSS). This analysis defined four promoter clusters (designated as clusters 1-4) for downstream analysis. Heatmaps of relative ATAC-seq and PRO-seq signal by cluster were generated based on relative signal over the windows described above. Values were $\log_2$-transformed, and sites were ordered based on cluster assignment as indicated. Sites within each cluster were unranked.

Relative Accessibility Analysis

Relative accessibility was calculated as the ratio of ATAC-seq signal in BRM014-treated samples compared to matched DMSO controls. For promoters, signal was summed from -450 to +149 bp relative to the TSS. For enhancers, signal was summed from -300 to +299 bp relative to the enhancer peak center. Values were $\log_2$-transformed before plotting.

Relative PRO-seq Analysis

Relative promoter-proximal PRO-seq was calculated as the ratio of sense-strand PRO-seq signal from the TSS to +149 nt in BRM014-treated samples compared to matched DMSO controls. Relative gene-body PRO-seq signal was calculated as the ratio of sense-strand PRO-seq signal from +250 nt downstream of the TSS until one of the following conditions was met: (1) 500 bp upstream of the nearest enhancer; (2) the TES (as defined by GGA); or (3) a maximum of 5 kb. Relative enhancer PRO-seq signal was calculated as the ratio of PRO-seq signal on both strands in a window of -300 bp to +299 bp relative to the enhancer peak center. All values were $\log_2$-transformed before plotting.

Differential Gene Expression Analysis

For each condition, PRO-seq 3' read positions around each gene were counted from the dominant TSS+250 nt to the dominant TES. Sense PRO-seq reads were then counted for each gene and used as input for differential gene expression analysis, using DEseq2 to

compare counts from each BRM014 treatment timepoint to those of matched DMSO controls. Up- and down-regulated genes were defined as genes exhibiting an increase or decrease of greater than 1.5-fold with BRM014 treatment, with an adjusted *P* value < 0.001.

Gene Ontology Analysis

Gene ontology analysis was performed using the Database for Annotation, Visualization and Integrated Discovery (DAVID) v6.8 (https://david.ncifcrf.gov/home.jsp) under default parameters.[94,95] Cluster 2 was designated as background, and cluster 1 was input as a gene list for analysis.

Analysis of Publicly Available mESC Data

Previously published MNase-seq data[28] were downloaded from the NCBI Gene Expression Omnibus as GSE85191 and aligned to mm10 according to the parameters described.[103,104] MNase-seq data from control cells and cells treated with BRM014 for 24 h were downloaded as normalized wig files (GSE158345).[21] Replicates were merged and converted to bedGraph format for metagene analysis. ATAC-seq data from control cells and BRG1-KO cells[8] were downloaded (GSE87822) as FASTQ files and mapped according to the parameters described above. Promoter accessibility was calculated by summing signal from -450 to +149 bp relative to the TSS, and relative accessibility was calculated as the ratio of signal in BRG1 KO samples vs. control. Values were $\log_2$-transformed before plotting. TT-seq data[34] were downloaded (GSE178230) and processed as described for PRO-seq data through mapping to the spike genome, after which STAR (v. 2.7.3a)[86] was used to align data to the mm10 mouse genome. H3K4me3 ChIP-seq data were downloaded from the same source and processed as described above. Associated H3K27ac ChIP-seq data were retrieved through the 4DN Data Portal (https://data.4dnucleome.org/) at accession no. 4DNESQ33L4G7. Published H3K4me1 ChIP-seq data[35] were downloaded from GSE56098. ChIP-seq data for CHD1, CHD2, CHD4, and EP400[3] were downloaded from GSE64825. TIP60 ChIP-seq data[62] were downloaded from GSE69671. SNF2H ChIP-seq data[61] were downloaded from GSE123670. All samples were processed as described above. Processed data for CTCF ChIP-seq were downloaded from GSE137272. Processed data for OCT4, SOX2, and NANOG ChIP-seq were downloaded from GSE87822. CpG Island and GC Percent data tracks for the mm10 genome were downloaded from the UCSC Genome Browser Database as bedGraph files using the Table Browser tool.[44] Previously published classifications were used to define bivalent genes,[105] and the Ensembl BioMart[100] was used to match Refseq and Ensembl gene IDs.

Cancer Cell Line RNA-seq and ATAC-seq Analysis

RNA-seq analysis

RNA-seq FASTQ data files from control and BRM014/AU-15330 treated samples MV411 (SRP350415[48]), MOLM13 (SRP350415[48]), LNCaP (SRP313558[25]), VCaP (SRP313558[25]), BT869 (SRP395732[52]), and DIPG007 (SRP432122[53]) cells were downloaded from the sequence read archive. GetGeneAnnotations (GGA) scripts (DOI listed in the key resources table)[106] were used to annotate dominant active TSS and TES positions from the downloaded datasets as well as our A549, and H1299 RNA-seq data. To quantify gene expression changes following BRM014 or AU-15330 treatment, RNA-seq samples were mapped to the hg38 genome using STAR version 2.7.3a.[86] Gene counts were generated using featurecounts function of the Rsubread package version 2.0.1,[87] and $\log_2$ fold-change following BRM014 or AU-15330 treatment calculated with DESeq2 version 1.26.0.[88] Protein-coding genes were filtered for a minimum of 0.3 FPKM counts in at least one condition and promoter ATAC-seq reads above the bottom 5th percentile.

MV411 ATAC-seq data processing and mapping

All custom scripts described here are accessible at Zenodo (DOIs listed in the key resources table).[101] Cutadapt 1.14[89] was used to remove adaptor sequences and low-quality reads. In order to identify spike-in reads, read pairs were next aligned to the *D. melanogaster* genome (dm6) using bowtie 1.2.2 (-k1 -v2 -X1000, –best –p 5 –allow-contain).[85] All reads that failed to align to the spike genome were subsequently aligned to the *H. sapiens* genome (hg38) using bowtie 1.2.2 (-k1 -v2 -X1000 –best -p 5 -S –allow-contain). Fragments were deduplicated and filtered to retain unique reads between 10 and 150 bp, representing regions of accessible chromatin, which were then converted to bedGraph format using the custom script extract_fragments.pl. As spike returns were consistently elevated in BRM014 and AU-5330 treated conditions, samples were spike-normalized using the custom script normalize_bedGraph.pl. Replicate samples were highly correlated across ATAC-seq peaks, so biological replicates were merged using the custom scripts bedgraphs2stdBedGraph.pl. Data was binned in 50 bp windows to generate bedGraph files for UCSC Genome Browser visualization and downstream analysis. Mapped read counts and Spearman correlations between replicates are shown below:

Sample	Total reads	Number of mapped reads	Replicate Spearman correlations (reads summed +/- 300 bp from peak centers)
MV411_ATACseq_1h_AU15330_rep1	17422822	15638875	0.96-0.97
MV411_ATACseq_1h_AU15330_rep2	17463612	15637034	0.96-0.97
MV411_ATACseq_1h_AU15330_rep3	17030548	15172048	0.96-0.97

(*Continued on next page*)

Continued

Sample	Total reads	Number of mapped reads	Replicate Spearman correlations (reads summed +/- 300 bp from peak centers)
MV411_ATACseq_1h_BRM014_rep1	17983974	16124142	0.96-0.97
MV411_ATACseq_1h_BRM014_rep2	17557774	15525055	0.96-0.97
MV411_ATACseq_1h_BRM014_rep3	19013075	17070772	0.96-0.97
MV411_ATACseq_1h_DMSO_rep1	11644740	10730855	0.90-0.91
MV411_ATACseq_1h_DMSO_rep2	15019014	13746773	0.90-0.91
MV411_ATACseq_1h_DMSO_rep3	15889335	14655099	0.90-0.91
MV411_ATACseq_2h_AU15330_rep1	17640274	15733692	0.96
MV411_ATACseq_2h_AU15330_rep2	21036807	18638757	0.96
MV411_ATACseq_2h_AU15330_rep3	16834928	15168706	0.96
MV411_ATACseq_2h_BRM014_rep1	19578571	17485150	0.96
MV411_ATACseq_2h_BRM014_rep2	17979067	16146574	0.96
MV411_ATACseq_2h_BRM014_rep3	18235185	16305432	0.96
MV411_ATACseq_2h_DMSO_rep1	13803920	12357528	0.87-0.92
MV411_ATACseq_2h_DMSO_rep2	17806159	16185591	0.87-0.92
MV411_ATACseq_2h_DMSO_rep3	16447045	15102912	0.87-0.92
MV411_ATACseq_4h_AU15330_rep1	21720994	19523743	0.93-0.95
MV411_ATACseq_4h_AU15330_rep4	15449037	13716501	0.93-0.95
MV411_ATACseq_4h_AU15330_rep5	15383362	13514610	0.93-0.95
MV411_ATACseq_4h_BRM014_rep1	19981587	17948468	0.94-0.95
MV411_ATACseq_4h_BRM014_rep4	12678223	11176617	0.94-0.95
MV411_ATACseq_4h_BRM014_rep5	17610603	15617695	0.94-0.95
MV411_ATACseq_4h_DMSO_rep1	15764713	14501673	0.88-0.91
MV411_ATACseq_4h_DMSO_rep4	14062481	12752247	0.88-0.91
MV411_ATACseq_4h_DMSO_rep5	12506852	11431714	0.88-0.91
MV411_ATACseq_8h_AU15330_rep1	20319858	18244886	0.95-0.96
MV411_ATACseq_8h_AU15330_rep2	18869618	16966018	0.95-0.96
MV411_ATACseq_8h_AU15330_rep3	17132937	15612731	0.95-0.96
MV411_ATACseq_8h_BRM014_rep2	14391283	12960222	0.96
MV411_ATACseq_8h_BRM014_rep3	18788433	17004873	0.96
MV411_ATACseq_8h_DMSO_rep1	16438301	14923545	0.91
MV411_ATACseq_8h_DMSO_rep2	15069431	13845500	0.91
MV411_ATACseq_8h_DMSO_rep3	15904985	14617631	0.91

H3K27ac ChIP-seq analysis

H3K27ac FASTQ data files from control MV411 (GSE82116[50]) cells were downloaded from the sequence read archive. H3K27ac data were mapped to hg38 using the same parameters described above for ChIP-seq mapping in mESCs. H3K27ac peaks were then called with HOMER (4.10.3) findPeaks using the "-style factor" argument.[93]

MV411 Enhancer annotations

MV411 enhancers were annotated similarly to those in mESCs. Briefly, peaks were called on ATAC-seq samples from DMSO treated MV411 cells (N=12) with HOMER (4.10.3) findPeaks using the "-style factor" argument.[93] Peaks located more than 1.5 kb away from a dominant TSS were classified as distal. As transcription correlates tightly with acetylation,[30,107] we used H3K7ac in lieu of dREG peaks. Distal ATAC-seq peaks that were located within 500 bp of a H3K27ac peak were classified as enhancers (n = 36,175) and retained for analysis.

MV411 promoter clustering

The kmeans function in R (3.6.1) was used to cluster promoters (n = 11,022) based on relative ATAC-seq signal ($\log_2$ normalized to DMSO control) across the BRM014 treatment time course (summed over a 600 bp window from -450 to +149 bp relative to the TSS). This analysis initially defined six promoter clusters, but as two sets of clusters were similar in subsequent analyses, these were merged to give 4 final clusters (designated as Clusters 1-4) for downstream analysis. Heatmaps of relative ATAC-seq signal by cluster were generated based on relative signal over the windows described above. Values were $\log_2$-transformed, and sites were ordered based on cluster assignment as indicated. Sites within each cluster were unranked.

Publicly available ATAC-seq analysis

ATAC-seq FASTQ data files from control MV411 (GSE190721[48]), MOLM13 (GSE190721[48]), LNCaP (GSE171523[25]), VCaP (GSE171523[25]), A549 (GSE169955[81]), H1299 (GSE141060[83]), BT869 (GSE212718[52]), and DIPG007 (GSE229452[53]) cells were downloaded from the sequence read archive. ATAC-seq data were mapped to hg38 using the same parameters described above for ATAC-seq mapping in mESCs. ATAC-seq counts for each gene were summed in a window of -500 bp to +499 bp around the dominant TSS.

H3K4me1 ChIP-seq analysis

H3K4me1 ChIP-seq FASTQ data files from control MV411 (GSE168647[51]), MOLM13 (GSE154985[84]), LNCaP (GSE122922[80]), VCaP (GSE148400[79]), A549 (GSE169955[81]), and H1299 (DRR016953[82]) cells were downloaded from the sequence read archive (see key resource table). ATAC-seq data were mapped to hg38 using the same parameters described above for mapping in mESCs. ATAC-seq counts for each gene were summed in a window of -500 bp to +499 bp around the dominant TSS.

Predicting genes sensitive or resistant to SWI/SNF inhibition

H3K4me1 and ATAC-seq were used to predict genes sensitive or resistant to SWI/SNF perturbation by BRM014 or AU-15330. Genes with promoter H3K4me1 in the top 15% and ATAC-seq in the bottom 15% were predicted to be sensitive. Genes with promoter H3K4me1 in the bottom 15% and ATAC-seq signal in the top 15% were predicted to be resistant. For ATAC-seq only predictions, genes in the bottom and top 5% ATAC-seq signal were predicted to be sensitive and resistant respectively. The number of genes predicted to be sensitive or resistant in each cell line is shown below:

Cell line	Prediction	Number of genes
MV411	Sensitive – H3K4me1 + ATAC-seq	678
MOLM13	Sensitive – H3K4me1 + ATAC-seq	574
A549	Sensitive – H3K4me1 + ATAC-seq	634
H1299	Sensitive – H3K4me1 + ATAC-seq	204
LNCaP	Sensitive – H3K4me1 + ATAC-seq	364
VCaP	Sensitive – H3K4me1 + ATAC-seq	567
MV411	Resistant – H3K4me1 + ATAC-seq	234
MOLM13	Resistant – H3K4me1 + ATAC-seq	514
A549	Resistant – H3K4me1 + ATAC-seq	370
H1299	Resistant – H3K4me1 + ATAC-seq	327
LNCaP	Resistant – H3K4me1 + ATAC-seq	252
VCaP	Resistant – H3K4me1 + ATAC-seq	444
MV411	Sensitive – ATAC-seq	624
MOLM13	Sensitive – ATAC-seq	550
A549	Sensitive – ATAC-seq	604
H1299	Sensitive – ATAC-seq	593
LNCaP	Sensitive – ATAC-seq	677
VCaP	Sensitive – ATAC-seq	704
BT869	Sensitive – ATAC-seq	668
DIPG007	Sensitive – ATAC-seq	586
MV411	Resistant – ATAC-seq	573
MOLM13	Resistant – ATAC-seq	550
A549	Resistant – ATAC-seq	598
H1299	Resistant – ATAC-seq	593
LNCaP	Resistant – ATAC-seq	580
VCaP	Resistant – ATAC-seq	668
BT869	Resistant – ATAC-seq	670
DIPG007	Resistant – ATAC-seq	582

DepMap analysis of SWI/SNF subunit mutations

Cell line gene mutation data were downloaded from the DepMap[108] (“OmicsSomaticMutations.csv” and "Model.csv" files downloaded May 23, 2023 from: https://depmap.org/portal/download/all/). Mutations in SWI/SNF subunits (SMARCA4, SMARCA2, SMARCB1, SMARCC1, SMARCC2, SMARCE1, SMARCD1, SMARCD2, SMARCD3, BCL7A, BCL7B, BCL7C, DPF1, DPF2, DPF3,

ARID1A, ARID1B, SS18, BCL11A, BCL11B, ARID2, PBRM1, BRD7, PHF10, BRD9, BICRA, BICRAL, ACTL6A, ACTL6B, ACTB) were analyzed in the following cell lines: NCIH1299, A549, MOLM13, MV411, VCAP, LNCAPCLONEFGC, HSJDDIPG007. The splice site mutation of *SMARCA4/BRG1* in H1299 cells is reported to function as a gene knockout.[26,109] While not in the DepMap database, characterization of the BT869 cell revealed no mutations in SWI/SNF subunits.[110]

Box plots and statistical analysis

Box plots were plotted in GraphPad Prism 9.0 (GraphPad Software, San Diego, CA, USA) and have a line at the median, and whiskers show the 10-90th percentiles. P-values were calculated in Prism, using the indicated statistical test, except for the overlap in Venn diagrams which were calculated using the phyper function in R (3.6.1).

Supplemental figures

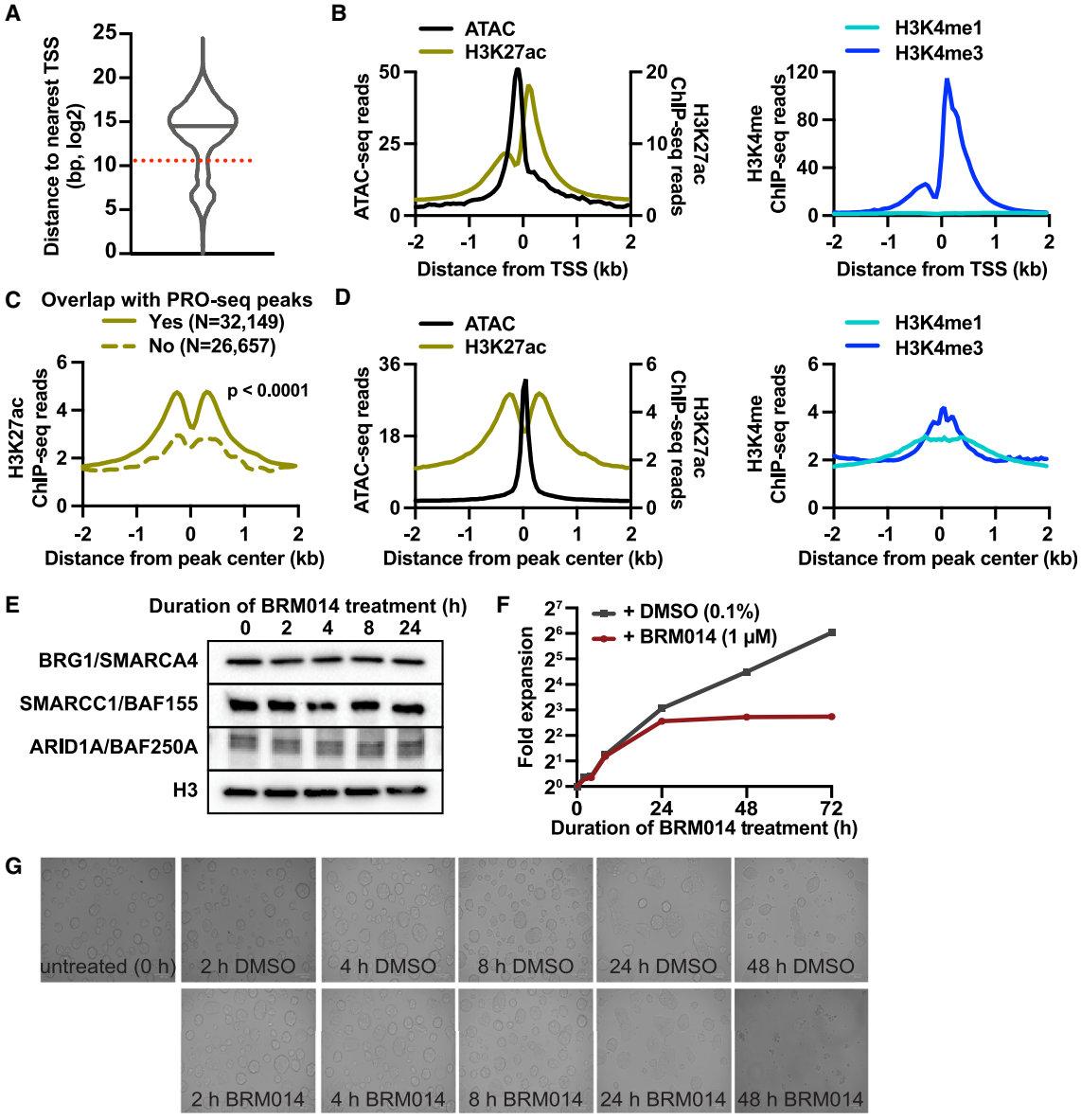

Figure S1. Promoter and enhancer characteristics and effects of BRM014 treatment in mESCs, related to Figure 1

(A) Distribution of distances between all ATAC-seq peaks (n = 83,201) and the nearest active, annotated TSS. Dotted red line indicates 1.5 kb threshold used to separate proximal and distal peaks.

(B) Data are shown around proximal peaks, hereafter referred to as promoter peaks (n = 13,536). Average metagene profiles of ATAC-seq and H3K27ac,[34] H3K4me1[35] and H3K4me3[34] ChIP-seq aligned around the associated TSSs, graphed in 50 bp bins.

(C) H3K27ac ChIP-seq[34] signal at distal ATAC-seq peaks that do or do not overlap with peaks of PRO-seq signal. Data are graphed in 50 bp bins. p values are from Mann-Whitney test, comparing H3K27ac reads ± 500 bp from enhancer center.

(D) For all enhancer peaks (n = 32,149), average profiles of ATAC-seq and H3K27ac,[34] H3K4me1,[35] and H3K4me3[34] ChIP-seq are shown, aligned around peak centers, graphed in 50 bp bins.

(E) Western blots of cells treated with 1 μM BRM014 for the indicated duration using antibodies against BRG1/SMARCA4, SWI/SNF subunits SMARCC1/BAF155 and ARID1A/BAF250A. Histone H3 is shown as a loading control.

(F) Proliferation of mESCs treated with BRM014 or DMSO for the indicated duration.

(G) Bright-field images of mESCs treated with 1 μM BRM014 or 0.1% DMSO for the indicated duration.

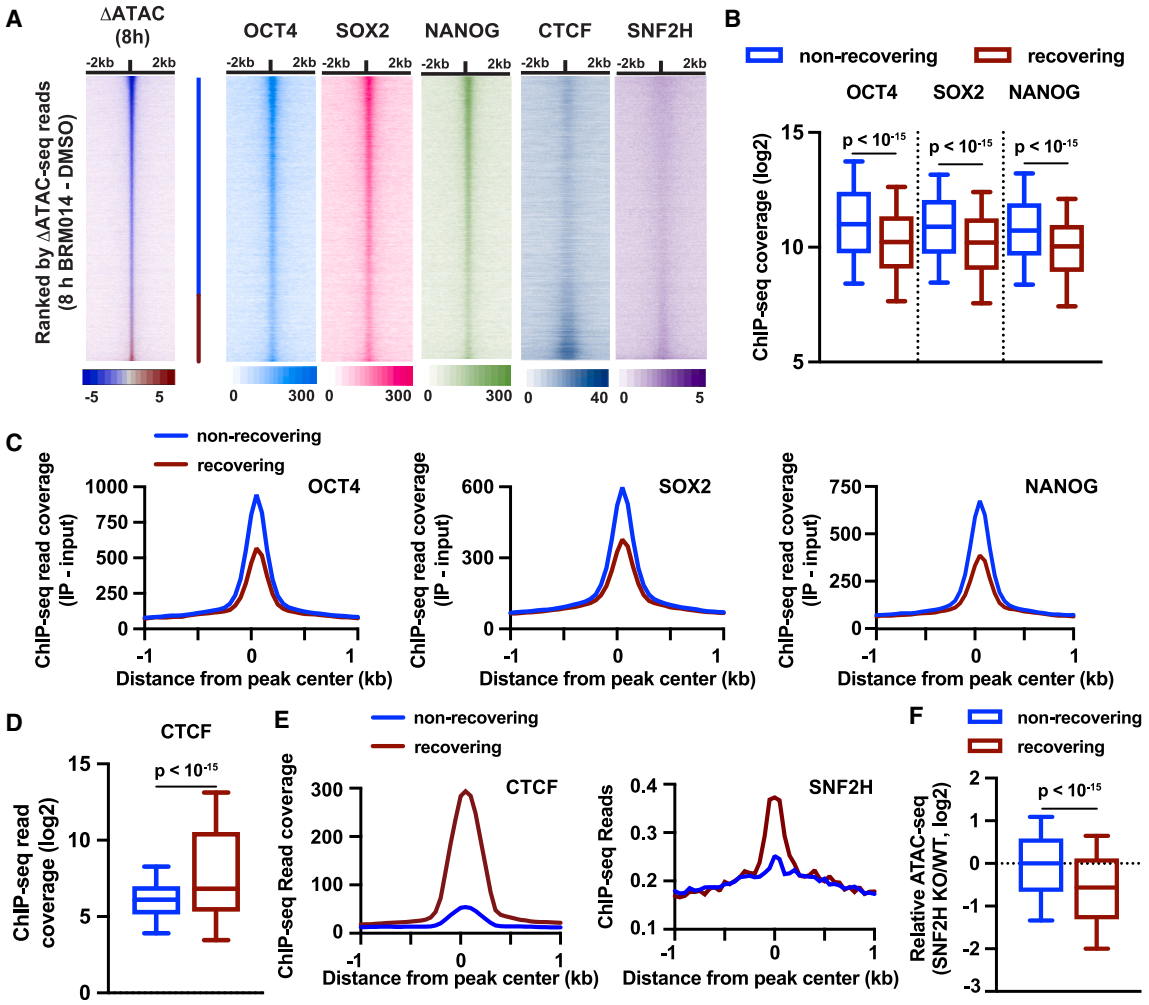

Figure S2. Enhancers bound by pluripotency-associated pioneer factors require SWI/SNF to retain accessibility, whereas SNF2H opens chromatin at CTCF-associated enhancers, related to Figure 1

(A) Heatmap of change in ATAC-seq signal after 8 h BRM014 treatment (ranked as in Figure 1D) across all enhancers is shown alongside heatmaps of ChIP-seq for OCT4,[8] SOX2,[8] NANOG,[8] CTCF,[78] and SNF2H,[61] shown in the same rank order. Data are aligned to the enhancer peak center and summed in 50 bp bins. The blue line indicates the positions of the non-recovering enhancers (N = 24,679) and the red line indicates the recovering enhancers (N = 7,470).

(B) Boxplots of ChIP-seq signals for the indicated factors (±300 bp from enhancer center). Whiskers show the 10–90th percentiles and p values are from Mann-Whitney test.

(C) Metagene plots of average ChIP-seq signal (in 50 bp bins) for the indicated TFs, at enhancers separated by whether they recover accessibility following 8 h of BRM014 treatment.

(D) Boxplots of CTCF[78] ChIP-seq signal (±300 bp from enhancer center). Whiskers show the 10–90th percentiles and p values are from Mann-Whitney test.

(E) Metagene plots of CTCF[78] (left) and SNF2H[61] (right) ChIP-seq signal at enhancers, separated by recovery capacity following BRM014 treatment, graphed in 50 bp bins.

(F) For non-recovering and recovering enhancers, relative change in ATAC-seq signal is shown (peak center ± 300 bp) in SNF2H knockout compared with control.[4] Whiskers show the 10–90th percentiles and p values are from Mann-Whitney test.

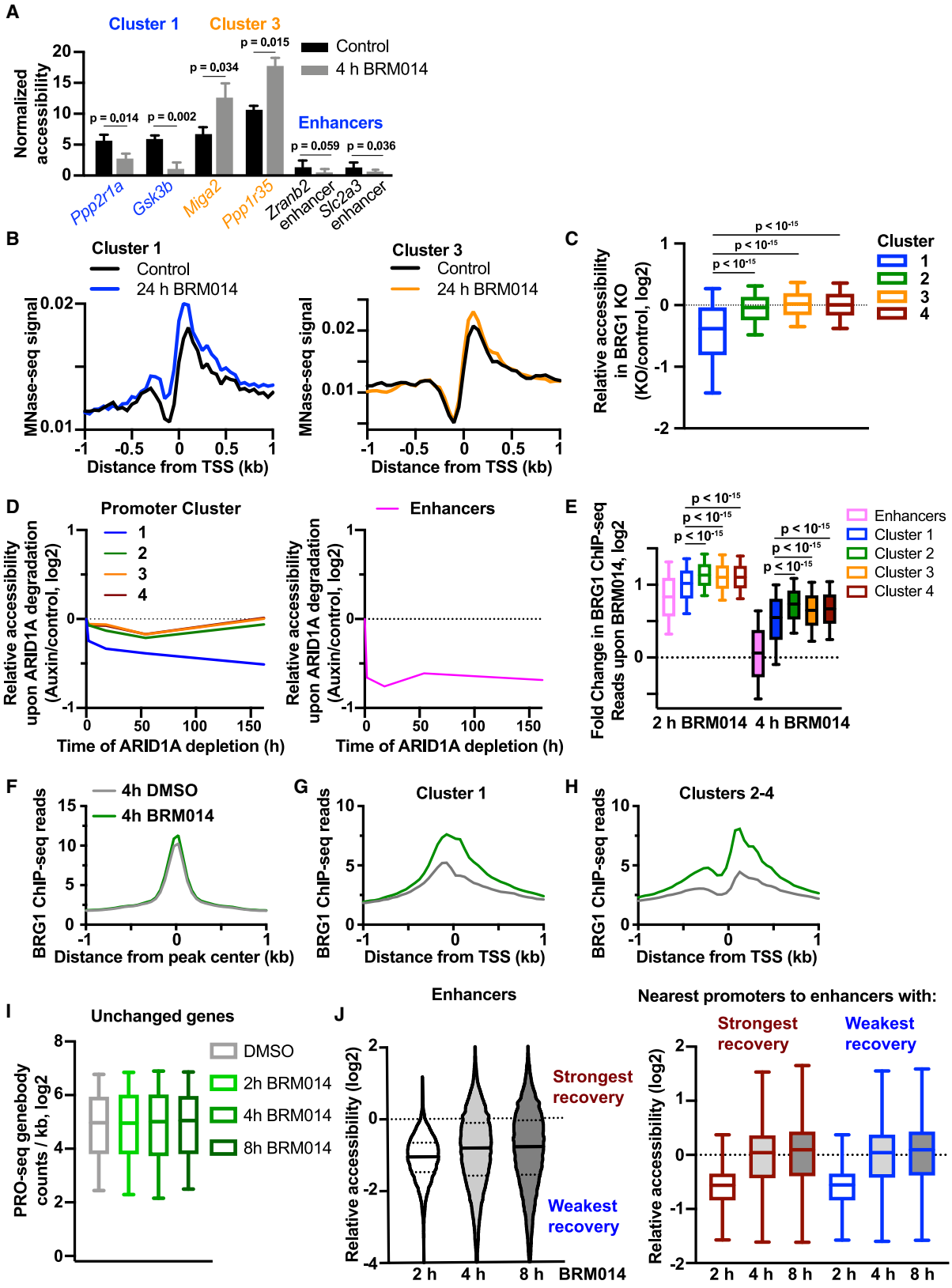

(legend on next page)

Figure S3. Cluster 1 promoters show sustained repression of accessibility in the absence of SWI/SNF remodeling, related to Figures 2 and 3

(A) ATAC-qPCR validation of accessibility changes following 4 h BRM014 treatment at selected promoters without evidence of recovery (cluster 1, *Ppp2r1a*, and *Gsk3b*), promoters with evidence of recovery (cluster 3, *Miga2*, and *Ppp1r35*), and enhancers (*Zranb2* and *Slc2a3* enhancers, neither of which recover). Cq values normalized to background signal of closed chromatin. p values calculated by Student's t test.

(B) Average MNase-seq signal around cluster 1 promoters (left) and cluster 3 promoters (right) in cells subjected to 24 h BRM014 treatment compared with control.[21] Data are graphed in 50 bp bins.

(C) Relative accessibility of promoters in each cluster (ATAC-seq signal from −450 to +149 bp relative to TSS) following conditional knockout of BRG1 via 72 h tamoxifen administration in BRG1 fl/fl cells expressing CRE-ER.[8] Whiskers show the 10–90th percentiles and p values are from Mann-Whitney test.

(D) Average relative accessibility of promoters in each cluster (left, ATAC-seq reads from −450 to +149 bp relative to TSS) or enhancers (right, ATAC-seq reads −300 to +299 bp from enhancer center) over an extended time course of ARID1A degradation.[39]

(E) Relative BRG1 ChIP-seq binding at enhancers and promoters in each cluster (BRG1 ChIP-seq signal ±500 bp relative to enhancer center or TSS) following treatment with BRM014 for 2 or 4 h. Whiskers show the 10–90th percentiles and p values are from Mann-Whitney test.

(F–H) Average BRG1 ChIP-seq reads at enhancers (F), promoters in cluster 1 (G), and promoters in clusters 2–4 (H). Data are graphed in 50 bp bins.

(I) Gene body PRO-seq read density (TSS + 250 nt to TES) at unchanged genes. Whiskers show the 10–90th percentiles. There are no significant differences in PRO-seq reads at 2, 4, or 8 h BRM014 treatment compared with the DMSO control (Mann-Whitney test, p values all > 0.05).

(J) Left: ATAC-seq reads were summed at each enhancer (−300 to +299 bp from the peak center, n = 32,149) over the time course of BRM014 treatment and read counts relative to time-matched DMSO samples are shown. As indicated, enhancers were separated into quartiles based on the level of accessibility after 8 h of BRM014. For each enhancer, the nearest gene promoter was identified. Right: the relative ATAC-seq signal is shown at the promoters (−450 to +149 bp relative to TSS) associated with the quartile of enhancers showing the strongest recovery in accessibility (red) and the weakest recovery in accessibility (blue) following 8 h of BRM014 treatment. There is no significant difference in the distribution of relative ATAC-seq signals at promoters associated with the strongest vs. weakest recovering enhancers (Mann-Whitney test, p value > 0.05). Whiskers show the 10–90th percentiles.

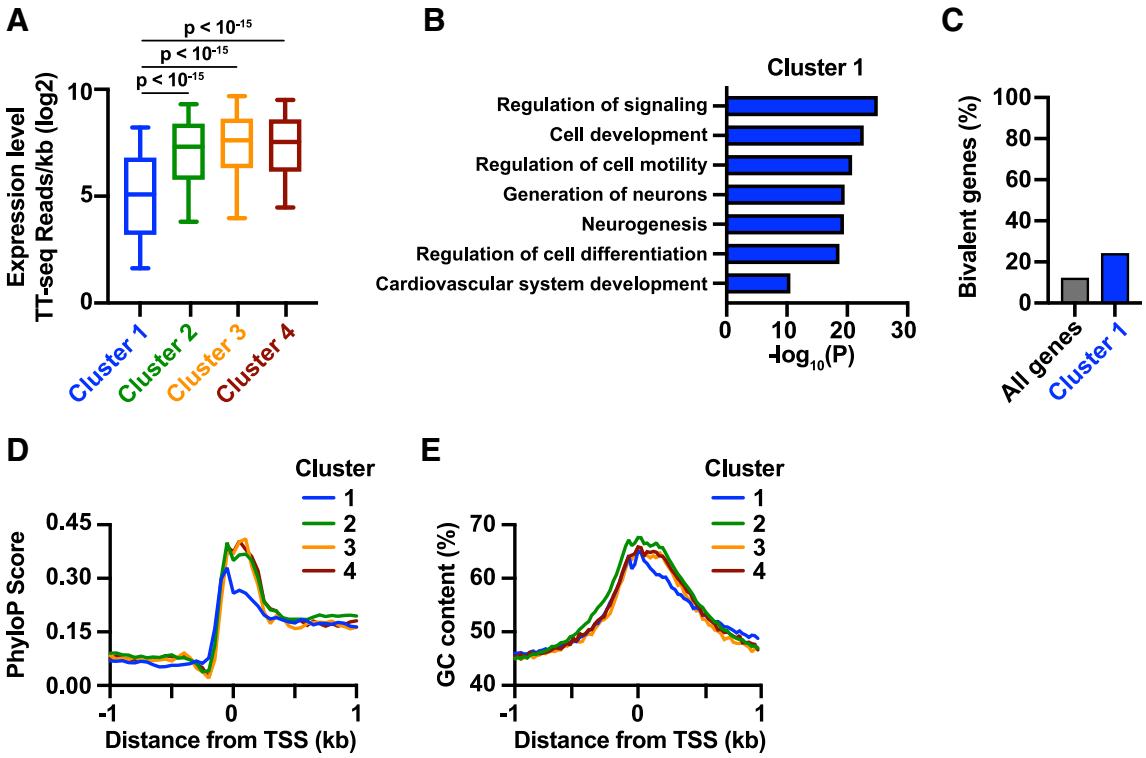

Figure S4. Characteristics of promoters of genes in clusters 1–4, related to Figure 4

(A) Transient transcriptome sequencing (TT-seq)[34] signal at genes by promoter cluster. Whiskers show the 10–90th percentiles and p values are from Mann-Whitney test.

(B) Select GO terms enriched in cluster 1 genes, using cluster 2 genes as background.

(C) Percentage of genes classified as bivalent.[105]

(D) Average PhyloP conservation score[44] for promoters by cluster, graphed in 50 bp bins. A higher PhyloP score indicates a higher level of evolutionary conservation, as determined across placental species.

(E) Average GC content[44] at promoters by cluster, graphed in 25 bp bins.

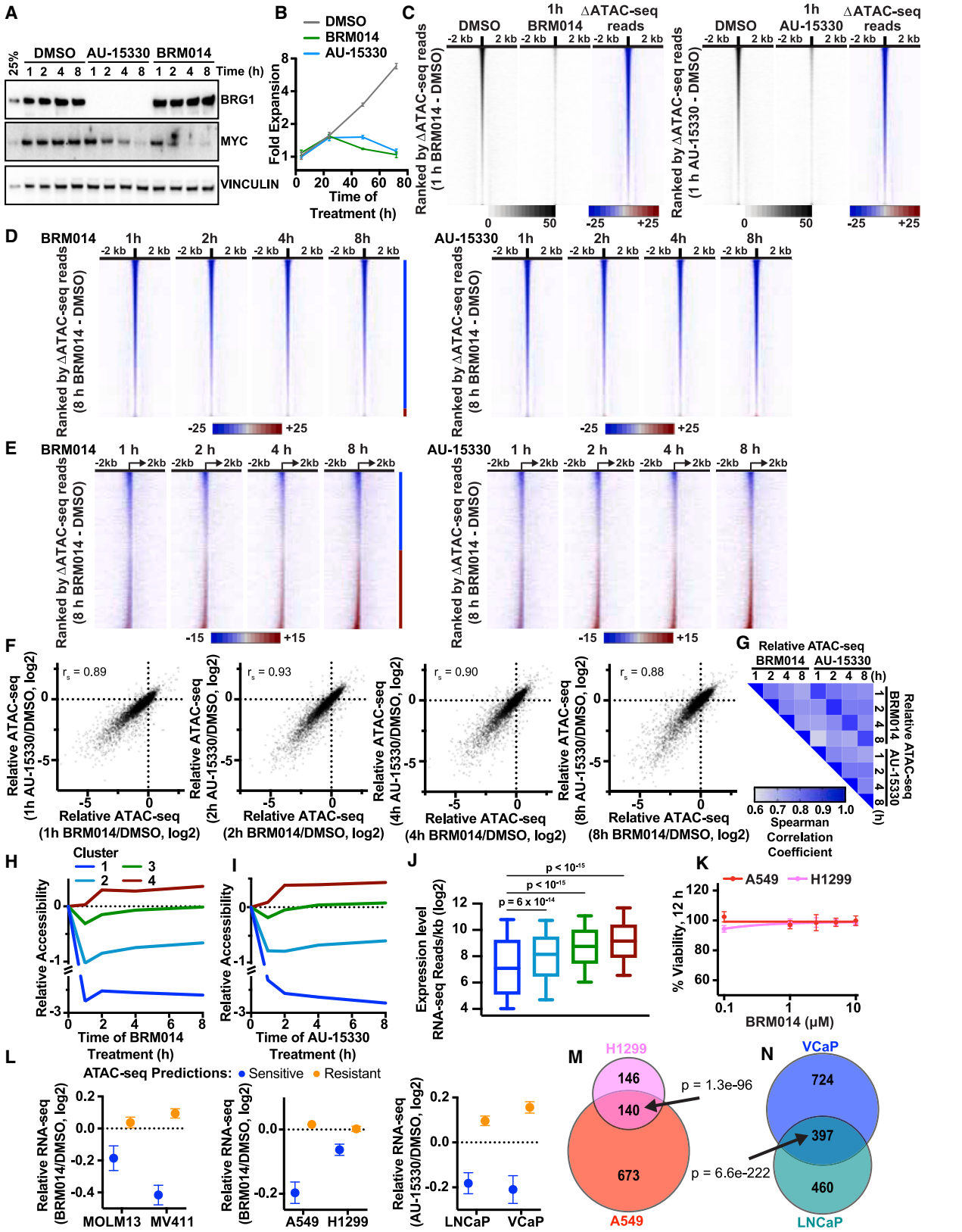

(legend on next page)

Figure S5. Effects of BRM014 and AU15330 treatment in human cancer cell lines, related to Figure 5

(A) Western blots of MV411 cells treated with 1 μM BRM014, AU-15330, or DMSO for the indicated duration, using antibodies against BRG1/SMARCA4 or MYC. As MYC expression in MV411 cells is known to depend on SWI/SNF activity,[48] it is used here as a positive control to confirm successful perturbation of SWI/SNF function. A dilution of the 1 h DMSO sample is loaded in the first lane to enable quantitative assessment of BRG1 and MYC protein levels. Vinculin is shown as a loading control.

(B) Proliferation of MV411 cells treated with 1 μM BRM014, AU-15330, or DMSO for the indicated duration. Error bars represent the standard error of the mean for three biological replicates.

(C) Heatmap representation of the effects of 1 h BRM014 (left) or AU-15330 (right) treatment on ATAC-seq signal at MV411 enhancers (n = 36,175). Normalized data from combined replicates (n = 3 per condition) were aligned to the enhancer center. Sites are ranked by difference in ATAC-seq reads (enhancer center ± 300 bp) between 1 h BRM014 (left) or 1 h AU-15330 (right) and 1 h DMSO control.

(D) Difference in ATAC-seq signal after BRM014 (left) or AU-15330 (right) treatment ($n \geq 2$ per condition) for all MV411 enhancers. Data were aligned to the enhancer center and rank ordered by the difference in enhancer ATAC-seq reads after 8 h BRM014 treatment. The blue line between heatmaps indicates the 95% of enhancers that fail to recover accessibility (N = 34,460), whereas the red line indicates enhancers that recover accessibility (N = 1,715).

(E) Difference in ATAC-seq signal after BRM014 (left) or AU-15330 (right) treatment ($n \geq 2$ per condition) for all active gene promoters in MV411 cells (n = 11,022). Data were aligned to TSSs and rank ordered by the difference in promoter ATAC-seq reads after 8 h BRM014 treatment. The blue line between heatmaps indicates the 50.8% of promoters that fail to recover accessibility (5,596), whereas the red line indicates promoters that fully regain accessibility (5,426).

(F) The fold-change in ATAC-seq signal at active gene promoters (−450 to +149 from the gene TSS) in MV411 cells is shown, comparing changes upon BRM014 or AU-15330 treatment for 1, 2, 4, and 8 h. Spearman's rho is indicated.

(G) Heatmap depicting Spearman's rho for the fold-change in ATAC-seq signal at MV411 gene promoters (−450 to +149 from the gene TSS) following BRM014 or AU-15330 treatment for 1, 2, 4, and 8 h.

(H and I) The average fold-change in ATAC-seq signal (−450 to +149 bp from the TSS) for each MV411 promoter cluster across the BRM014 (H) and AU-15330 (I) time courses.

(J) RNA-seq[48] signal at genes in each promoter cluster, as defined by ATAC-seq in MV411 cells. Whiskers show the 10–90th percentiles and p values are from Mann-Whitney test.

(K) Drug dose-response curves of BRM014 treated A549 or H1299 cell lines after 12 h of treatment. Viable cells counted using CellTiter-Glo. Error bars represent SEM of six technical replicates.

(L) Mean expression changes at genes predicted to be sensitive to SWI/SNF perturbation using ATAC-seq. The average $\log_2$ fold-change in RNA-seq following SWI/SNF inhibition by BRM014 (MOLM13,[48] MV411,[48] A549, and H1299 cells) or degradation by AU-15330[25] (LNCaP and VCaP cells) is shown. Error bars represent SEM. See STAR Methods for data sources and number of genes in each group.

(M and N) Overlap between genes downregulated (fold-change > 1.5 and p adj < 0.001) following BRM014 treatment in H1299 and A549 cells (K) or AU-15330 treatment in VCaP and LNCaP cells[25] (L). p values for the overlap of gene lists were calculated using the hypergeometric distribution with the phyper function in R.

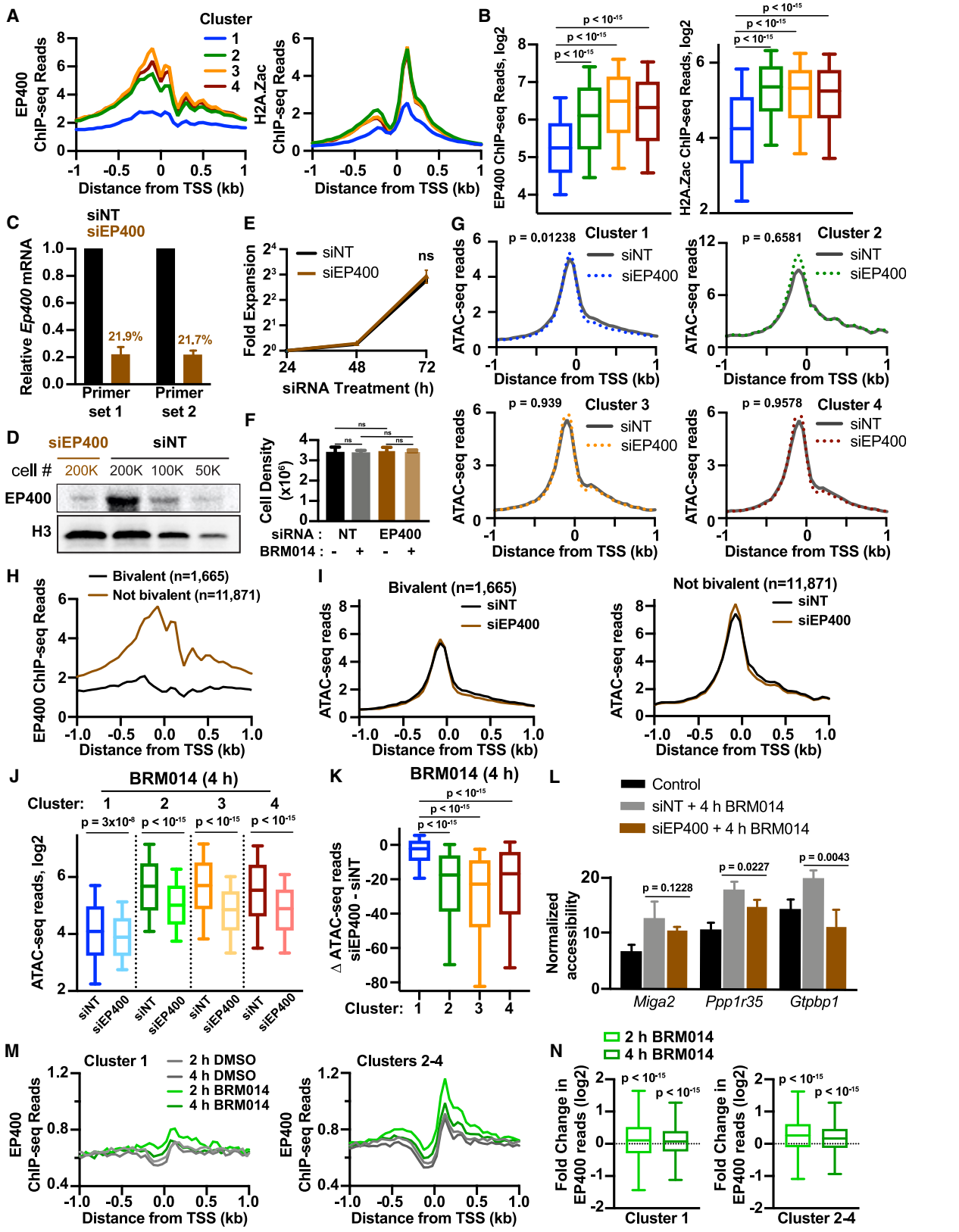

(legend on next page)

Figure S6. siRNA-mediated knockdown of EP400 for 72 h substantially reduces levels of EP400 mRNA and protein and impairs promoter recovery following BRM014 treatment, related to Figure 6

(A) Average EP400[3] and H2A.Zac[63] ChIP-seq reads by promoter cluster, graphed in 50 bp bins.

(B) For promoters by cluster, boxplots of EP400[3] and H2A.Zac[63] ChIP-seq reads per gene (TSS ± 500 bp). Whiskers show the 10–90th percentiles and p values are from Mann-Whitney test.

(C) RT-qPCR analysis of *Ep400* mRNA levels following 72 h treatment with siNT or siEP400. Two primer pairs targeting *Ep400* were used. Data were normalized for each primer pair by levels detected in siNT-treated cells.

(D) Western blot analysis of EP400 protein levels following 72 h treatment with siNT or siEP400. Histone H3 is shown as a loading control.

(E) Proliferation of mESCs treated with siRNAs against EP400 (siEP400) or a non-targeting control (siNT) (n = 2). p value was calculated using a paired t test. We note that the process of transfecting mESCs slows growth for 24–48 h, and cells were investigated at 72 h, after cell proliferation had fully recovered.

(F) mESCs were treated with siEP400 or siNT. 72 h post transfection, mESCs were treated with DMSO or 1 μM BRM014 for 4 h (as in Figure 6D; n = 3). Bar plots depict viable cell counts per indicated condition. p values were generated using a paired t test.

(G) For promoters by cluster, average ATAC-seq signal in siNT-treated and siEP400 cells, graphed in 50 bp bins. To assess differences between conditions, ATAC-seq signal was summed (−450 to +149 bp relative to TSS) in siNT-treated and siEP400 cells. p values were calculated by Wilcoxon signed ranks test.

(H) Average EP400[3] ChIP-seq reads for genes classified as bivalent[105] vs. those not classified as bivalent, graphed in 50 bp bins.

(I) For promoters classified as bivalent[105] (left) or not (right), average ATAC-seq signal in siNT-treated and siEP400 cells, graphed in 50 bp bins.

(J) For promoters by cluster, boxplots of ATAC-seq signal (−450 to +149 bp relative to TSS) in siNT and siEP400 cells following 4 h BRM014 treatment. Whiskers show the 10–90th percentiles and p values are from Mann-Whitney test.

(K) For promoters by cluster, boxplots of the difference in ATAC-seq signal (−450 to +149 bp relative to TSS) in BRM014-treated cells (siEP400 minus siNT). Whiskers show the 10–90th percentiles and p values are from Mann-Whitney test.

(L) ATAC-qPCR validation of accessibility changes following 4 h BRM014 treatment in siNT-treated and siEP400 cells at selected promoters with evidence of recovery (*Miga2*, *Ppp1r35*, and *Gtpbp1*). qPCR values were normalized to background signal of closed chromatin. p values calculated by Student's t test.

(M) Aggregate plots of EP400 ChIP-seq signal (n = 2 per condition) at promoters per indicated cluster in 2 or 4 h DMSO- and BRM014-treated cells. Clusters 2–4 are grouped together, and data are graphed in 50 bp bins.

(N) Boxplots of EP400 ChIP-seq reads per gene (TSS ± 500 bp) are shown per cluster, as in (M). Whiskers show the 10–90th percentiles and p values are from a one sample Wilcoxon signed rank test, comparing samples with a theoretical median of 0.

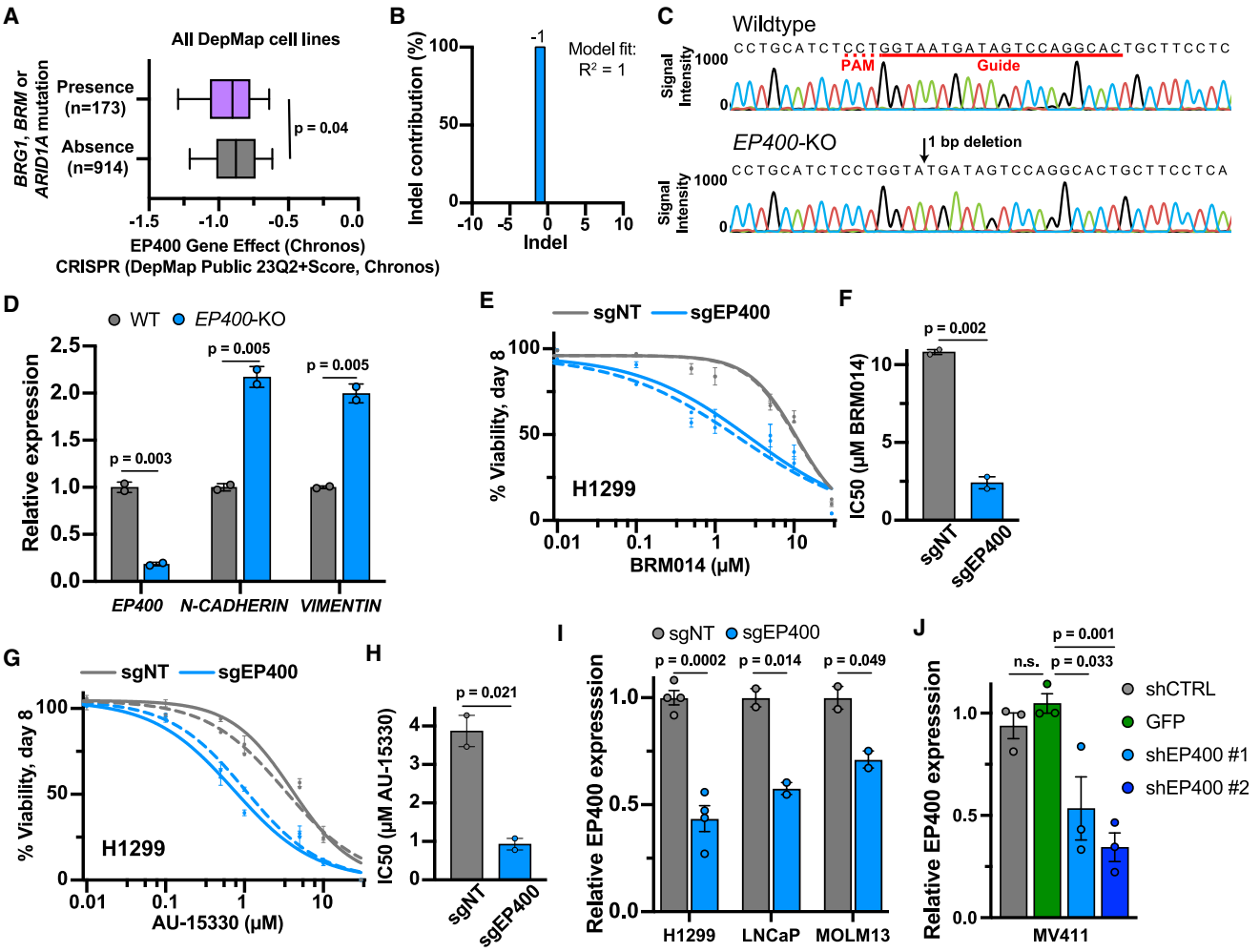

K

Cell line	Gene	Variant Info	Protein change	Allelic frequency
A549	SMARCA4	Frame shift deletion	p.Q729fs	0.984
H1299	SMARCA4	Splice site	NA	0.979
LNCaP	SMARCA2	Frame shift deletion	p.M1242fs	0.436
LNCaP	SMARCC1	Nonsense	p.Q789*	0.500
LNCaP	ARID1B	Nonsense	p.E2247*	0.348
LNCaP	SMARCA2	Missense	p.P889H	0.167
LNCaP	SMARCC2	Missense	p.R443Q	0.436
LNCaP	ARID1A	Frame shift deletion	p.G285fs	0.764
LNCaP	SMARCD1	Missense	p.D289G	0.554
LNCaP	BCL7B	Missense	p.G72S	0.375
VCaP	No reported mutations in SWI/SNF subunits			
MOLM13	No reported mutations in SWI/SNF subunits			
MV411	SMARCE1	Missense	p.S172N	0.559
BT869	No reported mutations in SWI/SNF subunits			
DIPG007	No reported mutations in SWI/SNF subunits			

(legend on next page)

Figure S7. Characterization of *EP400*-depleted cell lines, related to Figure 7

(A) EP400 gene effect Chronos scores[65–68] across DepMap cell lines with (n = 173) or without (n = 914) annotated mutations in *BRG1*, *BRM*, or *ARID1A*. Whiskers show the 10–90th percentiles and p value is from Mann-Whitney test.

(B) Indel contributions shown for the A549 *EP400*-KO cell line, indicating a homozygous 1 bp deletion.

(C) Sanger sequencing traces spanning the CRISPR guide cut site (in the coding sequence of *EP400* exon 2) from wild-type and *EP400*-KO A549 cell lines were compared using Inference of CRISPR Edits (ICE).[99] Raw sequencing traces shown with CRISPR guide and 1 bp deletion in KO indicated.

(D) *EP400*, *N-CADHERIN* and *VIMENTIN* transcript levels were assessed by RT-qPCR in parental (wild-type) and *EP400*-KO cells (n = 2 for each condition). *EP400* expression was normalized to *ActB* and then to the average expression in wild-type cells. Primers for *EP400* anneal to exons 29 and 30. Average expression per genotype plotted, with individual values shown as circles and error bars representing the SEM. p values calculated by Student's t test.

(E) Drug dose response curves of sgNT- and sg*EP400*-expressing NSCLC (H1299) cells following 8 days of treatment with BRM014. Each curve represents an independent experiment of the indicated cell line (n = 2). Errors bars represent the SEM of three technical replicates.

(F) Quantification of IC50 values from the dose response curves plotted in (E). Error bars represent SEM. Individual values plotted as circles. p values calculated by t test.

(G) Drug dose response curves of sgNT- and sg*EP400*-expressing (H1299) cells following 8 days of treatment with AU-15330. Each curve represents an independent experiment of the indicated cell line (n = 2). Errors bars represent the SEM of three technical replicates.

(H) Quantification of IC50 values from the dose response curves plotted in (G). Error bars represent SEM. Individual values plotted as circles. p values calculated by t test.

(I) *EP400* transcript levels were assessed by RT-qPCR in Cas9-expressing cells transduced with lentiviruses expressing non-target (sgNT) or EP400-targeting (sgEP400) guides (n = 2–4 for each condition). *EP400* expression was normalized to *ActB* and then to the average expression in wild-type cells. Primers for *EP400* anneal to exons 29 and 30. Average expression per genotype is plotted, with individual values shown as circles and error bars representing the SEM. p values calculated by Student's t test.

(J) *EP400* transcript levels were assessed by RT-qPCR in cells transduced with lentiviruses expressing the indicated shRNAs (n = 3 for each condition). *EP400* expression was normalized to *ActB* and then to the average expression in wild-type cells. Primers for *EP400* anneal to exons 29 and 30. Average expression per genotype is plotted, with individual values shown as circles and error bars representing the SEM. p values calculated by Student's t test.

(K) For the indicated cell lines, SWI/SNF subunits were analyzed for mutations annotated in the DepMap database, with mutations found for *SMARCA4*/*BRG1*, *SMARCA2*/*BRM*, *SMARCC1*/*BAF155*, *SMARCC2*/*BAF170*, *SMARCE1*/*BAF57*, *ARID1A*/*BAF250A*, and *ARID1B*/*BAF250B*. The splice site mutation of *SMARCA4*/*BRG1* in H1299 cells is reported to be deleterious, resulting in a loss of SMARCA4/BRG1 in these cells.[26,109] Note: the BT869 cell line, is not included in the DepMap database, but a published characterization of the cell line revealed no mutations in SWI/SNF subunits.[110]